Leaf and canopy responses to forest degradation and extreme climatic events: a remote sensing perspective

Matheus Henrique Nunes

Fitzwilliam College

University of Cambridge

December 2018

Dissertation submitted to the University of Cambridge

for the Degree of Doctor of Philosophy

Summary

Monitoring the responses of leaf functional traits and vegetation structure to environmental change is key to understanding the responses of ecological systems to anthropogenic global change. Advancement in earth observation technologies provide new opportunities to answer complex ecological questions at scales ranging from the community to the landscape level. This thesis investigates the impacts of environmental change on foliar traits and forest structure. In particular, it investigates the impacts of El Niño on leaf traits using hyperspectroscopy and on the structure of forests modified by oil palm plantations using airborne LiDAR. The first chapter explores the potential and limitations of using hyperspectral data to estimate leaf traits remotely. Working with six temperate tree species in contrasting soil types, I explore the relationship between leaf structure and chemistry and spectral characteristics. We show that interspecific differences in leaf traits were generally much stronger than intraspecific differences related to soil type. We highlight the difficulties that can arise in detecting within-species variation owing to "constellation effects" but demonstrate the power of spectroscopy to predict traits. The second chapter investigates the effects of drought on leaf traits and spectra, by taking measurements during and after an El Niño event. Pigments were particularly lower after the drought, when rain was more frequent, sunshine duration was shorter and radiation was lower, indicating increased greenness and forest resilience to climatic variation. Spectral information was also shown to be effective at detecting the impacts of droughts on leaf traits. Upscaling to the landscape level, the third chapter focuses on methods for estimating aboveground carbon stocks in oil palm plantations using airborne LiDAR. We show that an area-based approach is more accurate than tree-centric methods, although the latter may be useful to detect, extract and count individual oil palm trees from images. The fourth chapter explores the effects of El Niño drought on the canopy structure of tropical forests in Borneo using repeat airborne LiDAR. Our results reveal extensive leaf shedding caused by extreme high temperatures and Vapour-Pressure Deficit. Regenerating short forests on ridges were particularly more vulnerable to climatic variation owing to greater heat and atmospheric dryness. In conclusion, this thesis integrates field measurements and remote sensing to narrow down the uncertainties of vegetation responses to environmental changes.

This dissertation is the result of my own work and includes nothing which is the outcome of work done in collaboration except as declared in the Preface and specified in the text.

It is not substantially the same as any that I have submitted, or, is being concurrently submitted for a degree or diploma or other qualification at the University of Cambridge or any other University or similar institution except as declared in the Preface and specified in the text. I further state that no substantial part of my dissertation has already been submitted, or, is being concurrently submitted for any such degree, diploma or other qualification at the University of Cambridge or any other University or similar institution except as declared in the Preface and specified in the text.

It does not exceed the prescribed word limit of 60,000 for the Biology Degree Committee.

Acknowledgements

This thesis represents not only work in the past four years, it is a milestone seeking to become an academic in Ecology. I would like to firstly acknowledge my sypervisor David Coomes, who gave me this opportunity and brilliantly guided me through the past four years during my steep learning curve time (breaking and losing some equipment too!). Many thanks for trusting me and giving me the independence to think and learn, and for always pushing me to challenge myself. You are a very great leader and mentor! Many thanks.

I am extremely grateful to the Conselho Nacional de Pesquisa e Desenvolvimento (CNPq) for the PhD scholarship. It is necessary to recognise the importance of those investments to strenghten our country politically, socially and economically, that will ultimately bring ecological stability.

My family is a big support with their incentives and life stories: Agradeço muito à minha mãe que sempre soube de meus desejos em ser pesquisador. Depois de suas batalhas no Reino Unido, eu me aventurei pela bandas de cá para realizar este sonho que também foi dela. Um muito obrigado à minha família, especialmente avó Maria, tias (as donas bonitas Célia, Cláudia, Leca e Eva) e primos que sempre mantiveram o suporte e hoje são minha base de apoio. Fiquem tranquilas que não demora e eu voltarei! Muito do que faço é pensando em vocês.

A PhD becomes a much more encouraging process when surrounded by the brightest minds in Ecology. Many thanks for all the bites you brought from many travels, the laughters over coffee, suggestions, conversations, partnerships, parties, college lunch and friendships. In no particular order, Chloé Orland, Boris Bongalov, Sacha Khoury, Tommaso Jucker, Ruben Valbuena, Tom Swinfield, Alex Guizar, Javi Igea, Laura Bentley, Jon Williams, Jéssica Silva, Florian Zellweger, Erik Emilson, O'Neill Kyaw Sein, and Lauranne Gateau.

I am grateful to Fitzwilliam College for making life easier in many aspects. In particular, I am very pleased the college gave me some wonderful people. Katarzyna Doniec (the gorgeous Kasia), my personal life mentor, my spiritual guide, my second granny, the one who tells me the truth (or a bunch of lies) to make me happy. Você é uma inspiração em inteligência, companheirismo, humildade e fé. Muito do que tenho feito foi pensando nos valores que você tem me dado como exemplo. Quero você sempre do meu lado. Jamie Gawith, the (successful)

man who keeps me in the loop with the Cambridge life, my agenda man, the one who finds me shelter. If I am ever stressed I just need to meet you to get relaxed and keep myself calm (because I really need it!). Some absolutely fantastic people at Fitz, among others, Rob Liu, Fernando Caballeros, Mandy (oh Mandy!).

Thank you those people who have been very present at some stage within the last years. Richard Downes, my cycle buddy, thanks for all the long bike rides, the beers, food, coffee, the insights to become a more pragmatic man. Carolina Dias, for making me all the important decisions. Tibisay Morgandi, for all good times travelling and eating.

In the past months, I had the pleasure to spend a great amount of time with the family Takacs Battini, who ended up being a really great support during the final stages of the writing up. Amanda and Eduardo, your support has been fundamental to give me a boost and energy!

Being in the Cambridge University Brazilian Society committee for three years was great fun to meet extremely interesting Brazilians from different backgrounds, make good friends and participate more actively in all things Brazil. Tem um povo maravilhoso demais por essas bandas de cá fazendo a revolução intelectual, que vai de É o Tchan até Heitor Villa-Lobos, pensamento medieval ao pós-moderno, dos laboratórios avançadíssimos de genética e cimento aos buracos negros, da migração de plantas à migração de populações. Isabela Navarro, Aline Khoury, Lívia Ribeiro, Paulo Savaget, Bruno Vermandel, Giu Papallo, Flávia Bueno, Angélica Silva, Arthur Josie, Pedro Vianna, Chris Robinson, Camila Zanella, Erick Silva, Rafael Moraes, Fabiana Freitas, André Vasconcelos, espero ver alguns de vocês nos ministérios e instituições brasileiros!

The time spent in Malaysia in 2015 gave me some good friends – going through madly crazy experiences - who I ended up spending a good time with throughout the past four year. The artsy-fartsy Conor Bolas, whose life is a rich tapestry, you brought happiness to all the beings and non-beings of the very much humid rain forests full of gases and extended it to the slightly colder fens of England and mountainous lakes of Scotland. Man, you are unbelievable! Dena, quiero casarme contigo! Glen Reynolds, the great man who is so important to protect the forests of Borneo. Terima kasih banyak semua orang orang dari Malaysia yang saya kerja di dalam hutan.

I would like to thank the SAFE management team, South East Asia Rainforest Research Partnership, Sabah Forestry Department and Sabah Biodiversity Centre for their support, access to the field sites and for permission to carry out fieldwork in Sabah.

Finally, I would like to thank the people who mostly influenced me academically prior to coming to Cambridge and have certainly shaped my carrer. In chronological order, Gislene Carvalho, Eduardo van den Berg, Ana Carolina Silva, Pedro Higuchi, Marcela Nunes Terra, Ary Oliveira-Filho, Izabela Oliveira, Bruno Kanieski, Eric Gorgens and Greg Biging. Many thanks!

Matheus Nunes

27th December 2018

Contents

List of Tables

List of Figures

Preface

Chapters 2 – 5 were written as manuscripts for peer-reviewed journals as result of data collection, analysis, interpretation and writing. As these papers have multiple authors, I have specified the role of each person in the Author contributions sections. Co-author contributions included data collection, laboratory analysis and supervisory guidance. At the time of submission, **Chapter 2** and **Chapter 4** have been published, **Chapter 3** is in review, and **Chapter 5** is in preparation. Data collection was also done for 5 months in Borneo however the results have not been published as part of this thesis.

Chapter 2

Nunes, M.H., Davey, M.P. and Coomes, D.A., 2017. On the challenges of using field spectroscopy to measure the impact of soil type on leaf traits. *Biogeosciences*, *14*(13), pp.3371-3385.

Chapter 3

Nunes, M.H., S.; Both; Bongalov, B.; Brelsford, C.; Khoury, S.; Burslem, D.F.R.P.; Philipson, C.; Majalap, N.; Riutta, T.; Coomes, D.A.; Cutler, M.E.J. Changes in leaf functional traits of rainforest canopy trees associated with an El Niño event in Borneo. *Environmental Research Letters* (accepted)

Chapter 4

Nunes, M.H., Ewers, R.M., Turner, E.C. and Coomes, D.A., 2017. Mapping aboveground carbon in oil palm plantations using LiDAR: A comparison of tree-centric versus area-based approaches. *Remote Sensing*, *9*(8), p.816.

Chapter 5

Nunes, M. H., Jucker T., Swinfield T., Asner G., Vaughn N., Valbuena R., Svátek M., Kvasnica J., Both S., Elias D.M.O., Riutta T., Malhi Y. and Coomes, D.A. Extreme microclimate conditions driven by human modification and topography control forest canopy loss during El Niño. (*in preparation*)

Chapter 1 | General introduction

The interconnected nature of the biosphere means that the stability of biological communities is affected by man-induced and natural changes (Odum, 1983; Greegor, 1986). Land-use change is rapid in the tropical forests regions (Salas *et al*., 2000), contributing to declining biodiversity (Newbold *et al*., 2015), and subsequently affecting the stability and resistance of ecosystems to climate extremes (Isbell *et al*., 2015; Hautier *et al*., 2015). Southeast Asia has experienced the greatest rates of forest loss anywhere in the tropics (Sohdi *et al*., 2004; Miettinen *et al*., 2011), and extreme climate events in the region are becoming more frequent and intense (Thirumalai *et al*., 2017). Given that these forests are amongst the most diverse (Slik *et al*., 2015) and carbon dense in the tropics (Sullivan *et al*., 2017), these changes are threatening many species and exerting a large impact on the Earth's climate system (Patra *et al*., 2017).

In this introductory chapter, I briefly review forest responses to environmental change, with a focus on responses to climatic events at species, community and landscape levels. I describe the changes that have already occurred on the island of Borneo, in Southeast Asia, and discuss efforts to conserve what remains. I explain how functional traits can be used to investigate forest responses to environmental change, and how remote sensing techniques may contribute to investigating these traits. Finally, I outline the aims of my thesis, explaining how the chapters address the use of remotely sensed functional traits as a means to examining the impact of extreme climate events on human-modified forests in the tropics.

1.1 Anthropogenic changes at the centre of forest change

Human activity has profoundly affected tropical forests (Hansen *et al*., 2013) mostly due to change in land use (Sala *et al*., 2000). These changes have a large influence on biogeochemical cycles. Tropical forests store 471 billion tonnes of carbon in their live biomass, soils, deadwood and litter, which is equivalent to almost half the total atmospheric carbon stocks (Pan *et al*., 2011). They also influence the hydrological cycle (Kooperman *et al*., 2018) and trace gases such as isoprene (Vickers *et al*., 2009). Tropical forests have high transpiration rates (Schlesinger and Jasechko, 2014; Manoli *et al*., 2018), and land use change affects affect

precipitation (Malhi *et al*., 2009). Their loss contributes to increasing CO_2 in the atmosphere and influence physiological behaviour of plants (e.g. reduced stomatal conductance; Kooperman *et al*., 2018).

1.1.1 Climate change and El Niño-Southern Oscillation events`

El Niño events are the dominant interannual climate variation on Earth (McPhaden *et al*., 2006), driven by variability in the trade winds and the zonal contrasts in sea surface temperature that they generate (Cane, 2005). Trade winds along the equator usually lead to an accumulation of warm surface water in the western Pacific and upwelling of cold water off the west coast of South America. This east-west surface temperature contrast reinforces an east-west air pressure differences that drive the wind trades. During El Niño, these winds are weakened causing the warm surface waters to move into the central Pacific region, with major consequences for rain patterns in the region (McPhaden *et al*., 2006). Shifts in precipitation patterns in response to El Niño typically bring drought to Australia and some Southeast Asia's countries, and flood to central Pacific islands and west coast of South America (McPhaden *et al*., 2006). However, the position and duration of sea surface temperature anomalies affect the intensity of El Niño events (Trenberth and Stepaniak, 2001), and fluctuations in temperature and precipitation on land are irregular in amplitude, duration, temporal evolution, and spatial structure (Neelin *et al*., 1998).

The Southern Oscillations responsible for El Niño events have occurred for at least 130,000 years (Tudhop *et al*., 2001), suggesting ample opportunity for natural selection of trees capable of tolerating irregular drought events (Detto *et al*., 2018). However, there are concerns that anthropogenic climate change is increasing the frequency and intensity of El Niño events (Thirumalai *et al*., 2017; Wang *et al*., 2017) due to increases in upper-ocean stratification in the equatorial Pacific under global warming (Cai *et al*., 2018). The 2015/2016 El Niño was the third most intense since the 1950s, and exerted a large impact on the Earth's natural climate system (Patra *et al*., 2017). The Earth was then a net carbon source, contributing to an excess CO_2 emission from the Earth's surface primarily due to reduced vegetation uptake associated with drought, and to a lesser extent from increased biomass burning.

There is evidence that increasing drought severity is having catastrophic effects on forests in some regions, including California (Asner *et al*., 2016), Inner Asia (Liu *et al*., 2013) and South-

western USA (Williams *et al*., 2010; Williams *et al*., 2013). Increased air temperature is causing higher evaporative demand, resulting in greater water stress even if rainfall patterns remain unchanged (Clark *et al*., 2010; Allen *et al*., 2015). This increased evaporative demand has the potential to shift tropical forests from net carbon sinks to sources due to increased tree mortality and decreased productivity during drought (Gatti *et al*., 2014; Qie *et al*., 2017; Zuleta *et al*., 2017; Greenwood *et al*., 2017; Mitchard, 2018). However, we still have a poor understanding of how tropical forests in different regions are responding to extreme climate events, particularly because rainforest species vary in resilience (Nepstad *et al*., 2002; Doughty *et al*., 2015; Santos et al, 2018) and CO_2 concentration can enhance forest productivity (Norby *et al*., 2005). Stomatal regulation and plant physiological response strongly regulate evapotranspiration, and responses to drought may vary from leaf shedding (Wolfe *et al*.,2016), lower productivity to widespread death of trees (Saatchi *et al*., 2013). Understanding how tropical forests respond to extreme drought events has therefore emerged as a key priority if we are to forecast the impacts of climate change on the terrestrial carbon cycle (Mitchard 2018; McDowell *et al*. 2018).

1.1.2 Forest fragmentation and logging in the context of extreme climate events

Anthropogenic disturbance can have significant effects on forest responses to drought (Huang and Asner, 2010; Baccini *et al*., 2017; Putz *et al*., 2012; Qie *et al*., 2017; Brinck *et al*., 2017). Disturbance of vegetation results in changes in surface albedo, evapotranspiration and cloud cover, affecting the regional and global climate (Bala *et al*., 2007; McAlpine *et al*., 2018), as well as modifying canopy gap formation and dynamics, producing canopies with lower height and more spatially uniform surfaces (Vaughn *et al*., 2015). Selective logging lowers and thins the forest canopy, reducing its area index (Ewers *et al*., 2015; Hardwick *et al*., 2015), the number of vegetation strata it contains, and creating large forest gaps (Okuda *et al*., 2003). These logged forests can be especially vulnerable to global warming because structural changes increase evapotranspiration, leading to depleted soil moisture and creating stress for drought-sensitive plants (Laurance 2004). For example, canopy height affects air temperature and atmospheric dryness in the understory of forests in Malaysian Borneo, and these microclimatic changes may influence forest regeneration (Jucker *et al*., 2018c). Given that microclimate modulates plant responses to macroclimate warming (De Frenne *et al*., 2013), logged forest understories are less buffered from regional climate change than old

growth forests, experiencing much higher microclimate extremes and heterogeneity (Blonder *et al*., 2018).

Forest fragmentation can increase tree mortality around the fragment borders, with edge effects reported to penetrate from 100 m (Laurance *et al*., 2006, Lindenmayer *et al*., 2012, Laurance *et al*.,2011; Numata *et al*., 2011) to 1500 m from the forest edge (Chaplin-Kramer *et al*., 2015). A recent global analysis estimates that edge effects extend 100 m from the forest edge, and shows that 19% of tropical forests lie within this area leading to 31% of the estimated annual carbon emissions associated with deforestation (Brinck *et al*., 2017).

These disturbed forests contain a high proportion of pioneer tree species (Both *et al*., 2018; Riutta *et al*., 2018), whose physiological characteristics may make them more vulnerable to drought and higher temperatures (Bazzaz and Pickett, 1980; Lohbeck *et al*., 2013). Pioneer species are characterised by "acquisitive" traits that maximize carbon capture and growth (Lohbeck *et al*., Poorter *et al*., 2008; 2013; Both *et al*., 2018), and have biomass growth rates several times higher than old-growth forests (Blanc *et al*., 2009; Berry *et al*., 2010). However, acquisitive traits are associated with cheap-to-construct material with short lifespans (Lohbeck *et al*., 2008). High stem turnover in early successional stands creates canopy gaps which results in high irradiance and temperatures in the forest understory, making these stands susceptible to climate extremes (Lebrija-Trejos *et al*., 2011).

1.2 Anthropogenic change on the island of Borneo

The island of Borneo contains some of the richest and carbon dense forests on the planet (McKinnon, 1996; Sullivan *et al*., 2016). Before human disturbance, most of the island was covered in lowland, hill and montane dipterocarp forests, heath forests, mangroves forests, and freshwater and peat swamp forests (McKinnon, 1996). Lowland dipterocarp forests occur up to 1200 m elevation dominated in its upper and emergent canopy by the family Dipterocarpaceae and is the most extensive forest type in Borneo (Newbury *et al*., 1992). The forests of Borneo have been severely impacted by selective logging, fire and conversion to plantations, which has occurred at unprecedented rates since the early 1970s (Gaveau *et al*., 2014). Between 1973 and 2010, 30% of Borneo's intact forests were lost, mostly to logging (15%) and industrial plantations (10%). With a land area of 73 631 km^2, the state of Sabah

occupies just less than 10 % of Borneo, and is registered as the region with the highest forest loss rate on the island between 1973 and 2010 (Gaveau *et al*., 2014).

1.2.1 Drivers of forest loss and degradation in Borneo

The oil palm (*Elaeis guineensis*) is the most rapidly expanding crop in the tropics (Koh and Wilcove, 2008). Malaysia has increased its planted area by 150% over the last decade (FAO, 2017) and, along with Indonesia, represents over 80% of global palm oil production (Koh and Wilcove, 2007; FAO, 2017). Rapid conversion to industrial plantations represents ~25% (~20.5% oil palm and ~4.5% pulpwood) of deforestation in Borneo (Gaveau *et al*., 2016). Oil palm plantations are a major driver of national economic and social development in the region where labour and land costs are low (Gaveau *et al*., 2016). If planted on degraded lands (e.g. logged forests), oil-palm may contribute more effectively to economic development and to human welfare than any comparable crop (Sheil *et al*., 2009), however 76% of the industrial plantations have been developed at the expense of old-growth forests (Gaveau *et al*., 2016). Oil palm plantations continue to expand rapidly in Southeast Asia (Gaveau *et al*., 2016) and across the tropics (Fitzherbert *et al*. 2008). Although oil palm plantations continue to expand, the government of Malaysia has pledged to reduce the country's projected GHG emissions by 45% by 2030 (UNFCCC, 2017).

In addition, Borneo's forests have been impacted by logging. More round wood was harvested from Borneo than from Africa and the Amazon combined between 1980 and 2000 (Curran *et al*., 2004). Almost 50% of the total forest area in Borneo has been logged (Gaveau *et al*., 2014), and further degraded by illegal logging, droughts and fires (Page *et al*., 1997; Wooster *et al*., 2012). Since 2000 the rate of logging roads expansion has approximately halved, reflecting a growing scarcity of unlogged, accessible forests (Gaveau *et al*., 2014). Forest conversion has occurred with little regional planning and has created a mosaic of degraded, logged-over areas and non-native monocultures (Curran *et al*., 1999).

El Niño induced droughts have also caused forest loss and degradation in Southeast Asia (Siegert *et al*., 2001; Wooster *et al*., 2012). The exposed ground surface of logged forests dries out and becomes increasingly susceptible to fire, and fires are much more frequent in logged areas (Siegert *et al*., 2001). Borneo's intact forests become carbon source in El Niño years due to increased mortality of trees (Qie *et al*., 2017). In addition, viable seed production and

seedling establishment have declined in Borneo, affecting reproduction and regeneration processes (Curran *et al*., 1999). Furthermore, the underlying mechanisms of forest responses to extreme climate events, and the influences of logging and fragmentation on those responses remain poorly understood.

1.3 Plant responses to environmental change

Rising temperatures and evaporative demand are important components of anthropogenic global, threatening plants that are unable to acclimate to these changes (Vickers *et al*., 2009). Understanding the mechanisms underlying plant responses to heat and water shortage, and to determine which species are more vulnerable than others, are key topics in global change biology (McDowell *et al*., 2008). The use of functional traits has been key to exploring the relationship between climate and plant responses (Niinemets, 2001; Lamont *et al*., 2002; Barlett *et al*., 2012; Fortunel *et al*., 2014).

1.3.1 Plant morphological and physiological functional traits

An increasing number of plant morphological and physiological traits are measured routinely in plant communities, and global trade-offs among these traits are often interpreted in terms of the life histories of different species (Adler *et al*., 2014; Fry *et al*., 2014). Morphological traits include aboveground growth, foliar mass, leaf mass pert unit area (LMA), leaf longevity, canopy structure and architecture (Bloom *et al*., 1985; Ehleringer and Werk, 1986). Physiological traits include photosynthesis, light harvesting, water and nutrient acquisition, although they should be associated with structural investments (Field *et al*., 1992). Many of these traits covary; a study that compared six plant traits – adult plant height, stem specific density, leaf area, LMA, nitrogen (N) and diaspore mass of 46,085 species revealed two dimensions of trait variation that accounted for 74% of the variability in traits (Diaz *et al*., 2016). They found that plant height tends to increase with seed diaspore, whereas a second independent dimension of variation indicates whether leaves have conservative (high LMA and low nitrogen concentration per unit mass) or acquisitive (low LMA and high nitrogen) properties. LMA and leaf N express different aspects of leaf strategy for resource capture and conservation: LMA reflects a trade-off between carbon gain and longevity, whilst N reflects a trade-off between the benefits of photosynthetic potential and the costs of acquiring nitrogen and suffering herbivory. Other physiological leaf traits, such as pigments, describe light use at

the leaf level, controlling the amount of photosynthetically active radiation absorbed for photosynthesis (Ustin *et al*., 2009). Morphological traits, such as canopy height (vertical distance between canopy top and ground), are essential to describe canopy architecture, encompassing the horizontal and vertical structure of forests and influencing light availability, thus affecting competitive and complementary light use and ecosystem productivity (Ishii *et al*., 2004; Williams *et al*., 2017). As morphological or physiological plant traits represent species' strategies for acquiring and using resources, traits may determine their growth, reproduction and survival (Poorter and Bongers 2006). Measuring plant traits in different environments is therefore key to investigating plant's responses to climate change.

Canopy leaf area is an efficient way to control canopy water loss of an entire tree, while maintaining sufficient water supply to the remaining leaves to attain high levels of photosynthesis per unit of leaf area, albeit at the loss of whole tree productivity (Coomes and Grubb, 2000).

1.3.2 Trait responses to environmental change

Functional traits provide a way of predicting tropical forest responses to environmental changes (Reich, 2014). Variation in traits takes on a new importance in the context of global changes; populations that experience the greatest extent of variability in a given environmental condition are expected to be more plastic in traits to acclimate to those conditions (Sultan and Spencer, 2002). It has been suggested that this variability of traits within species help explain differences in growth and survival across resource gradients; for example, plant trait diversity might act as an insurance against climate change impacts on Amazon forests biomass, and considering the possible plasticity of traits, shifts of functional dominance enhance biomass resilience (Sakschewski *et al*., 2016). Morphological and physiological trait acclimation is linked in predictable ways by resource limitations, biotic factors, responses to disturbance or other aspects of the environment, and plant's allocation of energy to these morphological and physiological components should reflect the integration of multiple stresses and resource availability (Ustin and Gamon, 2004).

1.4 Functional traits from a remote sensing perspective

Tracking the consequences of land use, disturbance, and climate change on functioning of ecosystems requires remote sensing data at different scales. Advances in technology have progressively expanded capability for distinguishing the structure, phenology and physiology of vegetation. In particular, field spectrometers are making novel contributions to our understanding of functional traits (Ustin *et al*., 2004), whilst LiDAR is contributing new forms of explicit three-dimensional structural information (Lefsky *et al*., 1999; Gillespie *et al*., 2004; Vierling *et al*., 2008).

1.4.1 Field spectroscopy to study ecosystem functioning

Field spectroscopy involves the study of the inter-relationships between the spectral characteristics of plants and their biophysical attributes (Milton, 1987). Rapid, non-destructive determination of leaf traits *in vivo* and *in situ* using spectroscopy reduces the need to collect large amounts of material in the field, decreases processing time, lessens costly chemical analyses and eliminates sampling that could itself alter experimental conditions (Couture *et al*., 2013). Spectroscopy can provide predictions of a range of foliar traits at the leaf and canopy scales (Asner *et al*., 2011a; Doughty *et al*., 2011; Serbin *et al*., 2014). If variation in leaf traits associated with environmental change is large enough to influence remotely sensed patterns, these effects should be detectable in individual leaves. Hyperspectral reflectance signatures are related to the absorption features across a range of wavelengths: absorption in the visible (400 - 750 nm) portion of the spectrum is mainly driven by pigments (Sims and Gamon, 2002; Gitelson *et al*., 2005), while absorption in the near infrared (751-1300nm) and shortwave infrared (1301 - 2400nm) are driven by internal and external leaf structure, including water (Tucker, 1980), phenolics (Kokaly and Skidmore, 2009) and other organic constituents (Petisco *et al*., 2006; Asner *et al*., 2011a).

One challenge with the use of spectroscopy for traits prediction, is that some traits do not have absorption features within the visible and shortwave infrared spectral range of spectrometers conventionally used for vegetation analyses, but can be estimated indirectly through their covariance with traits that do have absorption features in the visible-to-shortwave-infrared region ("constellation effects" *sensu* Chadwick and Asner, 2016). These traits include elemental concentrations and stable isotopes (e.g. Serbin *et al*., 2014). In addition, structural

differences (i.e. leaf thickness, number of air water interfaces, cuticle thickness and pubescence) between leaves may have significant effects on the relationship between leaf reflectance and traits, and can complicate interpretation of data (Sims and Gamon, 2002; Wu *et al*., 2016). It is therefore key to gaining a critical understanding of the ability of spectroscopy to measure intraspecific variation in multiples traits in response to environmental change, particularly when some of those traits are indirectly determined through "constellation effects".

Nevertheless, it is poorly understood how climatic variation will affect leaf spectral properties; for example, it remains controversial whether a "green-up" phenomena in the Amazon during dry seasons is an artefact of optical sensors geometry (Morton *et al*., 2014) or whether leaves are actually investing in a photosynthetically apparatus and investing in greater leaf area (Saleska *et al*., 2005; Huete *et al*., 2006). From our knowledge, no study has repeatedly measured spectral properties of leaves to investigate the impact of extreme climate events on leaf spectra and traits.

1.4.2 LiDAR for aboveground carbon and canopy structure dynamics

Information about vegetation structure, from the leaf to the entire stand, is an essential component for assessing ecosystem functioning, and LiDAR instruments are contributing to the three-dimensional structural information (Lefsky *et al*., 2002). LiDAR uses internal energy sources to emit laser pulses in the near-infrared region (for terrestrial ecology applications) and precisely measures the time for the reflected signal (the pulse) to return to the detector, thus locating the position of the scattering object in space with high precision (Lefsky *et al*., 2002). LiDAR then can emit and measure sufficient numbers of pulses to characterize the plant canopy surface and the ground (topographic) surface.

Airborne LiDAR overcomes difficulties in scaling up estimates of forest structure made on trees or plots to larger scales by generating high resolution 3D maps of forest canopies (Marvin *et al*., 2014). LiDAR is able to resolve fine-scale heterogeneity in forest structural attributes within landscapes (Marvin *et al*., 2014; Asner *et al*., 2010; Coomes *et al*., 2017; Asner *et al*., 2018). Top-of-the-canopy height (TCH) measured by LiDAR is a useful metric for estimating forest structure and is relatively insensitive to sensor and flight specifications (Asner and Mascaro, 2014). Individual-tree-based approaches also make greater use of the three-dimensional information to quantify the architecture of single trees, but it is

challenging to identify all trees in a stand, owing to the complex nature of forests (Féret and Asner, 2013).

The use of LiDAR to map aboveground biomass of tropical plantations and neighbour forests is crucial for optimization of forest management and land-use planning (Carlson *et al*., 2012). Oil palm trees have been counted using airborne imaging spectrometry (Shafri *et al*., 2011) and their biomass estimated from satellite images (Thenkabail *et al*., 2004; Koh *et al*., 2011; Morel *et al*., 2011; Carlson *et al*., 2012), but nobody has yet developed equations and tested approaches to estimate carbon density in oil palm plantations from airborne LiDAR data. The development of carbon prediction models provides opportunities to assess the aboveground carbon density of oil palm plantations, which is essential for assessments of the environmental sustainability of human modified tropical landscapes (Carlson *et al*., 2012).

Repeat-survey LiDAR can be a powerful technique for monitoring forest dynamics over large spatial scales and tease apart the environmental effects on forest dynamics, (Zhao *et al*., 2018). Some studies have interpreted change in terms of mortality and growth (Kellner *et al*., 2009; Dubaya *et al*., 2010; Meyer *et al*., 2013; Englhart *et al*., 2013, Andersen *et al*., 2014; Réjou-Méchain *et al*., 2015), however repeat-LiDAR surveys can also detect leaf shedding and budburst through the effects on canopy height estimated from the point clouds (Wasser *et al*., 2013; Simonson *et al*., 2018). Repeat surveys then lead to a better understanding of the processes governing canopy turnover and the associated carbon fluxes associated with environmental change such as El Niño-induced droughts (Leitold *et al*., 2018).

1.5 Thesis aims

Working primarily in the forests of Sabah, this thesis uses field and remotely sensed data to address three broad questions:

1) How well can the traits of tropical forest trees be predicted remotely (**Chapters 3, 4, 5**)?

2) Did the 2015/2016 El Niño event affect leaf traits of old-growth tropical forests (**Chapter 3**)?
3) What are the environmental controls on canopy structure of tropical forests during El Niño (**Chapter 5**)?

Before approaching these questions, in **Chapter 2** I critically assess the ability of field spectroscopy to estimate intra-specific variation in leaf traits by comparing the traits of trees of the same species growing on contrasting soil types in temperate forests of the UK. I describe how the variation in foliar traits affect different regions of the spectra. In **Chapter 3**, I investigate trait variation in tropical forests that comprise a considerably larger number of species. I explore the effects of El Niño events on leaf traits including spectral reflectance. Expanding my work from the community to the landscape level, in **Chapter 4** I test different approaches to predict aboveground carbon of oil palm plantations from airborne LiDAR data. Having developed a reliable approach, we then explore the use of repeat LiDAR surveys in **Chapter 5** to explore the impacts of El Niño events on aboveground carbon of oil palm plantations and canopy structure of tropical forests. In particular, I ask whether fragmentation, logging and topographic variation modulate forest responses to El Niño, and investigate whether microclimate play a significant role in these responses. Finally, in **Chapter 6**, I discuss my findings, and consider the implications and limitations of my research.

Chapter 2 | On the challenges of using field spectroscopy to measure the impact of soil type on leaf traits

2.1 Summary

Understanding the causes of variation in plant functional traits is a central issue in ecology, particularly in the context of global change. Spectroscopy is increasingly used for rapid and non-destructive estimation of foliar traits, but few studies have evaluated its accuracy when assessing phenotypic variation in multiple traits. Working with 24 chemical and physical leaf traits of six European tree species growing on strongly contrasting soil types (i.e. deep alluvium versus nearby shallow chalk), we asked (i) whether variability in leaf traits is greater between tree species or soil type; and (ii) whether field spectroscopy is effective at predicting intraspecific variation in leaf traits as well as interspecific differences. Analysis of variance showed that inter-specific differences in traits were generally much stronger than intraspecific differences related to soil type, accounting for 25% versus 5% of total trait variation, respectively. Structural traits, phenolic defences and pigments were barely affected by soil type. In contrast, foliar concentrations of rock-derived nutrients did vary: P and K concentration were lower on chalk than alluvial soils, while Ca, Mg, B, Mn and Zn concentrations were all higher, consistent with the findings of previous ecological studies. Foliar traits were predicted from 400-2500 nm reflectance spectra collected by field spectroscopy using partial least square regression, a method that is commonly employed in chemometrics. Pigments were best modelled using reflectance data from the visible region (400 - 700 nm), whilst all other traits were best modelled using reflectance data from the shortwave infrared region (1100 - 2500 nm) region. Spectroscopy delivered accurate predictions of species-level variation in traits. However, it was ineffective at detecting intraspecific variation in rock-derived nutrients (with the notable exception of P). The explanation for this failure is that rock-derived elements do not have absorption features in the 400-2500 nm region, and their estimation is indirect, relying on elemental concentrations co-varying with structural traits that do have absorption features in that spectral region ("constellation effects"). Since the structural traits did not vary with soil type, it was impossible for our regression models to predict intraspecific variation in rock-derived nutrients via constellation effects. This study demonstrates the value of spectroscopy for rapid, non-

destructive estimation of foliar traits across species, but highlights problems with predicting intraspecific variation indirectly. We discuss the implications of these findings for mapping functional traits by airborne imaging spectroscopy.

2.2 Introduction

There is currently great interest in using plant traits to understand the influences of environmental filtering and species identity on the functioning of plant communities, and to model community responses to environmental change (MacGillivray *et al*., 1995; McGill *et al*., 2006; Green *et al*., 2008; Funk *et al*., 2016). Traits vary at multiple scales within individuals, within populations, between populations and between species (Albert *et al*., 2011), and analysis of this variation is key to evaluating the strength of various filtering processes on communities growing along environmental gradients (Davey *et al*., 2009; Violle *et al*., 2012). For example, intraspecific variation in traits may reflect differences in microclimate driven by competition, disturbance, environmental conditions and age (Funk *et al*., 2016), whereas inter-specific and inter-site variation may reflect both genetic variation and phenotypic plasticity in response to environment (Davey *et al*., 2009; Sultan, 2001; Donohue *et al*., 2005). Despite substantial advances in trait-based community ecology over the past decade (Kunin *et al*., 2009; Funk *et al*., 2016), the importance of environmental filters is still debated, especially at small scales where biotic factors may prevail over abiotic environmental constraints (Vellend, 2010). Global analyses of leaf nitrogen, phosphorus and leaf mass per unit areas (LMA) indicate that about half of all variation occurs within communities (Wright *et al*., 2004), underscoring the importance of community-level variation in traits.

An increasing number of leaf traits are measured routinely in plant communities and global tradeoffs among these traits are often interpreted in terms of life history of different species (Adler *et al*., 2014; Pillar *et al*., 2003; Aubin *et al*., 2009; Fry *et al*., 2014). In this study we measured 24 traits which we organise into three functional groups (Asner, 2014, Asner *et al*., 2014b; Asner *et al*., 2015): (i) *light capture and growth traits* include pigments, the maximum efficiency of photosystem II (PSII), nitrogen concentration which is closely related to protein concentration (Milton and Dintzis, 1981), soluble C compounds and leaf water content, C isotope discrimination ($\delta^{13}C$), N isotope discrimination ($\delta^{15}N$); (ii) *defence and structural traits* include silicon (Si) organic cell wall constituents (cellulose, hemicellulose and lignin), that are associated with leaf toughness, longevity and defence capability (Hikosaka, 2004),

polyphenols that are associated with defence against herbivores (Mithöfer and Boland, 2012), and LMA, a primary axis of specialization among plants (Grime *et al*., 1997; Lambers and Poorter, 1992), that plays a crucial role in herbivore defence as well as leaf longevity (Wright *et al*., 2004); finally, (iii) *rock-derived nutrients* include phosphorus (P), which is involved in many enzymatic, genetic and epigenetic processes (Schachtman *et al*., 1998), and calcium (Ca), magnesium (Mg), potassium (K), zinc (Zn), manganese (Mn), boron (B) and iron (Fe), which are involved in signalling pathways and/or cofactors of enzymes (Marschner, 2012). We recognise that leaf traits can contribute to more than one class (e.g. LMA is related to growth but also to defence, P is a rock-derived nutrient also associated with growth). Many analyses of traits have focussed on interspecific variation, but there is recognition that intraspecific variation can strongly influence species and community responses to environmental change (e.g. Weiner, 2004; Funk *et al*., 2016).

There is currently great interest in using hyper-spectroscopy as a tool for studying the chemical and structural traits of leaves, particularly because improved airborne sensors and faster computing make it possible to map functional traits from the air (Ustin *et al*., 2009; Asner and Martin 2016b; Jetz *et al*., 2016; Asner *et al*., 2017). Plans to put hyperspectral sensors into space (e.g. DRL plan to launch EnMAP in 2018; Guanter *et al*., 2015) will soon enable spectral response curves of vegetation communities to be assessed at the global scale. Rapid, non-destructive determination of leaf traits *in vivo* and *in situ* using spectroscopy reduces the need to collect large amounts of material in the field, decreases processing time, lessens costly chemical analyses, and eliminates sampling that could itself alter experimental conditions (Couture *et al*., 2013). Spectroscopy can provide predictions of a range of foliar traits at the leaf and canopy scales within diverse tropical ecosystems (Asner *et al*., 2011a; Doughty *et al*., 2011) and temperate forests (Wessman *et al*., 1988; Serbin *et al*., 2014). However, some traits do not have absorption features within the visible and shortwave infrared spectral range of spectrometers conventionally used for vegetation analyses, but can be estimated indirectly through their covariance with traits that do have absorption features in the visible-to-shortwave-infrared region ("constellation effects" *sensu* Dana Chadwick and Asner, 2016). These traits include elemental concentrations and isotope ratios (e.g. Serbin *et al*., 2014). In addition, structural differences (i.e., leaf thickness, number of air water interfaces, cuticle thickness, and pubescence) between leaves may have significant effects on the relationship between leaf reflectance and traits, and can complicate interpretation of data (Sims and Gamon,

2002; Wu *et al*., 2016). The ability of spectroscopy to measure intraspecific variation in multiples traits between soil types, particularly when some of those traits are indirectly determined through constellation effects, has not been critically evaluated.

This paper examines the drivers of leaf trait variation in temperate woodlands growing on chalk in southern England compared with woodlands growing on nearby alluvial soils. Several studies have evaluated change in species composition among British semi-natural habitats that differ markedly in soil type (Haines-Young *et al*., 2003; Smart *et al*., 2003), but none to our knowledge have compared within- versus between-species variation of leaf traits in this context. The alkalinity of calcareous soils gives rise to phosphorus limitation, preventing short-term responses to nitrogen addition (Grime *et al*., 2000), so comparisons of chalklands with less-alkaline soils nearby provide strong edaphic contrast. We investigated 24 leaf traits on these contrasting soil types and examined the ability of reflectance spectroscopy to quantify these leaf chemical and structural traits. We place these traits into groups based on ordination analyses, rather than working with pre-defined functional groups, and evaluate the functional significance of these groups. Our specific questions were: (i) is variability in leaf traits greater between tree species or soil type? (ii) is field spectroscopy effective at predicting intraspecific variation in leaf traits between soil types, as well as interspecific differences?

2.3 Material and methods

2.3.1 Field site and sampling

Leaves were collected from trees growing on deep alluvial soils and shallow chalk soils, near Mickleham in Surrey, UK (latitude = 51°16'N, longitude = 0°19'W). The alluvial soil, along the banks of the river Mole, was a loam of several metres depth. The chalk soil was located on a steep south-facing escarpment into which the river was cutting; the top soil was a few centimetres deep, underlain by solid chalk (i.e. a typical rendzina soil). The chalk soils were alkaline with an average pH and standard deviation of 7.9 $\pm$ 1.0 (n = 10), whereas the alluvial was near neutral having a pH of 6.7 $\pm$ 0.2 (n = 10). Phosphorus becomes unavailable to plants in alkaline chalk soil (Gerke, 1992), and greater depth of loamy soil on the alluvial surfaces must result in much greater availability of nutrients to plants.

Across both sites, leaves were collected from 66 trees, representing six species. The six species common to both sites were: *Acer campestre* (field maple), *Acer pseudoplatanus* (sycamore), *Corylus avellana* (hazel), *Crataegus monogyna* (hawthorn), *Fraxinus excelsior* (ash) and *Sambucus nigra* (elder). Two fully sunlit branches were selected, cut and placed in a cool box, and subsequently transported to a laboratory for processing within two hours. For each branch, ten mature leaves were selected. Three samples of 15 leaf disks were cored from these leaves using a 6 mm corer, wrapped in aluminium foil and frozen in liquid N for later chemical analyses. Leaf area was measured from fixed-height photos against a white background analysed in *imageJ*. The scanned leaves were weighed to give hydrated mass, then dried at 70 °C for a minimum of 72 h to obtain dry mass. Leaf mass per area (LMA) was calculated as dry mass per unit of fresh leaf area. Leaf water content was computed as the ratio between the quantity of water (fresh weight – dry weight) and the fresh weight. A further 22 leaf chemical traits were measured on these samples (see below).

2.3.2 Chemical assays

Protocols for chemical assays are adapted from those developed by the Carnegie Airborne Observatory (see http://spectranomics.ciw.edu). Briefly, oven dried leaves were ground and analysed for a variety of elements and carbon fractions. Concentration of elements (B, Ca, K, Mg, Mn, P, Si, Fe, Zn) were determined by ashing samples in a muffle furnace followed by digesting them in nitric acid and analysis on an inductively-coupled plasma mass spectrometry (Perkin Elmer SCIEX, Elan DRCII, Shelton, CT, USA). Nitrogen and carbon concentrations were determined using a Thermo Finnigan 253 with elemental analyser using a gas chromatographic separation column linked to a continuous flow isotope ratio mass spectrometer. This technique also provided foliar concentrations of the stable isotopes of N and C. Carbon fractions, including hemicellulose, cellulose, lignin and soluble carbon (mainly carbohydrates, lipids, pectin and soluble proteins), were determined by sequential digestion of increasing acidity (Van Soest, 1994) in an Ankom fiber analyzer (Ankom Technology, Macedon, NY, USA). These carbon fractions are presented on an ash-free dry mass basis. Concentrations of photosynthetic pigments (chlorophyll *a*, *b*, anthocyanins and total carotenoids) were measured by spectroscopy of solution derived from frozen leaf disks on area basis. Absorbance values of the supernatant were measured at wavelengths 470 nm, 649 nm and 665 nm for chlorophyll *a*, *b* and total carotenoids determination and published equations used to calculate pigment concentrations as in Lichtenthaler (1987). Absorbance values were

also measured at wavelengths 530 nm and 650 nm for anthocyanins determination and published equations used as per Giusti *et al*. (1999), but corrected for possible chlorophyll contamination as per Sims and Gamon (2002). The maximum efficiency of photosystem II (PSII) was calculated according to Genty *et al*. (1989) by measuring the maximum fluorescence (F_m) and the yield of fluorescence in the absence of an actinic (photosynthetic) light (F_o) using a PAM fluorometer. Total phenolic concentration of the upper methanol/water layer was determined colorimetrically using the Folin-Ciocalteau method, based on absorbance at 760 nm on a spectrophotometer, and quantified using tannic acid equivalents with water serving as a blank as per Davey *et al*. (2007).

2.3.3 Leaf and canopy spectroscopy

The remaining leaves were detached from the branches, and 10 leaves selected at random, avoiding damaged and soft or young leaves. These leaves were laid on a matt black surface. Reflectance within bands ranging from 400–2500 nm was measured using a FieldSpec 4, produced by Analytical Spectral Devices (ASD, Boulder, Colorado, USA). The spectrometer's contact probe was mounted on a clamp and firmly pushed down onto the sample, so that no light escaped through the sides. The spectral measurements were taken at the mid-point between the main vein and the leaf edge, approximately half-way between the petiole and leaf tip, with the abaxial surface pointing towards the probe. The readings were calibrated against a Spectralon white reference every 5 samples. In all statistical analyses, the mean reflectance values of the 10 measurements per branch were used.

2.3.4 Statistical analyses

Analyses were performed within the R statistics framework (R Team, 2014). To evaluate the correlation among traits, Spearman rank correlation coefficient was calculated between all trait pairs and the variables were ordered in the figure by hierarchical clustering. Analyses of variance (ANOVA) were used to examine the influences of species identity and soil type on each of the 24 leaf traits. Species, soil and soil x species terms were included in the model, and the ratio of sum of squares of these terms versus the total sum of squares was used as an index of species- versus site-level variation. This partitioning of variance quantifies the variation between species, between soil types, the interaction between soil and species, and the unexplained variance (residual variance). The residual variance comprises analytical error and

various types of intraspecific variation including micro-site and within-canopy variation. Where necessary, variables were log transformed to meet assumptions of ANOVA (see Table 1 for details). In addition, permutation-based multivariate analysis of variance (PERMANOVA; Anderson 2001) was applied to the matrix of dissimilarity among traits to evaluate the importance of soil type, species identity and the interaction soil-species as a source of variation in the 24 traits simultaneously. The non-parametric permutation-based analysis of variance (PERMANOVA) was then performed on the resulting distances (10000 permutations). An alpha level of 0.05 was used for all significance tests, and no effort was made to test for or address non-normal data distributions. The PERMANOVA used distance matrices calculated using the *adonis* function in the *vegan* package of R.

Leaf traits were grouped using principal component analysis (PCA) using Simca-P (2016) software (Umetrics MKS Data Analytics Solutions, Sweden). The principal components for the variables were obtained by the correlation matrix modelling *in lieu* of covariance matrix modelling. We used the unit variance scaling (van den Berg *et al*., 2006) to avoid the effects of variables with high variance. The PCA was used to obtain score scatter and loadings plots to show the relatedness of all leaf traits in the dataset. R^2 and Q^2 overview plots were computed from the cumulated PCA axes 1-5. R^2 values denote how well a trait can be explained in the model and Q^2 denote how well a trait can be predicted from the dataset. The traits are ranked in descending R^2 order of how well they correlate with the other traits in the data set. These plots were used to evaluate whether traits clustered into functional groups.

Partial least squares regression (PLSR) was used to evaluate whether field spectroscopy can reliably predict leaf traits (Haaland and Thomas, 1988). The spectral reflectance values of each sample were transformed into pseudo-absorption values, that is log [1/ R]) where R is reflectance (see Bolster *et al*., 1996; Gillon *et al*., 1999; Richardson and Reeves III, 2005; Petisco *et al*., 2006; Kleinebecker *et al*., 2009). There is strong autocorrelation in pseudo-absorption values, so PLSR involves dimensionality reduction, producing orthogonal uncorrelated latent vectors containing the maximum explanatory power in relation to the trait data (Wold *et al*., 2001). The number of latent variables (nL) used in the PLSR analysis was predicted by minimising the Prediction Residual Error Sum of Squares (PRESS) statistic (Chen *et al*., 2004; Zhao *et al*., 2015). We adopted a leave-one-out cross-validation for each PLSR model. Model accuracy and precision were expressed by the coefficient of determination (R^2) and root mean square error (RMSE). We also standardised RMSE to the percentage of the

response range (RMSE%) by dividing each RMSE by the maximum and minimum values of each leaf trait, as in Feilhauer *et al*. (2010). RMSE and R^2 were acquired during both model calibration and after model validation. PLSR was conducted initially using all available wavelengths (i.e. 400-2500 nm), but we then evaluated whether models based on smaller regions of the spectrum performed any better (see Serbin *et al*., 2014), based on comparisons of RMSE. The smaller regions were selected from absorption features recognised in previous papers (Curran, 1989; Elvidge, 1990; Kokaly *et al*., 2009). The visible (VIS, 400-700 nm), near infra-red (NIR, 700-1500 nm) and shortwave infra-red I (SWIR I, 1500-1900 nm), shortwave infra-red II (SWIR II, 1900-2500 nm) regions, as well as combinations of the regions (700-1100 nm, 700-1900 nm, 700-2500 nm, 1100-1500 nm, 1100 -1900 nm, 1100-2500 nm, 1500-2500 nm and 400-2500 nm) were tested and the best-supported model selected based on minimisation of RMSE. To evaluate the effectiveness of field spectroscopy at measuring variation in traits related to soil type and species identity, we partitioned variance in model-predicted trait values using exactly the same approach as we used with lab-measured traits (i.e. first paragraph of methods).

2.4 Results

2.4.1 Soil and species controls on leaf traits

Foliar concentrations of rock-derived nutrients varied with soil type, but few other traits varied strongly with soil. Foliar concentrations of the macronutrients N, P and K were 17 %, 43 % and 24 % higher on alluvial compared to chalk soils (Table 2.1). Nitrogen isotope discrimination ($\delta^{15}N$) varied greatly between the two soils, from -3.8 ‰ in the chalk soil to 3.4 ‰ in the alluvial. Foliar concentrations of nutrients required in smaller quantities (Si, Ca, Mg, B, Mn and Zn) showed the opposite trend: they were higher in chalk soils (by 22%, 37%, 50%, 19%, 23% and 49%, respectively). In contrast, hemicellulose, cellulose, lignin and LMA were completely unaffected by soil type, and pigments and traits related to water status ($\delta^{13}C$ and water content) varied little with soil type, with the exception of carotenoids concentration, which was 25 % higher in alluvial soil. The efficiency of PSII showed only a slight increase of 4 % in alluvial soil. The percentage contribution of soluble C was affected by soil, with an increase in soluble C of 9 % in the alluvial soil.

Table 2.1 | Average, standard deviation (SD) and coefficient of variation (CV) in percentage for leaf traits of six generalist species growing on alluvial and chalk soils. Foliar trait was statistically different between soil types with *P*-value < 0.05 *, < 0.01 ** and < 0.001 ***. Note that water content and the concentrations of defence and structure compounds are invariant of soil type, as this is key to understanding why variation in elemental concentrations between soil types cannot be predicted indirectly by "constellation effects".

Leaf trait	Alluvial		Chalk	
	Mean ± SD	%CV	Mean ± SD	%CV
Light capture and growth				
N (%) ***	2.53 ± 0.81	32.1	2.16 ± 0.73	34.0
$\delta^{15}N$ (‰) ***	3.43 ± 2.65	77.3	-3.83 ± 2.01	52.3
$\delta^{13}C$ (‰)	-28.2 ± 1.2	4.5	-28.7± 1.0	3.6
$^{+}$Chlorophyll a (mg m^{-2})	338.8 ± 116.0	34.2	279.6 ± 89.2	31.9
Chlorophyll b (mg m^{-2})	78.6 ± 27.6	35.1	64.7 ± 22.4	34.7
Anthocyanins (mg m^{-2})	423.3 ± 143.8	33.9	362.8 ± 121.6	33.5
Carotenoids (mg m^{-2}) *	110.5 ± 40.4	36.5	88.2± 35.5	40.2
Efficiency of PSII **	0.74 ± 0.05	7.1	0.71 ± 0.06	9.8
Soluble C (%) **	73.6 ± 6.5	8.8	70.3 ± 7.5	10.6
Leaf water content (%)	59.1 ± 8.2	14.0	58.5 ± 7.9	13.5
Defence and structure				
$^{+}$LMA (g cm^{-2})	60.8 ± 24.0	39.4	60.6 ± 23.6	38.9
Phenolics (%)	83.7 ± 64.1	76.5	84.3 ± 49.7	59.0
$^{+}$Hemicellulose (%)	10.9 ± 3.2	29.8	12.5 ± 3.6	29.4
Cellulose (%)	10.1 ± 1.8	18.6	11.0 ± 2.1	19.3
Lignin (%)	3.9 ± 1.9	49.8	4.7 ± 3.1	64.8
$^{+}$Si (%) *	0.91 ± 0.56	62.2	1.11 ± 0.79	71.5
Rock-derived nutrients				
$^{+}$P (%) ***	0.20 ± 0.05	25.5	0.14 ± 0.03	26.8
K (%) ***	0.98 ± 0.49	50.0	0.79 ± 0.50	64.4
$^{+}$Ca (%) *	1.67 ± 0.75	45.1	2.29 ± 1.24	54.1
$^{+}$Mg (%) ***	0.24 ± 0.11	47.1	0.36 ± 0.15	43.8
$^{+}$B (µg g^{-1}) ***	29.0 ± 8.7	30.1	34.5 ± 12.4	36.0

$^{+}$Fe (μg g^{-1})	122.3 ± 24.6	20.1	125.4 ± 32.0	25.5
$^{+}$Mn (μg g^{-1}) *	84.7 ± 64.3	75.9	103.8 ± 69.5	66.9
$^{+}$Zn (μg g^{-1}) ***	22.9 ± 12.6	55.0	34.1 ± 18.7	54.9

+log transformed prior to ANOVA.

Most traits varied greatly between species and that variation was far greater than the soil effects (Fig. 2.1). Interspecific variation (green bars, Fig. 2.1) accounted for $\geq$ 60% of the variation of eight traits (in descending order Si, water content, B, soluble C, N, LMA, K and cellulose concentrations), and $\geq$ 40% of the variation of another six traits (in descending order, lignin, hemicellulose, Mg, Zn, phenolics and Fe). Species identity exerted little or no influence on pigment concentrations, efficiency of PSII, $\delta^{13}C$, $\delta^{15}N$, P, Ca or Mn concentrations. The interactions between species and soil (blue bars, Fig. 2.1) explained little variation and were significant for $\delta^{15}N$, P, Mn and Zn, but for no other traits. The pigments, efficiency of PSII and $\delta^{13}C$ had the largest unexplained variance. PERMANOVA analyses showed that, overall, species identity accounted for 25% of the variation in leaf traits, soil type accounted for 5%, while the interaction between species and soil accounted for virtually no variation (i.e. the traits of different species responded similarly to soil type).

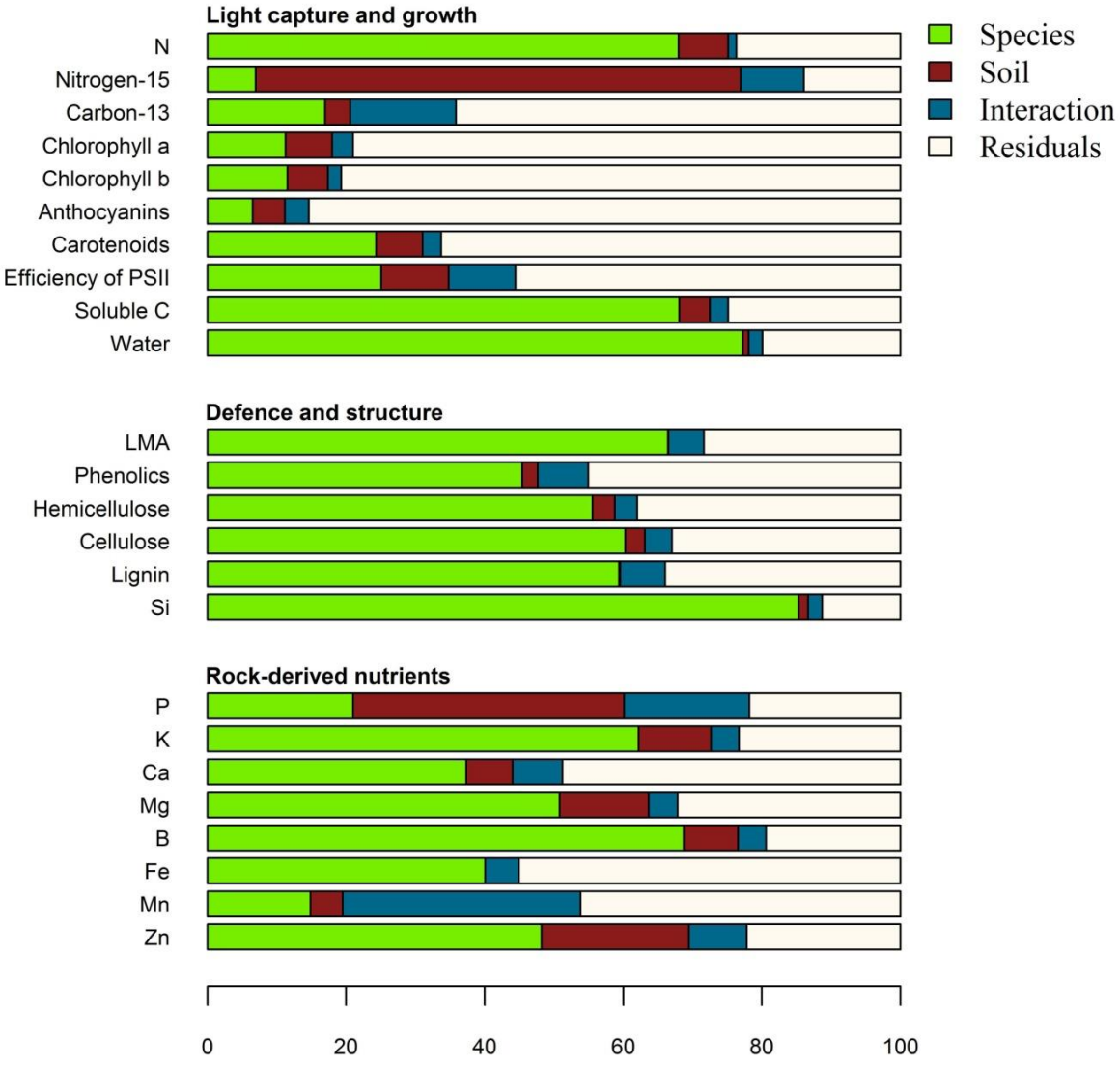

Figure 2.1 | Partitioning of variance of foliar traits between species, soil, species-soil interaction and residual components for six generalist species found on both chalk and alluvial soils. Residual variation arises from within-site intraspecific variation, micro-site variability, canopy selection and measurement error variance.

The Principal Component Analysis (PCA) was able to distinguish species across component 1 and 2 (Fig. 2.2A), with less separation of species within the same genus (i.e. *A. campestre* and *A. pseudoplatanus*). The first two components of PCA explain 45% of the total variance. Separation of individuals between the soil types was weak. Growth vs structural/defence traits were separated in its first axis and area-based vs concentration-based traits in its second axis. The first two components of PCA explain 46% of the total variance. Considering only traits that were well-predicted by PCA (i.e. had $Q^2 > 0.5$), the first component distinguishes the traits

associated in growth (i.e. N, K and soluble carbon concentrations, and water content) from traits associated with leaf defence and structure (i.e. hemicellulose and Si). The second component is chlorophyll *a*, chlorophyll *b*, carotenoids, anthocyanins and LMA, and mainly separates the traits that were calculated on area basis. The first component distinguishes species relatively well, with less separation of species within the same genus (i.e. A. *campestre* and A. *pseudoplatanus*).

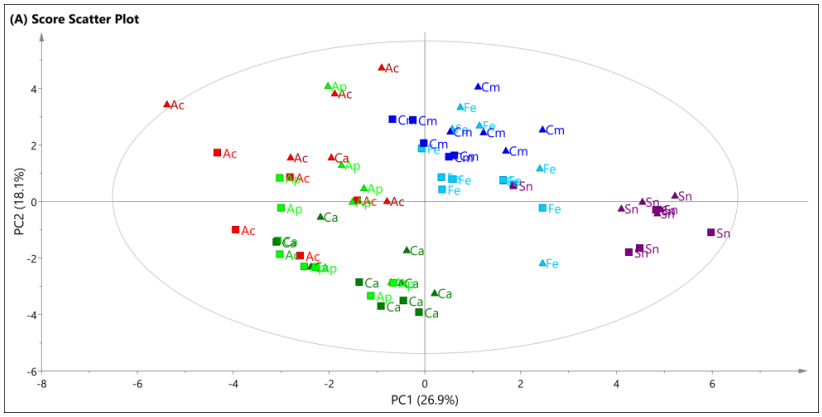

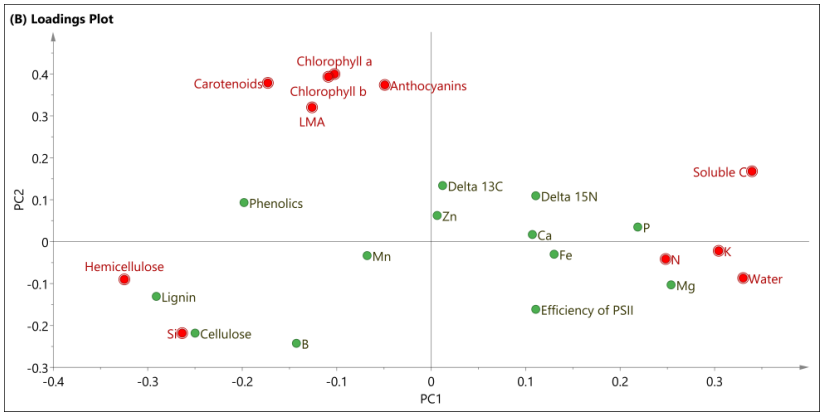

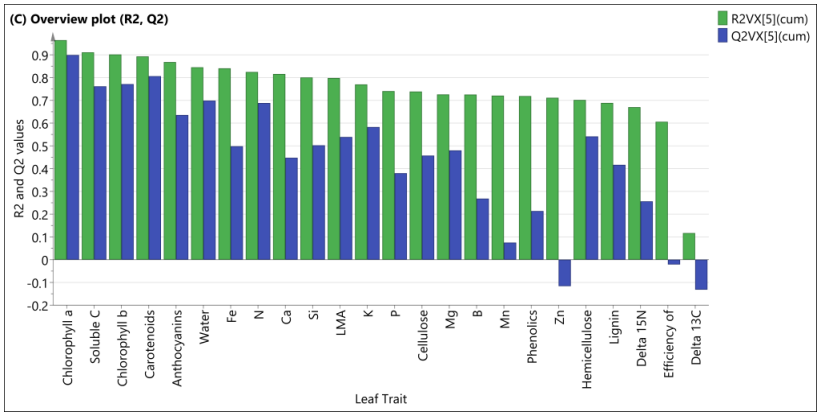

Figure 2.2 | Principal component analysis of all leaf traits (unit variance scaled) measured across all species and sites. (A) Score scatter plot showing first and second principal components using all six species for which data exist for all 24 traits on two contrasting soil types. Colours represent species identity: Fe = *Fraxinus excelsior*; Sn = *Sambucus nigra*; Ac = *Acer campestre*; Cm = *Crataegus monogyna*; Ca = *Corylus avellana*; Ap = *Acer pseudoplatanus*. Samples from chalk sites are denoted by squares symbols and alluvium sites are denoted by triangles. (B) Loadings plot showing position and correlation of all leaf traits. Traits highlighted in red denote are those with $Q^2 > 0.5$; (C) cumulated R^2 of PCA axes 1-5 (Green bars denote how well a trait can be explained in the model) and Q^2 (Blue bars denote how well a trait can be predicted) values for each trait. The traits are in descending R^2 order of how well they correlate with the other traits in the data set.

2.4.2 Spectroscopy of leaf traits

The ability to predict leaf traits from hyperspectral reflectance spectra varied greatly among the 24 traits (Table 2.2). The R^2 values of validation data varied from 0.92 to 0.16, with traits ranked by goodness of fit as follows (highest first): LMA, leaf water content, Si, phenolics, carotenoids, K, B, efficiency of PSII, N, chlorophyll *a* and chlorophyll *b*. Some minerals, such as P, Zn and Mn, as well as $\delta^{13}C$ and $\delta^{15}N$ showed low R^2. There was virtually no difference in the average reflectance curves of leaves of trees growing on chalk and alluvial soils (Fig. 2.3a), but the coefficient of variation among plants was greater on the chalk soil (Fig. 2.3b). Pigments were most accurately modelled using reflectance data from the visible region of the spectra, whilst other traits were most accurately modelled using spectral data in the 1100 - 2500 nm range (Fig. 2.3). Efficiency of PSII and Fe were the only foliar traits for which the strength of relationship was greatest when all wavelengths between 400 and 2500 nm were used in the model.

Table 2.2 | Partial Least Squares Regression (PLSR) on spectral data and leave-one-out cross-validation for 24 leaf traits of 6 species occurring on both alluvial and chalk soils. The model calibration (indicated with subscript cal) and validation (indicated as subscript val) performance was evaluated for each leaf trait by calculating the coefficient of determination (R^2), root mean square error (RMSE) and the percentage root mean square error (%) based on the given number of latent variables (nL) for each PLS model.

Leaf trait	Spectral range (nm)	nL	R2		RMSE		RMSE%	
			Cal	Val	Cal	Val	Cal	Val
Light capture and growth								
N (%)	1100 – 2500	3	0.61	0.55	0.49	0.52	15.0	16.0
$\delta^{15}N$ (‰)	1100 – 2500	9	0.41	0.16	3.28	4.01	23.5	28.7
$\delta^{13}C$ (‰)	1100 – 2500	6	0.46	0.30	0.85	0.96	16.1	18.2
$^{+}$Chlorophyll *a* (mg m^{-2})	400 – 700	7	0.65	0.53	60.05	69.62	13.5	15.7
Chlorophyll *b* (mg m^{-2})	400 – 700	4	0.59	0.50	16.48	18.57	15.2	17.1
Anthocyanins (mg m^{-2})	400 – 700	4	0.45	0.33	99.20	110.70	18.0	20.1
Carotenoids (mg m^{-2})	400 – 700	7	0.75	0.62	19.31	23.54	11.0	13.4
Efficiency of PSII	400 – 2500	6	0.68	0.55	0.03	0.04	13.4	15.9
Soluble C (%)	1100 – 2500	4	0.54	0.46	4.76	5.15	18.1	19.6
Leaf water content (%)	1100 – 1500	5	0.87	0.83	2.89	3.29	9.0	10.1
Defence and structure								
$^{+}$LMA (g cm^{-2})	1100 – 2500	6	0.94	0.92	1.09	1.12	6.1	6.9
Phenolics (%)	1500 – 1900	6	0.78	0.70	26.20	30.48	9.7	11.3
$^{+}$Hemicellulose (%)	1100 – 2500	4	0.44	0.35	1.28	1.30	18.4	19.8
Cellulose (%)	1100 – 2500	4	0.44	0.34	1.52	1.66	17.0	18.6
Lignin (%)	1100 – 2500	4	0.57	0.47	1.72	1.89	13.0	14.2
$^{+}$Si (%)	1100 – 2500	4	0.77	0.72	1.50	1.55	14.4	15.5
Rock-derived nutrients								
$^{+}$P (%)	1500-2500	7	0.43	0.22	1.26	1.30	17.8	20.2
K (%)	1500 – 2500	7	0.70	0.61	0.27	0.31	11.9	13.6
$^{+}$Ca (%)	1500-2500	7	0.53	0.40	1.40	1.47	15.9	17.9
$^{+}$Mg (%)	1900 – 2500	3	0.54	0.46	1.39	1.42	15.2	16.5
$^{+}$B (μg g^{-1})	1500-1900	6	0.66	0.56	1.24	1.28	13.6	15.2
$^{+}$Fe (μg g^{-1})	700 – 2500	5	0.56	0.46	1.17	1.19	15.6	17.2

$^{+}$Mn (μg g^{-1})	1500-1900	6	0.35	0.20	1.83	1.95	20.5	22.7
$^{+}$Zn (μg g^{-1})	1500-1900	7	0.41	0.21	1.50	1.60	19.5	22.4

$^{+}$ Trait values were natural log-transformed for PLSR.

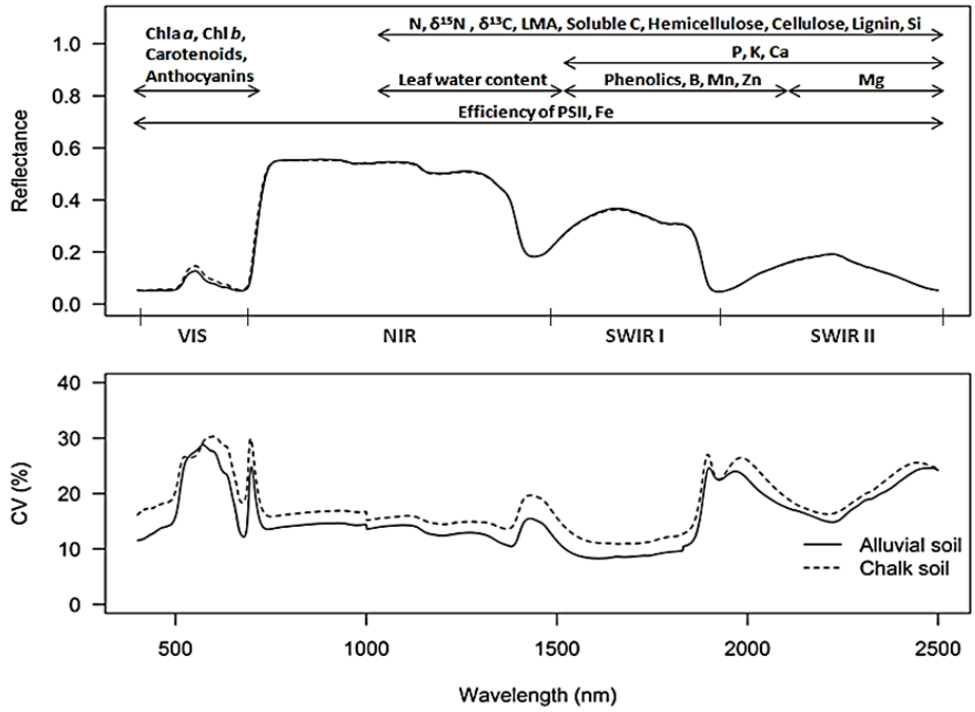

Figure 2.3 | Spectral reflectance and percentage coefficient of variation (CV) of reflectance of six generalist species for alluvial and chalk soils. The spectral regions for each trait were selected based on the model that minimised RMSE.

Some leaf traits which appeared to be predicted accurately by PLSR do not have absorbance features in the 400-2500 nm range, and were instead predicted because of their close association with leaf traits that do have absorbance features in that range (see correlations in Fig. A.1).

For instance, Si and B do not have absorption features in the 400-2500 nm range, but their concentrations are highly correlated to hemicellulose, cellulose and lignin concentrations, and these organic polymers do have strong absorbance features in the SWIR region. Likewise, K do not have absorption features in the 400-2500 nm range, but K concentration is highly

correlated to leaf water content, soluble carbon, lignin, hemicellulose and cellulose, all of which have absorbance features in the region. The importance of these "constellation effects" (*sensu* Chadwick and Asner 2016) becomes apparent when we examine the partitioning of variance of PLSR-predicted trait values: several rock-derived nutrients vary significantly with soil type when measured in leaves but little of that variation is successfully modelled by PLSR (Fig. 2.5). The explanation for this failure to model soil-related variation correctly is that concentrations of their associated traits remain invariant of soil type. The use of PLSR also considerably under-predicted the importance of soil (~ 37 %) on the $\delta^{15}N$ variation, presumably for similar reasons. Some species-soil interaction effects were detected by PLSR modelling, except for traits that showed strong interaction (Mn, P and $\delta^{13}C$). PLSR models were better able to detect intra-specific variation in foliar N concentrations, because much of the nitrogen is contained in proteins, which have strong absorbance features.

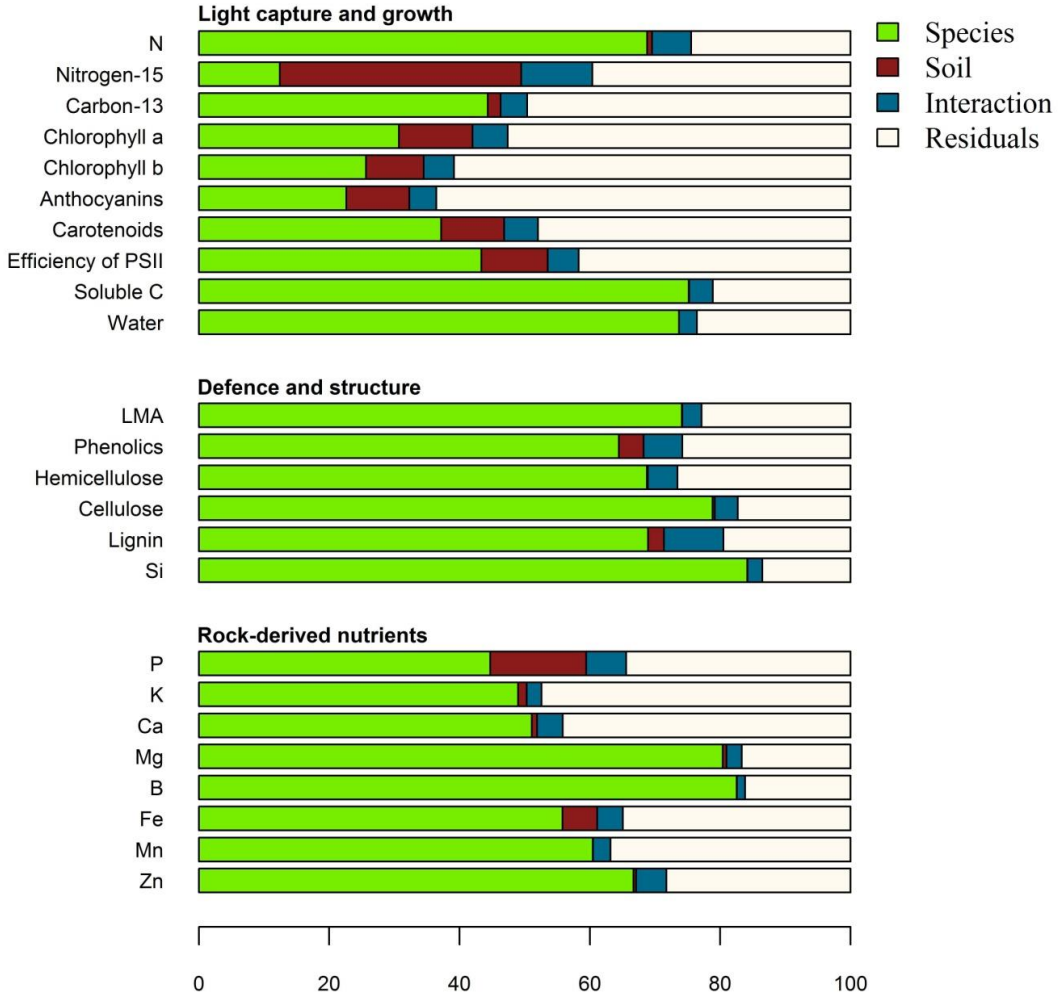

Figure 2.4 | Partitioning of variance of foliar traits between species, soil, species-soil interaction and residual components for six generalist species found on both chalk and alluvial soils from predicted data. Residual variation arises from within-site intraspecific variation, micro-site variability, canopy selection but not measurement error variance, and is therefore smaller than for field measurements (Fig. 2.1). Predicted data were obtained from partial least square regression (PLSR).

2.5 Discussion

2.5.1 Patterns of variation in leaf traits

Compared with trees growing on deep alluvium, trees on thin chalk soils had low concentrations of N, P and K macronutrients in their leaves, but high concentrations of several micronutrients. Similar findings have been reported for herbaceous species growing on chalk (Hillier *et al*., 1990). Phosphorus and several micronutrients form low-solubility compounds in alkaline soils and become less available for plant uptake (Marschner, 1995; Misra and Tyler, 2000; Tyler, 2002; Sardans and Peñuelas, 2004), while the low N concentrations may reflect stoichiometric constraints (Niklas *et al*., 2005). The lower efficiency of PSII in the chalk soil is likely to be a consequence of phosphorus deficiency (Santos *et al*., 2006). Importantly for our later discussion on indirect estimation of traits by spectroscopy, species did not vary between soil types in their structural and defensive traits (i.e. LMA, lignin, phenolics) despite these differences in rock-derived nutrients. A similar lack of intraspecific change has been found in New Zealand rainforest trees growing on alluvium versus phosphorus-depleted marine terraces (Wright *et al*., 2010) and in several other studies (Koricheva *et al*., 1998; Boege and Dirzo, 2004; Fine *et al*., 2006).

Species had a greater influence on trait values than soils for all traits except P, and PCA analyses demonstrated that species with traits associated with fast growth had low concentration of traits associated with defence and structure (see Coley, 1983; 1987; Fine *et al*., 2006). Traits favouring high photosynthetic rate and growth are usually considered advantageous in rich-resource soil environments, while traits favouring resource conservation are considered advantageous in low-resource environments (Aerts and Chapin, 1999; Westoby

et al., 2002), but in this study the species were generalists growing on both soil types. The traits most influenced by species (in descending order) were Si, leaf water content, B, soluble C, N, LMA, K, cellulose, lignin, hemicellulose, magnesium, Zn, phenolics and Fe. It is interesting to note that two trace elements were near the top of this list; it is likely that strong differences in B and Si concentrations between species reflect differences in ion channel activity in roots (Ma and Yamaji, 2006). Previous studies have also shown Si to be under strong phylogenetic control, and to be little affected by environmental conditions (Hodson *et al*., 2005). We also found Si and B concentrations to be positively correlated, which might ameliorate the effects on B toxicity as Si can increase B tolerance of plants (Gunes *et al*., 2007). High Zn organization at the species level corroborates earlier analyses that showed more than 70% of Zn variation occured within family and substantial differences existed between and within species (Broadley *et al*., 2007).

The patterns revealed by our variance partitioning analysis of six temperate species (Fig. 2.1) bear similarities to those emerging from an analysis of 3246 species from nine tropical regions (Fig. 5 of Asner and Martin, 2016a). The tropical analyses included a "site" term which captured variation due to soil and geology, among other factors. They, like us, found that taxonomic identity explained far more variation than site for most traits. Additionally they found foliar concentrations of P and other rock-derived minerals varied strongly with site, while nitrogen concentrations varied little; found that soluble carbon, structural and defensive traits hardly varied between sites; and observed that pigments (in their case just chlorophyll) was the least predictable of traits, probably because photosynthesis is rapidly up- and down-regulated in response to light environment among other factors (Asner and Martin, 2011). Similarly, $\delta^{13}C$ is known to vary strongly with light condition and with relative humidity (Buchmann *et al*., 1997; Yan *et al*., 2012) which may explain why species and soil explained little of its variance in our study. These parallels between tropical and temperate systems suggest broad similarities in plant responses to soil across different regions that differ greatly in temperature.

2.5.2 Measuring interspecific variation in leaf traits with field spectroscopy

The spectral regions selected by our PLSR models match the locations of known spectral absorption features related to proteins, starch, lignin, cellulose, hemicellulose and leaf water content (Knipling, 1970; Curran, 1989; Elvidge, 1990; Fourty and Baret, 1998; Kokaly *et al*.,

2009). In the region between 700 and 2500 of the electromagnetic spectrum, absorption features are commonly the result of overtones and combinations of fundamental absorptions at longer wavelengths. The visible region was useful to predict pigments concentrations and contributed to the predictions of the efficiency of PSII and Fe only, whereas the infra-red region was associated with most traits. The region of importance with correlated wavelengths with nitrogen varies between 1192 nm in deciduous forest (Bolster *et al*., 1996) to 2490 for forage matter (Marten *et al*., 1983), which results directly from nitrogen in the molecular structure. According to Kumar *et al*. (2002), three main protein absorption features reported as important for N estimation are located around 1680 nm, 2050 nm and 2170 nm. In this study, pigments were found to influence the visible region of the spectrum while PSII-efficiency was predicted from features across the VSWIR range. The spectra of chlorophylls are distinct from those of proteins because C-H bonds in their phytols tails create a strong absorption feature not found in proteins (Katz *et al*., 1966). However, pigments are tightly bound by proteins to form photosynthetic antenna complexes that capture light energy and transfer it to the PSI and PSII reaction centres (Liu *et al*., 2004). The vibration of the bonds in the pigment–protein complex adds additional absorption features to the spectra of pigments and may help explain why so many bands were involved in PSII-efficiency prediction (Porcar-Castell *et al*., 2014). The 1500-1900 nm region was important for phenolic compounds prediction, which includes the 1660 nm feature across a variety of species and phenolic compounds (Windham *et al*., 1988; Kokaly and Skidmore, 2015). The primary and secondary effects of water content on leaf reflectance are greatest in spectral bands centred at 1450, 1940, and 2500 nm (Carter and Porter ,1991), but has also been predicted using bands between 1100-1230 nm absorption features (Ustin *et al*., 1998; Asner *et al*., 2004). With respect to the other rock-derived nutrients, Galvez-Sola *et al*. (2015) also showed that near-infrared spectroscopy can constitute a feasible technique to quantify several macro and micronutrients such as N, K, Ca, Mg, Fe and Zn in citrus leaves of different leaves with coefficient of determination (R^2) varying between 0.53 for Mn and 0.98 for Ca, whereas B showed less accurate results with the use of spectroscopy. The regions of importance for prediction described in those studies were relatively similar to all the mineral nutrients analysed in our study, except for B that had the band between 1500 and 1900 as the best predictive region.

Some of most accurately predicted traits have no absorption features in the visible-to-near-infrared, but were instead estimated indirectly via constellation effects. Leaf mass per unit area

(LMA) is consistently among the more accurately predicted traits using spectroscopy (Asner and Martin, 2008; Serbin *et al*., 2014; Chavana-Bryant *et al*., 2016), but is measured indirectly via its close coupling with water content and leaf structural traits (Asner *et al*., 2011). Silicon (Si) concentrations were well-predicted by field spectroscopy, as recently reported by Smis *et al*. (2014). Silicon is absorbed by plants from the soil solution in the form of silicic acid (H_4SiO_4), being translocated to the aerial parts through xylem, and then deposited as phytoliths (Tripathi *et al*., 2011). Si is closely associated with phenol- or lignin-carbohydrate complexes (Inanaga *et al*., 1995), cellulose (Law and Exley, 2011), and polysaccharide and peptidoglycans (Schwarz, 1973). It seems that spectroscopy is able to predict Si concentrations reliably because it integrates information on several of these foliar traits to make the predictions. Similarly, the relative high precisions for K, Fe and B predictions may be as strong as they are because information on several foliar traits are integrated. Unfortunately, foliar P concentrations are not closely predicted by spectroscopy. RNA and DNA absorb in the ultraviolet (e.g. Tataurov *et al*., 2008) and phosphates in the longwave infrared, but there are no pronounced absorption features in the VSWIR region (Homolová *et al*., 2013) and covariance with other traits is weak, making constellation effects unreliable. Whilst a few spectroscopy studies have modelled P with some success, the spectral bands chosen differs among studies (Homolová *et al*., 2013) suggesting that constellation effects cannot be relied upon.

2.5.3 Difficulties in measuring intraspecific variation by field spectroscopy and its implications for mapping functional traits

Rock-derived nutrients lack absorption features in visible to shortwave-infrared region of the electromagnetic spectrum so cannot be measured directly by spectroscopy. They can, nevertheless, be estimated indirectly by virtue of the fact that element concentrations co-vary with organic molecules that do have strong absorption features ("constellation effects", see above). This paper identifies a problem with this approach: there were strong differences in rock-derived mineral nutrients between soil types, but we could not measure these because the concentrations of defence and structural traits were barely affected by soil type. We have shown many similarities between our study and those in tropical forests, demonstrating that this problem is likely to be widespread.

There are likely to be implications of the constellation-effect problem for mapping functional

traits using imaging spectroscopy. Ever larger areas of earth are being mapped with airborne spectrometers (e.g. Asner *et al*., 2017) and the anticipated launch of satellite-borne sensors (e.g. EnMAP; DLR 2015; Guanter *et al*., 2015) will soon enable vegetation and ecosystem function to be characterised at a global scale. The effectiveness of indirect prediction of traits using constellation-effect approaches will depend critically on whether soils act as a strong filter on tree species within a particular region. In the Amazonian lowlands, Asner *et al*. (2015) found that variation in soil P was mirrored by changes in species composition, and that P variation among species was correlated with changes in structural and defence compounds: in this instance, indirect estimation should be effective (e.g. Chadwick and Asner, 2016). However, in low-diversity temperate forests, a single tree species is often found to span many different soil types and show substantial phenotypic plasticity in some traits (Oleksyn *et al*., 2002; Turnbull *et al*., 2016). The six species growing on both chalk and alluvial soils in this study are a case in point. In these low diversity systems, it will be much more difficult to map variation using constellation effects, for the reasons explained above. Our study confirms the power of spectroscopy for predicting biochemical and structural plant traits, but we urge caution in interpreting results when species range across contrasting soil types.

2.5.4 Conclusions

Trees on thin chalk soils had low concentrations of N, P and K macronutrients in their leaves than trees growing on deep alluvium, but had high concentrations of several micronutrients. Phosphorus is sequestered in insoluble forms in alkaline soils. This shortage of plant available phosphorus was associated in this study with low concentrations of foliar N and low efficiency of PSII, but had no effect on structural and defensive traits. Trait differences were far greater among species than between soil types, for all traits except foliar P. Foliar traits predicted from VSWIR reflectance spectra matched the locations of known spectral absorption features related to proteins, starch, lignin, cellulose, hemicellulose and leaf water content. Some of the most accurately predicted traits have no absorption features in the VSWIR range, and were estimated indirectly through their covariance with structural traits that do have absorption features in that spectral region ("constellation effects") including cell wall constituents. Since these structural traits did not vary with soil type, our models were unable to reliably predict intraspecific variation in rock-derived nutrients via constellation effects. Similarities between our results and those of large-scale tropical studies suggest this problem is likely to be widespread. This study demonstrates the value of spectroscopy for rapid, non-destructive estimation of foliar

traits across species, but highlights the difficulties that can arise in detecting within-species changes along environmental gradients.

2.6 Authors' Contributions

Study design: David Coomes. *Data collection*: David Coomes. *Laboratory analysis*: Matthew Davey. *Data analysis*: Matheus Nunes. *Manuscript writing*: Matheus Nunes with support from all the co-authors.

Chapter 3 | Changes in leaf functional traits of rainforest canopy trees associated with an El Niño event in Borneo

3.1 Summary

El Niño generates periods of relatively low precipitation, low cloud cover and higher irradiation over the rainforests of Southeast Asia, but its impact on tree physiology remains poorly understood. Here we use a functional trait approach - commonly used to understand plant adaptation along environmental gradients - to evaluate rainforest responses to El Niño. Leaf chemical and structural traits, and hyperspectral reflectances, were measured on 104 Malaysian trees from 65 species during and after the 2015/16 El Niño. Chlorophyll and carotenoid concentrations were ~35% higher during the El Niño than afterward, suggesting greening-up of the canopy in response to higher irradiance. Concentrations of mineral nutrients (N, P, K, Mg and Ca) were unaffected, suggesting that mineralisation and transportation processes were unaffected by the El Niño. Leaves also contained more phenolics and tannins during the El Niño, and differences in concentrations were highly organised by species. We show that reflectance spectra provide reliable estimates of these changes in traits. Our study provides evidence that pigments increase during the El Niño, contributing to the debate over canopy-level responses to dry periods in tropical forests.

3.2 Introduction

El Niño bring periods of low rainfall and low cloud cover to tropical rainforests typically supplied with plentiful water (Lopes *et al*., 2016), but the responses of rainforests to these events remain poorly understood. The Southern Oscillations responsible for El Niño events have occurred for least 130,000 years (Tudhop *et al*., 2001) suggesting ample opportunity for natural selection of trees capable of tolerating irregular drought events (Harrison, 2000; Detto *et al*., 2018). However, global warming is increasing the severity and frequency of El Niño events (Breshears *et al*., 2005; Allen *et al*., 2010; Thirumalai *et al*., 2017; Wang *et al*., 2017). For example, higher than average temperatures recorded across Southeast Asia in 2015 were attributed to an El Niño event amplified by global warming (Thirumalai *et al*., 2017); those higher temperatures increase evaporative demand and increase the severity of drought events

(Adams *et al*., 2009). Recent research has demonstrated a variety of biotic responses to El Niño-induced droughts (O'Brien *et al*., 2017; Qie *et al*., 2017; Detto *et al*., 2018). There is evidence of increased mortality in the Amazon (Phillips *et al*., 2009; Doughty *et al*., 2015) but West African forests are more resilient owing to a gradual shift in species composition toward drought-tolerant species (Fauset *et al*., 2012). There is also evidence of forest greening in periods without rain based on optical remote sensing (Saleska *et al*., 2007); one interpretation of these data is that the greatest photosynthetic activity coincides with peaks in solar irradiance associated with reduced cloud cover and perhaps primary forests are deep-rooted and continue to access sufficient water in dry periods (Huete *et al*., *et al*., 2006).

The functional trait approach provides a way of dealing with large uncertainties in predicting tropical forest responses to short- and long-term climate changes that arise from the high diversity of tropical tree species (Reich, 2012; Reich, 2014; Doughty *et al*., 2018). Traits help explain differences in growth and survival across resource gradients; for example, plant trait diversity might act as an insurance against climate change impacts on Amazon forests biomass, and considering the possible plasticity of traits, fast shifts of functional dominance enable enhancement of biomass resilience (Sakschewski *et al*., 2016). Nevertheless, repeated trait measurements on the same plants are less frequent. Recent studies have measured traits over time to investigate leaf aging impacts (Chavana-Bryant *et al*., 2017), but this approach has not been used previously to track traits changes through an El Niño event.

If variation in leaf traits associated with El Niño is large enough to influence remotely sensed patterns, these effects should be detectable in individual leaves. Hyperspectral reflectance signatures are related to the electromagnetic radiation and leaf matter across a range of wavelengths; the visible (400 - 750 nm) portion of the spectrum is mainly driven by pigments (Sims and Gamon, 2002), the near infrared (751 - 1300 nm) and shortwave infrared (1301 - 2400 nm) driven by internal and external leaf structure (Slaton *et al*., 2001), including water (Tucker, 1980; Ustin *et al*., 2004), phenolics (Kokaly and Skidmore, 2009) and organic constituents (Petisco *et al*., 2006; Asner *et al*., 2011). The spectral diversity observed among plants is coupled with their functional and evolutionary divergence and may be used to predict ecosystem function (Schweiger *et al*., 2018), expressing leaf traits that are important for resource capture and stress tolerance. Earth observation studies using MODIS satellite spectroscopy have shown positive impacts of dry seasons on EVI (Huete *et al*., 2006; Saleska *et al*., 2007), an enhanced vegetation index which is a combination of chlorophyll content and

leaf area that does not saturate in dense forests, indicating a "green up" phenomenon associated with light availability during dry seasons. However, it remains controversial whether trees are actually investing in photosynthetically apparatus or whether this phenomenon is an artefact of optical sensors (Morton *et al*., 2014). We then propose that leaf-level reflectance can provide an efficient and accurate method to monitor short-term climate change, on the basis that trait variation affects reflectance in different portions of the spectrum, and indicates forest resilience to short-term climate change.

This paper presents observations of changing leaf traits in a Bornean tropical forest associated with the 2015/16 ENSO-induced drought, and determines whether these can be observed through spectral analysis as well as *in situ* sampling. In terms of drought stress, there may be species-specific responses at the leaf level (Maréchaux *et al*., 2015). A change among several of these factors could indicate a combination of canopy physiological and structural responses to drought. No studies have previously reported such responses in the context of tropical forest remote sensing from repeatedly measured traits. We investigate variation in 17 foliar traits and leaf-level spectroscopy in response to the El Niño event to address the following questions: 1) how do foliar traits change with El Niño events? 2) Can response to El Niño affect leaf spectral properties? To answer these questions, we measured a diverse range of leaf properties to investigate the response to El Niño effects that comprise higher than average temperatures, reduced rainfall and longer sunshine duration, and used spectroscopy to capture the variation in leaf traits. We aim to offer a new spectral approach for determining the response of forest canopies to climatic variations from a temporal perspective. Leaf samples and field spectroscopy data were acquired in two field campaigns, one during the El Niño event (September 2015) and one after the rains had returned (October 2016). By taking repeat measurements of physico-chemical and spectral properties on the same trees, this is the first study to measure leaf-level responses to El Niño events, providing a unique perspective on rainforest tree acclimation to short-term climatic variation.

3.3 Material and methods

3.3.1 Site Description and 2015-16 ENSO in Southeast Asia

The study was conducted in Danum Valley Conservation Area in the Malaysian state of Sabah, on the island of Borneo (Reynolds *et al*., 2011). Vegetation is classified as lowland mixed

dipterocarp forest (Fox, 1972) on clay soils (Wright, 1975). Data collection was carried out within two 1-ha plots located in old growth forests (plot coordinates 4.951° N, 117.796° E and 4.953° N, 117.793° E) characterised by high species richness and tall and emergent trees where there was no evidence of logging or recent human disturbance (Riutta *et al*., 2018).

Borneo experiences variability in climate due to influences from both the Pacific and Indian Oceans. The National Oceanic and Atmospheric Administration (NOAA) considers El Niño conditions to be present when the Oceanic Niño Index (ONI) is + 0.5 or higher. The strong El Niño of 2015-16 El (Fig. 3.1a) coincided with a period of higher diurnal range in surface air temperatures across the island, peaking during the months November 2015 to April 2016 which were on average 0.6° – 1.2° higher than average seasonal temperatures (Colledge, 2017). Precipitation during 2015 and 2016 varied considerably across the region, but in North-eastern Borneo seasonal total rainfall in May to October 2015 was between 75% to 100% of normal rainfall (based on a 1981-2010 seasonal average), reducing to 50% to 75% of normal rainfall for the period November 2015 to April 2016, returning to long-term seasonal average amounts for May to October 2016 (typically 900 – 1000 mm) (Colledge, 2017). At Danum Valley Conservation Area itself, mean daily rainfall (mm) in the latter half of 2015 and early 2016 was lower than typically recorded for the site (Fig. 3.1b), before increasing rapidly in the latter half of 2016. In the months immediately preceding the two surveys (May to August) the average number of days when no rain was recorded was 16 in 2015 and 10 in 2016, whilst the longest run of consecutive days without rain was 10 in 2015, and just 3 in 2016. Coupled with reduced rainfall, an increase in sunshine duration was also recorded at Danum Valley, with mean daily sunshine of 5.9 hours in May to August 2015, reducing to 5.4 hours for the same months in 2016. Thus, at Danum Valley Conservation Area, the forest experienced reduced rainfall and longer sunshine duration before the first survey (September 2015) compared to higher rainfall and fewer hours of sunshine in the months before the second survey.

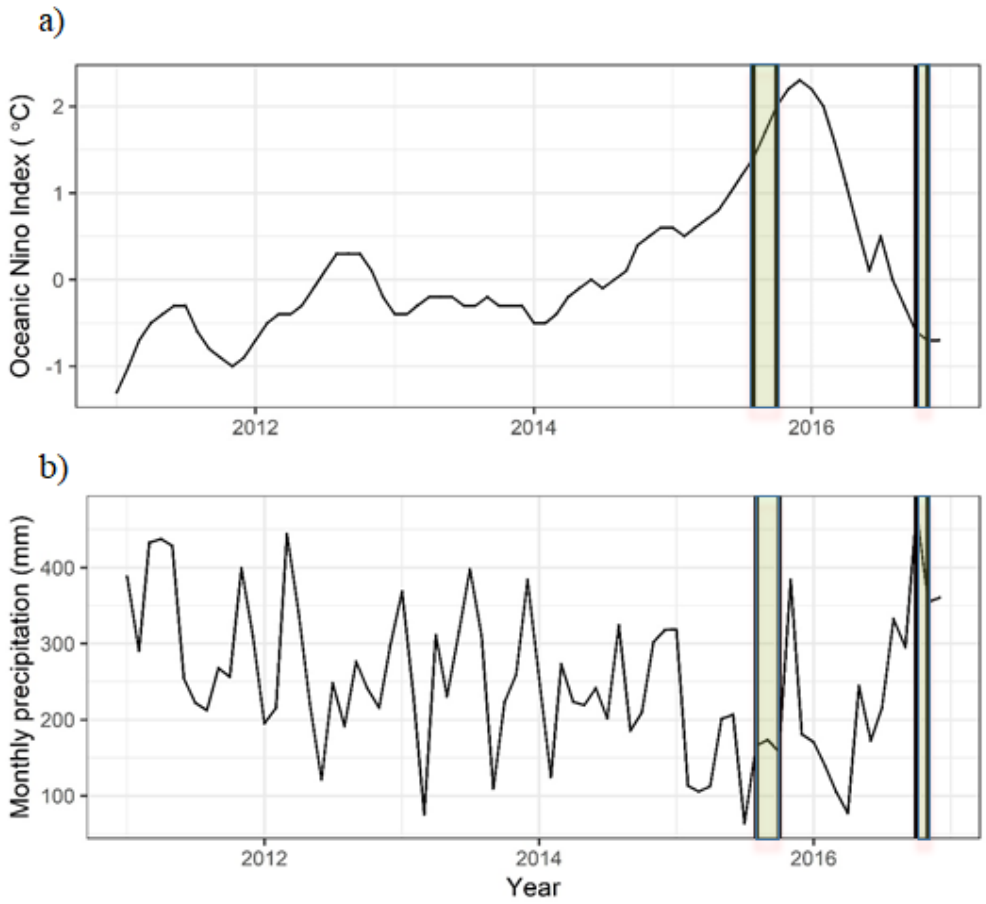

Figure 3.1 | a) Oceanic Niño Index based upon surface temperature anomalies; and b) monthly precipitation (mm) recorded at Danum Valley Field Centre in Malaysian Borneo. Shaded regions represent the periods of trait collection during and after the 2015/2016 El Niño event.

3.3.2 Sampling design and field data collection

Seventeen functional traits were measured on 104 individual trees ≥ 10 cm diameter at breast height (DBH) during and after the 2015/2016 El Niño. The first measurement was conducted in September 2015 during a period of dry conditions, and the second in October 2016 after a return to wetter conditions (Fig. 3.1b). We combined two strategies to sample functional traits in each plot that included sampling the species that most contributed to 90% of the total plot basal area, followed by a stratified random and taxon-independent sampling of all trees in three randomly selected subplots (400 m^2) to ensure representation of understory and potentially rare species (see Both *et al*., 2018 for details). Tree height ranged from 2.3 m to 73.7 m. Branches were collected from 104 trees representing 65 species from 44 genera and 24 families. We attempted to sample fully sunlit canopy branches and fully shaded branches, but it was

uncommon for large-canopy trees to have fully shaded branches or for small understory trees to have fully sunlit branches, so in many cases only one branch was sampled.

Physico-chemical traits were determined using standardised laboratory approaches selected so that measurements are directly comparable with other international trait campaigns (see Both *et al*. 2018 for details). Branch samples were collected by tree climbing or by cutting from the ground with telescopic branch cutters. Undamaged mature leaves were collected and cleaned with water for subsequent analyses. Dried bulked and milled leaf material was used for determination of Ca, K, Mg, P and N concentrations, $\delta^{13}C$ and $\delta^{15}N$ stable isotope composition, soluble carbon, cellulose, hemicellulose and lignin concentrations (for analyses see Perez-Harguindeguy *et al*., 2013). Analyses of pigments (Chlorophyll *a*, Chlorophyll *b* and carotenoids), phenols and tannins were conducted on 0.7-cm-diameter leaf discs punched from fresh leaves immediately after field collection and frozen in liquid N. The analyses of chlorophyll *a*, chlorophyll *b* and bulk carotenoid concentrations in leaf discs included an internal laboratory standard derived from a single batch of Macaranga leaves sampled prior to the first set of analyses, as well as a commercial common reference material. Chlorophyll *a* and chlorophyll *b* concentrations were summed and treated herein as chlorophyll *a* + *b*. These standards assured consistency of results across both sets of laboratory analyses. Leaf scans were obtained using a high resolution scanner (CanoScan LiDE 220, Canon Inc., Japan) shortly after collection and their area estimated via contrast analysis of the images. We extracted the blue channel of each image and converted it to grayscale values where pixels belonging to the white background have values close to one and pixels belonging to the dark leaf have values close to zero. We applied a binary segmentation algorithm in the *EBImage* package in R (Pau *et al*., 2010, R Core Team, 2018) to identify dark (leaf) clusters and filled any gaps within those clusters. Filling in of gaps is necessary as lighter colour irregularities such as necrosis or fungal infections may be otherwise mistakenly identified as background. We also applied a masking kernel via a moving window over the image that removed small patches identified by the binary segmentation algorithm. Doing so ensured that accidental dirt patches on the image are not counted as leaf area. The number of pixels within each leaf segment were summed and divided by the scanner resolution to obtain leaf area. Fresh and dry leaf weight were determined in a field laboratory and leaf mass per area (LMA) were calculated. Herbarium voucher specimens were taken for identification of tree species and were deposited in the herbarium at Danum Valley Field Centre (see Both *et al*., 2018).

Analyses were performed within the R statistics framework (R Core Team, 2018). We conducted analyses that considered the hierarchical structure of the data, and analyses focussing on species-level responses: (a) to evaluate the relative influence of the drought, shading and taxonomic level on each trait, we developed hierarchical models using the lme4 package in R. We included the phylogenetic levels of family, genus nested within family, species nested within genus, and branch type (shaded or sunlit) nested within species, as well as a temporal effect. All effects were treated as random. In each model, the response variable (y) is any chemical trait for each canopy sample. The total variance of the mean for a given trait was quantitatively separated into variance explained by each taxonomic level, El Niño and unexplained variance was treated as a residual comprised of micro-environment, sample selection and measurement errors associated with laboratory analyses; (b) To examine the influence of El Niño at the species level, trait values sampled from different branches of the same species were averaged to generate species-level values for each of the 17 leaf chemical traits. One-way analysis of variance (ANOVA) were used to examine the influence of the El Niño event.

3.3.3 Spectroscopy collection

For both surveys, five leaves attached to the branches were selected at random, avoiding damaged and young leaves. Reflectance spectra (350 to 2500 nm) were acquired using a FieldSpec 4, produced by Analytical Spectral Devices (ASD, Boulder, Colorado, USA). The spectroradiometer's contact probe was mounted on a clamp and firmly pushed down onto the sample against a black background, so that no light escaped through the sides. The spectral measurements were taken at the midpoint between the main vein and the leaf edge, approximately halfway between the petiole and leaf tip, with the abaxial surface pointing towards the probe. The readings were calibrated against a Spectralon white reference panel every five samples. In all statistical analyses, the spectral data were trimmed to the 400–2500-nm range, and the mean reflectance values of the 5 spectra per branch were used.

Partial least squares regression (PLSR) was initially used to predict leaf traits from spectral reflectance. There is strong autocorrelation in reflectance values, so PLSR involves dimensionality reduction, to produce orthogonal uncorrelated latent vectors containing the maximum explanatory power in relation to the trait data (Wold *et al*., 2001). To avoid over-fitting the calibration models, the number of latent variables was chosen according to the "one

standard error" rule that selects the least complex model with the average cross-validated accuracy within one standard error from that in the optimal model (Breiman *et al*., 2017). We determined the contribution of wavelengths within the visible (VIS; 400 – 750 nm), near infrared (NIR; 751 - 1300) and shortwave infrared (SWIR; 1301 – 2400 nm) to the model performance (Serbin *et al*., 2014; Nunes *et al*., 2017a). We also combined two or more spectral regions to evaluate performance. In general, previous research indicates that the SWIR contains absorption features for most traits (Curran, 1989; Kokaly *et al*., 2009; Nunes *et al*., 2017a), with the visible being useful for pigments (Curran *et al*., 1991; Sims and Gamon, 2002), and the NIR for leaf mass per area (LMA; Asner *et al*., 2011). Performance of the final models was evaluated using an 80/20 split of the data for calibration/validation, respectively, over 100 randomized permutations of the dataset. For each such permutation, we tracked the model fit (R^2) and the percentage root-mean-square error over the data range (%RMSE). These analyses generated a distribution of model coefficients and fit statistics and allowed for the assessment of model stability as well as uncertainty in predictions. Models were built using the packages *caret* and *vegan* in R (www.r-project.org). Additionally, we explored whether the data collected using spectroscopy could be used as a surrogate for the reference data to determine the effect of El Niño on leaf traits. To test this question, we used ANOVA separately for both reference and predicted data, as well as bias of the estimates.

3.4 Results

3.4.1 The influence of the El Niño event on traits

Pigment concentrations and some other chemical traits at the species level varied in response to the El Niño event that impacted Southeast Asia in 2015/2016 (Table 3.1). In general, most traits decreased in concentration after the El Niño, tracking the increased precipitation and reduction in irradiance in the post-ENSO period. Pigment concentrations, namely chlorophyll *a* + *b* and carotenoids, were about a third higher during the El Niño event, thereby representing the highest variation among all traits (Fig. 3.2). We also observed that phenolics decreased post El Niño by ~19%, and δ^{13} C decreased by 9%. Carbon fractions, including soluble C, hemicellulose, cellulose and lignin, N, δ^{15} N and rock-derived nutrients, namely P, K, Ca and Mg, did not change between sampling periods. LMA and water content did not vary with El Niño. Correlation analysis (Fig. B.1) indicates that plants with high LMA have more phenolics

and pigments but less water and lower N concentrations, however a decrease in pigments and phenolics did not cause a decrease in LMA.

Table 3.1 | Descriptive statistics and ANOVAs comparing foliar traits of species average values for 65 species during and after the El Niño event. Mean ± standard deviation of each trait is provided along with the change magnitude and significance (adjusted *P* value using the False Discovery Rates-based method) of the comparison. Traits in bold represent those statistically significant according to the adjusted *P-value*.

Foliar trait	**During El Niño**	**After El Niño**	**During - After change**	***P-adj***
LMA (g cm^{-2})	94.0 ± 17.4	88.5 ± 19.0	5.4 ± 11.0	0.06
Water content (%)	59.1 ± 6.6	57.4 ± 8.1	1.7 ± 4.5	0.26
N (%)	1.81 ± 0.52	1.86 ± 0.43	-0.05 ± 0.32	1
δ^{13} C (‰)	**-32.0 ± 1.35**	**-32.5 ± 1.24**	**0.5 ± 1.0**	**0.01**
δ^{15} N (‰)	1.23 ± 1.51	0.86 ± 1.11	0.37 ± 1.4	1
Chl a + b (mg m^{-2})	**326.2 ± 73.7**	**221.5 ± 91.3**	**109.4 ± 87.0**	**<0.001**
Car (mg m^{-2})	**58.1 ± 14.9**	**38.8 ± 17.1**	**19.3 ± 17.3**	**<0.001**
Sol. carbon (%)	50.7 ± 9.3	50.2 ± 9.2	0.5 ± 5.0	1
Phenolics (mg g^{-1})	**34.4 ± 19.0**	**27.8 ± 18.4**	**6.5 ± 13.2**	**0.01**
Tannin (mg g^{-1})	7.8 ± 5.3	6.4 ± 4.5	1.4 ± 3.7	0.26
Hemicellulose (%)	12.3 ± 3.2	12.1 ± 3.1	0.2 ± 1.1	1
Cellulose (%)	20.8 ± 4.2	19.9 ± 3.8	0.9 ± 2.4	0.24
Lignin (%)	16.1 ± 6.1	17.6 ± 6.4	-1.5 ± 3.5	0.07
P (mg g^{-1})	1.31 ± 0.48	1.31 ± 0.41	0.0 ± 0.35	1
K (mg g^{-1})	10.8 ± 7.2	10.4 ± 5.9	0.4 ± 3.5	1
Mg (mg g^{-1})	4.3 ± 3.0	4.2 ± 3.1	0.1 ± 1.0	1
Ca (mg g^{-1})	13.9 ± 8.8	14.9 ± 8.0	-1.0 ± 4.7	1

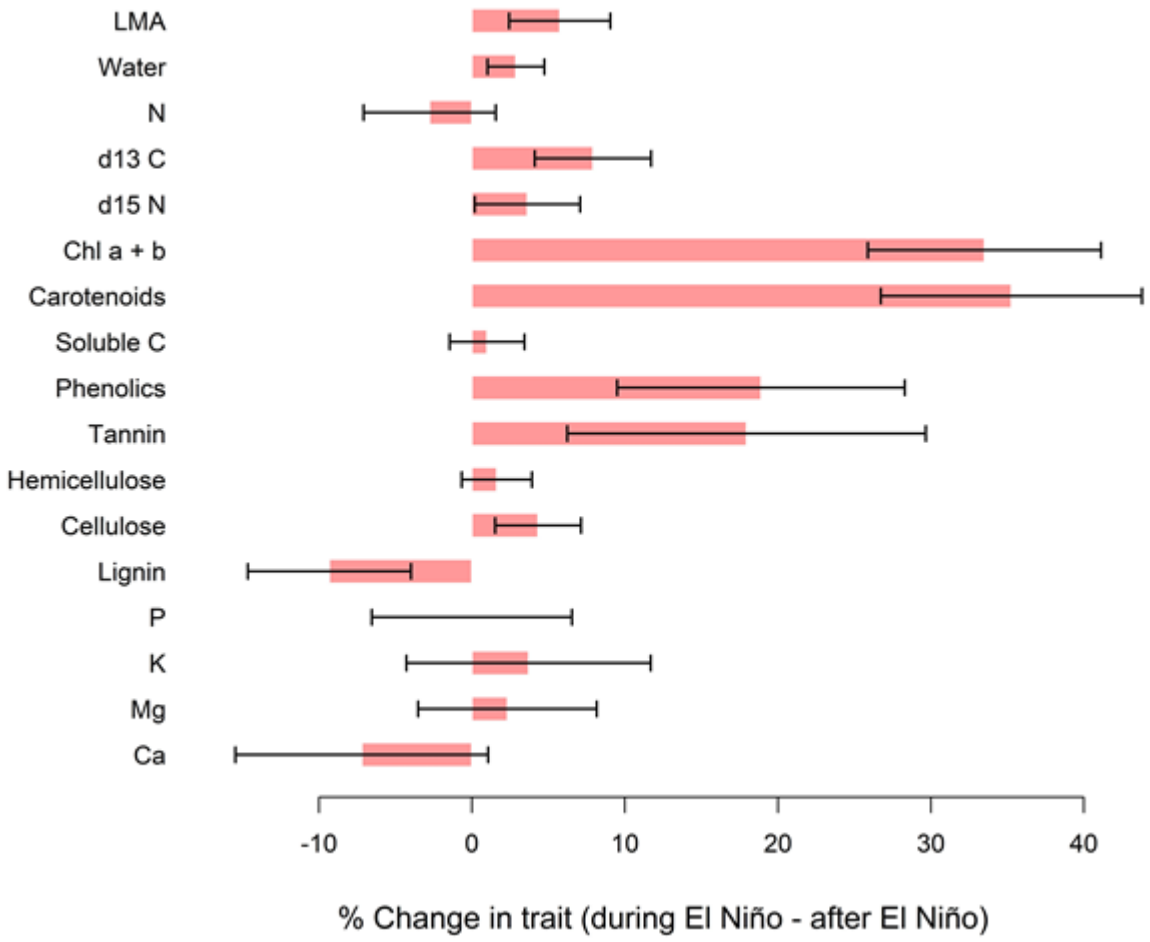

Figure 3.2 | Percentage differences in the ratio of each canopy chemical trait during and after El-Niño induced droughts. Differences (coloured boxes) were calculated from the species average value and error bars represent relative 95% confidence intervals of the average change. Percentage difference for δ^{15} N and δ^{13} C isotopes were calculated as trait change / trait range ratio.

3.4.2 Organisation of traits by taxonomy, light exposure and El Niño

Using hierarchical models for variance partitioning to analyse the dataset, we found evidence for strong taxonomic organization of multiple traits operating independently of variation in climate (Fig. 3.3). Our analysis also incorporates branch type (sunlit or shaded branches) to indicate traits highly variable within canopies. Residuals variation may result from variation in micro-environment, sample selection and analytical error. High trait diversity among coexisting trees is driven by differences between taxa rather than by environmental conditions. Water content, rock-derived nutrient concentrations, lignin, phenolics and tannin were all

strongly phylogenetically conserved; species-level differences were usually greater than family- or genus-level differences, although K, water, tannins, N and lignin had strong family-level effects. Pigments had the highest impact by El Niño and δ^{15} N was the least taxonomically organised trait and the highest unexplained variation. For most traits, branch type accounted for more variance than the El Niño event, in particular LMA, N, δ^{13} C and carbon fractions. LMA was conspicuously variable within canopies, indicating the dependence of environmental attributes associated with the vertical canopy profile, and is less affected by short-term climatic variation. Our analysis suggests that sun exposed leaves can have variable responses to El Niño.

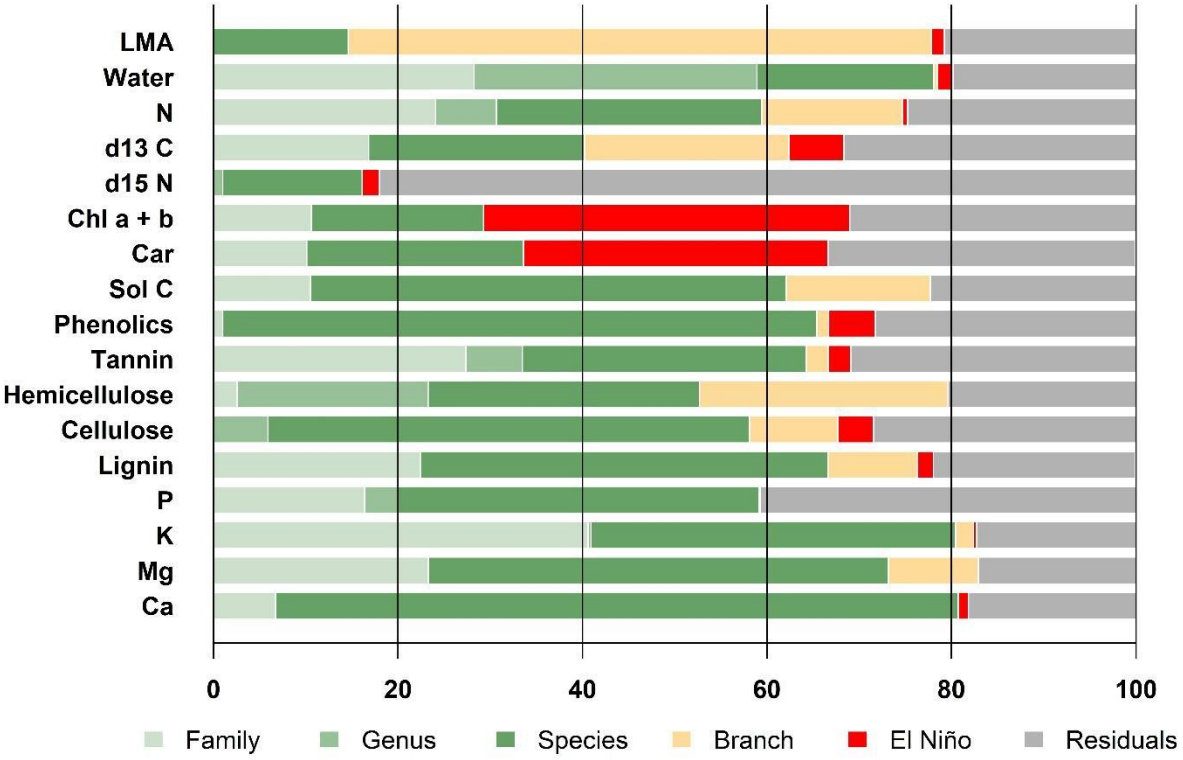

Figure 3.3 | Variance partitioning of functional traits into taxonomic level (family/genus/species), branch (sun exposed vs shaded), the El Niño event (during and after), and unexplained residual components from 104 trees in an old growth forest in Danum Valley Conservation Area, Malaysian Borneo.

3.4.3 Spectral analyses of leaf trait responses to El Niño

PLSR indicates that many of the 17 chemical traits can be estimated using leaf spectral reflectance (Table 3.2). Variation in water content, LMA, N, phenolics and cellulose

concentrations were explained particularly well using spectral reflectance. On the other hand, P, K, δ^{13} C and δ^{15} N were poorly predicted using reflectance, confirming previous studies that show the difficulties in detecting these traits from reflectance. In general, the highest absolute spectral sensitivity was observed in the SWIR portion of the spectrum between 1301 and 2400 nm, with all traits influencing this spectral region. The visible portion of the spectrum (400 - 750 nm) was influenced only by chlorophyll *a* + *b*, carotenoids and LMA, and the near infrared (751 - 1300 nm) influenced by LMA, phenolics and P.

Table 3.2 | Spectroscopy estimation of leaf chemical and structural properties using leaf spectral reflectance of 104 trees in Malaysian Borneo during and after an El Niño event. NComp is the number of latent components using partial least square regression and the average ± standard deviation of metrics to assess predictive power using. Performance of the final models was evaluated using an 80/20 split of the data for calibration/validation, respectively, over 100 randomized permutations of the dataset.

Trait	Region	ncomp	R^2	%RMSE
LMA(g cm^{-2})	VIS – NIR - SWIR	10	59.2 ± 9.4	14.1 ±1.4
Water content (%)	SWIR	5	67.3 ± 8.0	7.1 ± 0.9
N (%)	SWIR	16	58.8 ± 8.8	17.4 ± 2.7
δ^{13} C (‰)	SWIR	14	32.6 ± 10.7	17.1 ± 1.6
δ^{15} N (‰)	SWIR	1	3.2 ± 3.1	7.5 ± 2.5
Chl a + b (mg m^{-2})	VIS - SWIR	8	40.0 ± 12.5	28.4 ± 2.6
Car (mg m^{-2})	VIS - SWIR	7	41.2 ± 12.7	28.3 ± 2.9
Soluble carbon (%)	SWIR	18	38.8 ± 10.8	14.2 ± 1.6
Phenolics (mg g^{-1})	NIR - SWIR	9	53.8 ± 10.1	40.3 ± 4.6
Tannin (mg g^{-1})	SWIR	11	42.9 ± 9.9	47.6 ± 4.8
Hemicellulose (%)	SWIR	12	45.1 ± 9.7	21.3 ± 2.3
Cellulose (%)	SWIR	19	53.3 ± 10.1	15.2 ± 1.7
Lignin (%)	SWIR	17	34.8 ± 11.9	30.0 ± 4.3
P (mg g^{-1})	NIR - SWIR	10	27.7 ± 14.6	27.9 ± 6.1
K (mg g^{-1})	SWIR	9	24.5 ± 10.7	50.4 ± 7.0
Mg (mg g^{-1})	SWIR	13	43.0 ± 11.3	57.8 ±7.6
Ca (mg g^{-1})	SWIR	11	36.7 ± 9.3	47.1 ± 6.6

Following conversion of each reflectance spectrum to chemical values, usually referred to as spectranomic traits, we compared the predicted data and the observed data for traits affected by El Niño (Table 3.3). We only compared traits significantly affected by El Niño to investigate whether remote sensing is able to detect patterns of variation. El Niño influence on traits, except on water and δ^{15} N, were detected using spectral reflectance. We plotted the observed traits against spectranomic traits to further investigate the ability of remote sensing to detect El Niño influences (Fig. 3.4). The influence of El Niño on pigments was apparent by the separation of the data-set into during and after El Niño classes, indicating the spectral ability to detect the "green-up" phenomenon associated with the El Niño.

Table 3.3 | Comparison of foliar trait values predicted from spectral reflectance to the observed change in traits significantly affected by El Niño. Partial-least square regression was used to generate models relating leaf traits measured during and after an El Niño event to spectral reflectance data collected by field spectroscopy. Regression analyses did not include sampling date in model calibration, so the predicted during and after El Niño values indicate predictive power to detect El Niño influences on each trait. Mean $\pm$ standard deviation of each spectranomic trait change is provided along with the significance (adjusted *P* value) of the change and predictive bias.

Trait	**Predicted Change**	**Observed Change**	***P*-value**	***Bias***
δ^{13} C (‰)	-0.4 $\pm$ 0.7	-0.5 $\pm$ 1.0	<0.001	0.02
Chl *a* + *b* (mg m^{-2})	-79.8 $\pm$ 43.4	- 109.4 $\pm$ 87.0	<0.001	18.3
Carotenoids (mg m^{-2})	-15.2 $\pm$ 7.5	- 19.3 $\pm$ 17.3	<0.001	2.0
Phenolics (mg g^{-1})	-5.7 $\pm$ 7.0	- 6.5 $\pm$ 13.2	<0.001	1.1

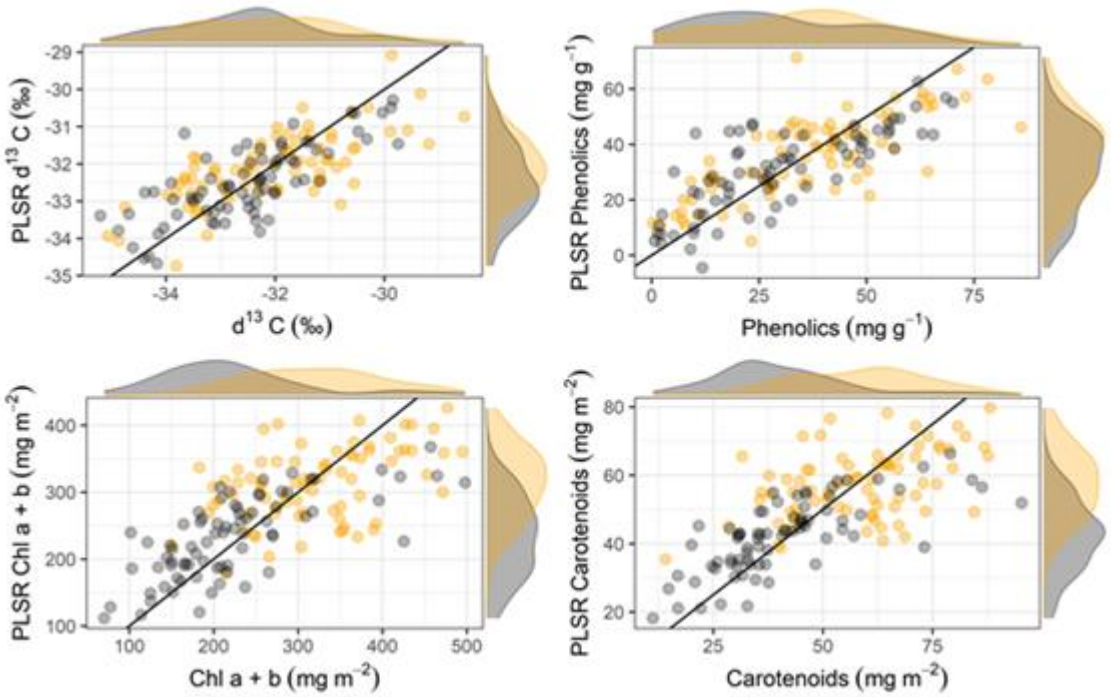

Figure 3.4 | Observed traits against traits predicted from spectral reflectance data, using Partial-Least Square regression, for traits significantly influenced by El Niño. The findings show that remote sensing is able to detect accurately traits during (yellow) and after (black) El Niño.

3.5 Discussion

The repeated measurements of a range of foliar traits and leaf reflectance for 104 trees in an intact forest in Malaysian Borneo shed light on the responses of plants to El Niño. Pigment concentrations were particularly high during the El Niño event, corroborating the hypothesis of a leaf-level "green up" phenomenon associated with dry seasons when irradiance is promoted by the absence of clouds (Nemani et al., 2003). To our knowledge, this paper provides field-based evidence of this phenomenon for the first time. The "green up" phenomenon can also be detected from proximal spectral reflectance, which strengthens the hypothesis that "green up" observed during dry periods in other tropical forests is caused by an increase in pigment and/or leaf area index (Huete *et al*., 2006; Saleska *et al*., 2007). We also detected an accumulation of phenolic compounds during El Niño, demonstrating that plants can also invest in defense alongside enhanced photosynthetic machinery. These results demonstrate the importance of understanding temporal changes in the expression of plant functional traits when studying short-term responses to climatic variation; these trait changes may represent acclimation to lower precipitation, higher temperatures but also higher

irradiance associated with reduced cloud cover. We also demonstrate the power of spectral reflectance data to predict the effects of El Niño on leaf level processes. Considering the expected increase in frequency of El Niño events associated with global warming (Wang *et al*., 2017), our results display the capacity of plants to express short-term acclimation to these conditions, and suggest that remote sensing may successfully predict these responses.

3.5.1 Leaf trait responses to an El Niño event

The repeated measurements indicate that forests responded to the environmental changes imposed by the El Niño event by investing in pigments and phenolics, and enhancing leaf-level water use efficiency. These rapid shifts in multiple leaf chemical traits reveal the sensitivity of forest functioning to El Niño. The differential dynamics of chemical traits in leaves may reflect their function. Chlorophylls control the amount of photosynthetically active radiation absorbed for photosynthesis, while carotenoids absorb radiation for photosynthesis and protect leaves from over-exposure to solar radiation by releasing the excess energy as heat (Ustin *et al*., 2009). The amount of these photosynthetic pigments per unit leaf area enhances photosynthetic capacity in high light (Poorter at al., 2009). In our study, pigment concentrations were ~35% higher during the El Niño event than afterwards, which suggests that the plants had a capacity to acclimate rapidly to the loss of the high irradiance conditions during wet periods and to up-regulate pigment synthesis when sunshine hours were high. The increase in photosynthetic pigment concentrations occurred during a dry spell, which suggests that the climatic water deficits may not have been sufficient to inhibit photosynthetic rates. Photosynthesis can be maintained at the same or even higher levels than during the wet La Niña phase of the ENSO cycle because of increased light availability during the relatively dry El Niño phase (Guan *et al*., 2015).

Forests green-up during drought events, as previously reported in a study examining the 2005 drought over the Amazon basin from satellite remote sensing (Saleska *et al*., 2007). The authors proposed that forests might be more resilient to drought that previously thought, because plants invest in photosynthetic apparatus during drought. However, a plot-based approach demonstrate that the 2005 drought negatively affected forest carbon through increased mortality (Phillips *et al*., 2009). Although our study provides evidence of a rapid shift to maximise water use efficiency, as well as a large investment in photosynthetic and defensive machineries, we cannot infer information about mortality and productivity of trees. We only

consider functional traits associated with light capture and gas exchange, not wood, root traits, canopy-level properties such LAI, height or tree architecture. Hence it is difficult to predict the responses to El Niño events.

During the El Niño event, leaves had higher δ^{13} C values. Water-use efficiency can be effectively measured with foliar δ^{13}C values (Farquhar *et al*. 1989). Our results indicate higher water-use efficiency when precipitation was lower and higher temperatures. A decrease in δ^{13}C post El Niño may have resulted from a high ratio of stomatal conductance to net photosynthesis and consequently higher intercellular CO2 / ambient CO2 ratios. The rapid shift in water-use efficiency indicate the ability of plants to acclimate to these short-term climate variation, but also may indicate the prospect of more frequent droughts could increase selection towards greater intrinsic water-use efficiency (Cernusak *et al*., 2009).

Defensive compounds, namely phenolics, were also at higher concentration during the El Niño. A number of plant products typically associated with anti-herbivore defenses, such as phenolic compounds, accumulate in larger quantities in plants exposed to UV-B radiation than in plants receiving no UV-B radiation (Tegelberg *et al*., 2004). Phenolic compounds are secondary metabolites with antioxidant effects in plants exposed to oxidative stress (Olsson *et al*., 1998; Tattini *et al*., 2004; Tatinni *et al*., 2005; Mansori *et al*., 2015). In a controlled environment study, several clover varieties were compared under combined treatments of drought and high UVB fluxes (Hofmann *et al*., 2003). Drought and UV-B radiation were tested synergistically in clover varieties resulting in a substantial increase of UV-B radiation-absorbing compounds, including phenolics, in drought stressed plants (Hofmann *et al*., 2003). These changes were linked to an improved water status of the plants. Solar UV-B radiation induces a variety of acclimation responses, which typically include accumulation of phenolic compounds that serve as “sunscreens” or UV filters (Caldwell *et al*., 2003). Phenolic compounds accumulate in large quantities in the vacuoles of epidermal cells and effectively attenuate the UV component of sunlight with minimal change in the visible region of the spectrum. The increase in defence-related compounds in plants exposed to UV-B radiation correlates with a lower forage quality in tissues from these plants (Izaguirre *et al*., 2006).

3.5.2 Hierarchical structuring of traits

By concentrating on functional traits without reference to species identities or individuals, we are able to account for intra-specific variability, often neglected when functional diversity is indirectly calculated from taxonomic data. Strong taxonomic organisation probably indicates low plasticity within species. The strong phylogenetic signal in water indicates selective pressure among coexisting species. Although plants can quickly adjust investment in the photosynthetic apparatus, water-use efficiency and defence, minerals stored in tissues may be reused and changes in those traits may take longer to manifest.

Our finding suggests that the efficiency of C fixation and pigments is increased during El Niño which could potentially correlate to high photosynthetic capacity (Girardin *et al*., 2010). High growth rate environments likely create the conditions under which competition and defense are the most critical factors determining how maximum productivity is achieved and maintained (Asner *et al*., 2014a), and traits associated with defense would be taxonomically organized within communities, and a divergence in functional strategies to ensure high growth rates under varying abiotic conditions (Coley, 2014). Our results suggest that the El Niño may favour individuals, but not necessarily species, that invest more in light capture, as well as species that can maintain strong defenses during extreme climatic events. The old growth forests of Borneo may have high levels of interspecific spectral variability associated with high biological diversity, and increased diversity in response to short-term climatic variation. A clearer sense of the diversity and organization of canopy chemical traits may help us to forecast winners and losers within specific communities in response to El Niño.

3.5.3 Application of spectroscopy to predict trait variation

To our knowledge, our study is the first to analyse changes in physico-chemical leaf traits and spectral reflectance during and after El Niño. Many previous papers have shown that leaf reflectance can predict morphological and biochemical leaf traits in the tropics (Asner *et al*., 2012b; Asner *et al*., 2014a; Doughty *et al*., 2017) that are commonly used for determining functional diversity (Schweiger *et al*., 2018). We demonstrate that repeated reflectance measurements can also predict variation of the El Niño effects at the leaf level. In particular, the variation of traits affected by El Niño such as pigments, $\delta^{13}C$ and phenolics were successfully detected.

The effects of El Niño on pigment content were detected from the visible (400 – 750 nm) portion of the spectra, as expected from previous studies (Curran *et al*., 1991, Sims and Gamon, 2002; Serbin *et al*., 2014). From a remote sensing perspective, a potential leaf-level green-up phenomenon during El Niño could be then a factor contributing to the "green-up" phenomenon observed during the dry season in Amazonia (Huete *et al*., 2006; Saleska *et al*., 2007), although some studies argue that it could be driven by an artefact of sun-sensor geometry (Morton *et al*., 2014) or that dry-season droughts do not co-vary with green-up of the Amazon whatsoever (Samanta *et al*., 2010). Our results demonstrate that trees do increase chlorophyll concentration in their leaves during El Niño and this change can be detected from spectral reflectance.

Large areas of earth are being mapped with airborne spectrometers (e.g. Asner *et al*., 2017) soon enable vegetation and ecosystem functioning to be characterised at the global scale. Evidence that plant acclimation during short-term climate change can be accurately predicted using spectrometers may be of great contribution to understand tropical forests.

3.6 Authors' Contributions

Study design: Mark Cutler, David Burslem, David Coomes, Sabine Both and Christopher Phillipson. *Data collection*: Matheus Nunes, Sabine Both, Christopher Phillipson, Craig Brelsford. *Laboratory analysis*: Sabine Both, Christopher Phillipson, Noreen Majalap, Matheus Nunes, Boris Bongalov. *Data analysis*: Matheus Nunes. *Manuscript writing*: Matheus Nunes with support from all the co-authors.

Chapter 4 | Mapping aboveground carbon in oil palm plantations using LiDAR: a comparison of tree-centric versus area-based approaches

4.1 Summary

Southeast Asia is the epicentre of world palm oil production. Plantations in Malaysia have increased 150% in area within the last decade, mostly at the expense of tropical forests. Maps of the aboveground carbon density (ACD) of vegetation generated by remote sensing technologies, such as airborne LiDAR, are vital for quantifying the effects of land use change for greenhouse gas emissions, and many papers have developed methods for mapping forests. However, nobody has yet mapped oil palm ACD from LiDAR. The development of carbon prediction models would open doors to remote monitoring of plantations as part of efforts to make the industry more environmentally sustainable. This paper compares the performance of tree-centric and area-based approaches to mapping ACD in oil palm plantations. We find that an area-based approach gave more accurate estimates of carbon density than tree-centric methods and that the most accurate estimation model includes LiDAR measurements of top-of-canopy height and canopy cover. We show that tree crown segmentation is sensitive to crown density, resulting in less accurate tree density and ACD predictions, but argue that tree-centric approach can nevertheless be useful for monitoring purposes, providing a method to detect, extract and count oil palm trees automatically from images.

4.2 Introduction

Southeast Asia has been the epicentre of the oil palm industry for over 50 years (Gutiérrez-Vélez and DeFries, 2013). Oil palm is one of the most profitable land uses in the humid tropics (Sayer *et al*., 2012). Malaysia has increased its planted area by 150% over the last decade (FAO, 2017) and, along with Indonesia, currently represents over 80% of global palm oil production (FAO, 2017; Koh and Wilcove, 2007). The planted area increased from 6 to 16 million hectares between 1990 and 2010, an area which now accounts for about 10 percent of the world's permanent cropland (MPOB, 2016). Conversion of forests to plantation agriculture represents a substantial source of greenhouse gas (GHG) emissions, especially in tropical peatlands (Foley *et al*., 2009), generating 10–20% of net global emissions (van der Werf *et al*., 2009). Although oil palm plantations continue to expand, the government of Malaysia has pledged to reduce their projected GHG emissions by 45% by 2030 (UNFCCC, 2017).

High-resolution forest biomass maps can provide detailed and spatially explicit estimates of aboveground carbon density (ACD, units of Mg C ha^{-1}) to assist natural resource management and assess emissions from deforestation. LiDAR (light detection and ranging) has become a commonly used technology to remotely predict ACD in many forest types (Asner *et al*., 2010; Simonson *et al*., 2016; Coomes *et al*., 2017). Carbon mapping by airborne LiDAR is significantly more accurate than approaches based on radar or passive optical measurements from space (Hyde *et al*., 2007; Nelson *et al*., 2007; Zolkos *et al*., 2013). Oil palm trees have been counted using airborne imaging spectrometry (Shafri *et al*., 2011) and their biomass estimated from satellite images (Thenkabail *et al*., 2004; Morel *et al*., 2011; Carlson *et al*., 2012; Koh *et al*., 2011), but nobody has yet developed equations to estimate carbon density in oil palm plantations from airborne LiDAR data. The development of carbon prediction models provides opportunities to assess the aboveground carbon density of oil palm plantations, which is essential for assessments of the environmental sustainability of human modified tropical landscapes.

Airborne LiDAR provides detailed information about forest structure within scanned areas, which can extend over hundreds of square kilometres (Lim *et al*., 2003; Dassot *et al*., 2011; Nguyen *et al*., 2016), but it also poses the challenge of how best to use these data to estimate aboveground carbon (Jucker *et al*., 2016). It has been demonstrated that top of canopy height (TCH), as measured by LiDAR, is a useful metric for estimating ACD of natural tropical forests and is relatively insensitive to sensor and flight specifications (Asner and Mascaro, 2014). However, the generality of TCH-based approaches to plot-aggregate carbon stock estimation has not been examined for oil palm plantations. There is current interest in developing individual-tree-based approaches to make greater use of the 3D information contained in airborne LiDAR data (Duncanson *et al*., 2013; Ferraz *et al*., 2016; Dalponte and Coomes, 2016). The tree-centric method is fundamentally similar to field-based approaches based on inventory plots (Coomes *et al*., 2002; Chen *et al*., 2015), so individual-based modelling has a strong theoretical basis (Shugart *et al*., 2015). Nevertheless, over- or under-segmentation of trees can lead to biases in biomass estimation (Coomes *et al*., 2017). To our knowledge, no study has used tree-centric approaches to map carbon in tropical plantations.

This paper develops methods for mapping the aboveground carbon density of oil palm plantations using LiDAR. Sabah has a larger percentage of oil palm plantation than any other state in the world (MPOB, 2016), so has become an important testbed to examine the effects

of oil palm plantations within human modified tropical landscapes. We compare the Dalponte and Coomes (2016) tree-centric approach with area-based methods (Asner and Mascaro, 2014; Coomes *et al*., 2017; Jucker *et al*., 2018a), and critically evaluate whether the advantages of working with individual trees outweigh any disadvantages associated with the accuracy of tree detection. We also explore the relationship between ACD and canopy gap fraction measured by LiDAR, and then use this finding to refine the area-based approach. Our study site contained plots with oil palm plantation that varied in age from 8 to 14 years at the time of sampling, providing an opportunity to test the generality of the approaches used.

4.3 Methods

4.3.1 The SAFE Degradation Landscape

The oil palm plantations are within the Stability of Altered Forest Ecosystem (SAFE) Project (4° 38′ N to 4° 46′ N, 116° 57′ to 117° 42′ E), located within lowland dipterocarp forest regions of East Sabah in Malaysian Borneo (Fig. 4.1). SAFE reflects Sabah's predominant land use change over the past decades, characterised by industrial harvesting and large-scale forest-to-palm conversions (Reynolds *et al*., 2011). The region has a tropical climate with high rainfall (>2000 mm/year) and varying topography, although all study plots are below 800 m altitude. The geology comprises a mixture of sedimentary rocks, including siltstones, sandstones and others that are easily eroded (Douglas, 1999).

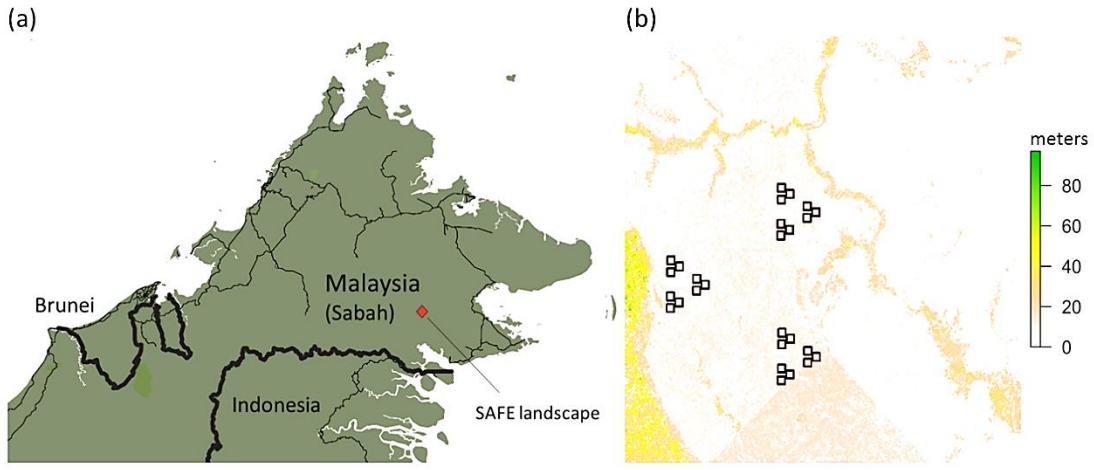

Figure 4.1 | Panel (**a**) shows the location of the Stability of Altered Forest Ecosystem (SAFE) landscape within Sabah, Malaysia and (**b**) the LiDAR Canopy Height Model (greener shades

corresponding to higher heights in metres) of the SAFE Project landscape including 27 plots located in oil palm plantations.

4.3.2 Field Data

Twenty-seven vegetation plots (25 m × 25 m, 0.0625 ha) with North–South orientation were set out at SAFE in 2010 using a Garmin GPSMap60 device. Vegetation plots were established according to a hierarchical sampling design based around a triangular pattern to assess regional forest attributes (Ewers *et al*., 2011). Plots were located at roughly equal altitude = 400 m and oriented to minimise potentially confounding factors such as slope. Oil palm is generally grown on fairly flat surfaces under Roundtable on Sustainable Palm Oil guidelines, recommendations from the Malaysian Palm Oil Board, and Standards for Oil Palm Production. On top of that, production on flat surfaces is higher. Therefore, these conditions will commonly be shared in oil palm plantations across SE Asia and are therefore valid. Plots were distributed among three oil palm plantation blocks of two different ages (OP1 and OP2 planted in 2006 and OP3 planted in 2000), henceforth referred to as 8-year-old and 14-year-old plots. In each 0.0625 ha plot, all oil palm individuals had their stem height measured in 2013 and remeasured in 2015; we used the average height between these years (Fig. 4.2). The average height and standard deviation (in metres) was 6.1 ± 2.3 for OP1, 5.4 m ± 1.5 for OP2 and 8.5 ± 2.0 for OP3. Palms have vascular bundles embedded in their trunks, in contrast to most tree species which have meristem cells just beneath their bark, so trunks do not increase in diameter as the trees grow taller. Thus, as secondary thickening does not occur in palm trees, we did not include tree diameter in our field measurements or biomass equation.

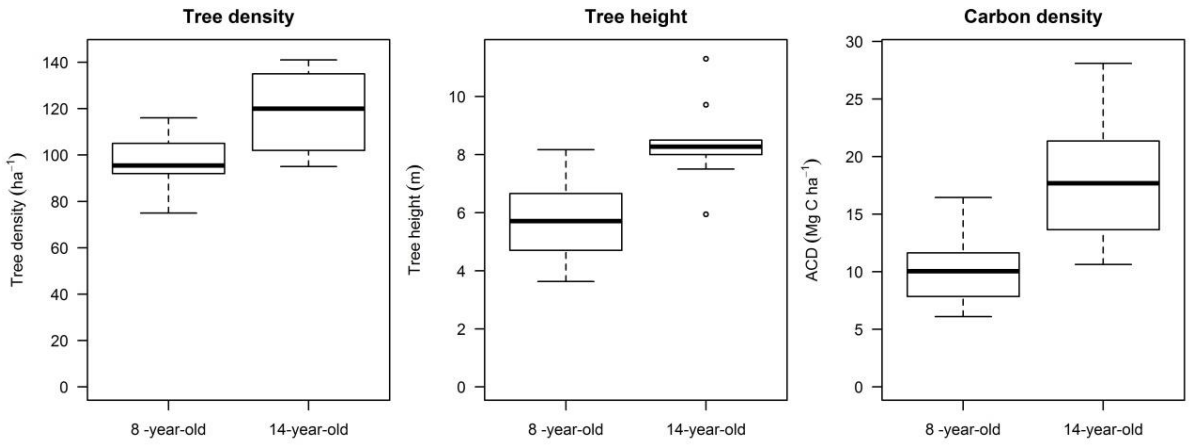

Figure 4.2 | Boxplots contrasting the structural attributes of oil palm plantations of two different ages (x axis), based on measurements taken in 27 1-ha plots. ACD is aboveground carbon density (Mg C ha^{-1}).

A 1-ha plot was created that was centred on each 0.0625-ha plot, to expand the plot size for aboveground carbon density calculations and minimize plot size effects on LiDAR model performance (Zolkos *et al*., 2013). We then used Earth Imaging data from the Pléiades satellite constellation (EADS Astrium), acquired over the SAFE landscape in June 2016, to visually count the tree density within each 1-ha plot. Pléiades data comprises a 0.5-m resolution panchromatic band, and four spectral bands (blue, green, red, and near infrared) with a 2.8 m spatial resolution, resampled to 2 m (Fig. 4.3a). The panchromatic band has sufficiently high resolution to distinguish the rows of trees in oil palm stands, as inter-row spacing is approximately 8 m. The average height of each 1-ha plot was assumed to be the same as in the 0.0625 ha plots, embedded at the centre. We recognise that spatial autocorrelation magnitude could impact the 1-ha plot data; however, we emphasize that the plots are not being used for landscape sampling, rather they are intended for calibration and validation purposes only. Areas within oil palm are all planted at the same time and managed in the same way, and are therefore likely to be extremely homogeneous.

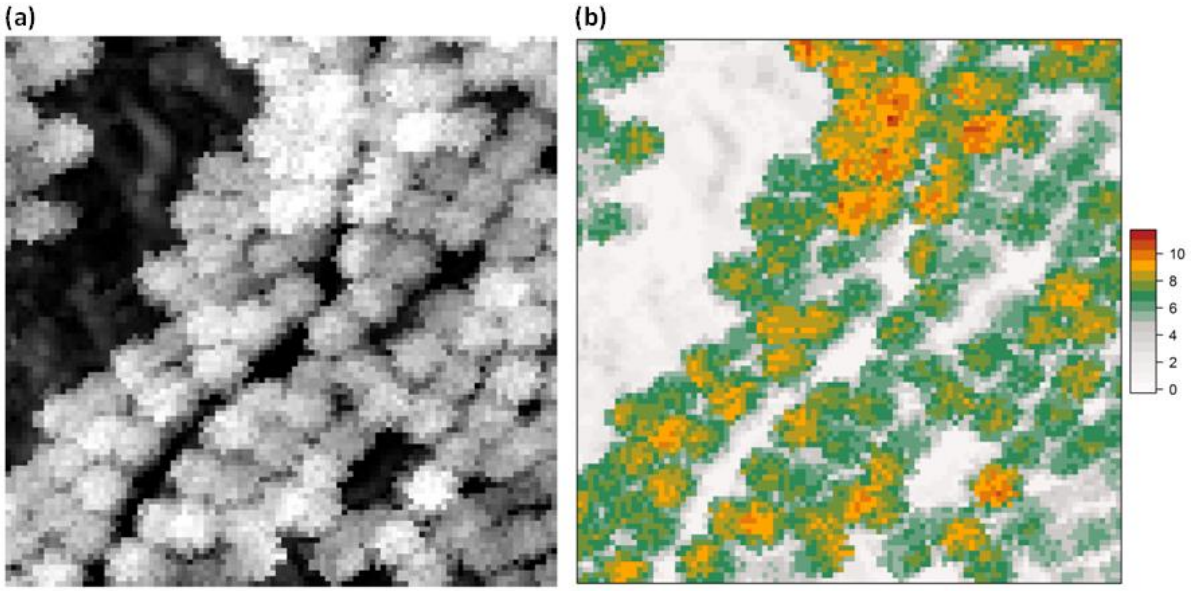

Figure 4.3 | (**a**) A monochromatic image from the Pléiades satellite constellation and (**b**) an airborne LiDAR image of a 1-ha plot to show a typical oil palm plantation canopy. The legend refers to height in metres of individual palms displayed on the LiDAR image.

4.3.3 LiDAR Data Acquisition and Processing

Airborne LiDAR data were acquired on 5 November 2014 using a Leica LiDAR50-II flown at 1850 m altitude on a Dornier 228–201 travelling at 135 knots. The LiDAR sensor emitted pulses at 83.1 Hz with a field of view of 12.0°, and a footprint of about 40 cm diameter. The average pulse density was 7.3 /m^2. The Leica LiDAR50-II sensor records full waveform LiDAR, but for the purposes of this study the data were discretised, with up to four returns recorded per pulse. Accurate geo-referencing of LiDAR point cloud was ensured by incorporating data from a Leica base station running in the study area concurrently to the flight. The LiDAR data were pre-processed by NERC's Data Analysis Node and delivered in standard LAS format. All further processing was undertaken using LAStools (http://rapidlasso.com/lastools/). Points were classified as ground and non-ground, and a digital elevation model (DEM) was fitted to the ground returns, producing a raster of 1 m resolution. The DEM elevations were subtracted from elevations of all non-ground returns to produce a normalised point cloud, and a canopy height model (CHM) was constructed from this on a 0.5 m raster by averaging the first returns. Finally, holes in the raster were filled by averaging neighbouring cells (Fig. 4.3b).

4.3.4 Estimating Tree- and Plot-Level Aboveground Carbon Density

Oil palm aboveground biomass (AGB_{palm}) was computed as dry mass in kg for each palm tree from its height (H) in metres using the equation of Thenkabail (2004):

$$AGB_{palm} = 37.47 \times H + 3.6334 \qquad \text{(Eqn. 4.1)}$$

Note, as explained above, palm trees do not increase in diameter as they increase in height, so the formula is based only on height. The average AGB_{palm} within the field plot was multiplied by the number of individuals counted in the 1-ha plots from the Pléiades images to give the total AGB within each 1 ha plot. A carbon content conversion factor of 0.47 was then applied, following Martin and Thomas (2011).

4.3.5 Area-Based Approach

Asner and Mascaro (2014) proposed a generalised approach to estimate ACD using top of canopy height estimated by LiDAR. As recommended by the authors, least squares regression was used to relate field measured TCH and ACD as follows:

$$ACD = a\,TCH^{b} \quad \text{(Eqn. 4.2)}$$

This model was fitted to data from the 27 1-ha SAFE plots and the estimates were obtained by leave-one-out cross validation. TCH was the mean height of CHM pixels within each 1-ha plot extracted using the raster package of R, while *a* and *b* are the parameters of the nonlinear model.

We also tested whether canopy cover (CC) - the proportion of area occupied by crowns at a given height aboveground - could be used as an alternative LiDAR metric to predict ACD. CC is calculated by creating a horizontal plane in the canopy height model (CHM) at height h above ground, and calculating the number of pixels for which the CHM lies beneath the plane divided by the total number of pixels in the plot. CC was calculated for h from 1 m to the maximum canopy height encountered in the plots (23 m). There were a few individuals of other tree species encountered in the 1-ha plots.

$$ACD = a\,CC^{b} \quad \text{(Eqn. 4.3)}$$

We also tested whether TCH and canopy cover could both be included as a predictor of ACD (Coome *et al*., 2017; Jucker *et al*., 2018a). The model requires accounting for multi-collinearity, considering that TCH is closely correlated to CC. This can be done by regressing one variable against the other, and replacing the variable with the residuals from the regression (Graham, 2003). We therefore first modelled the relationship between CC and TCH using logistic regression, validated the model using a leave-one-out procedure, and then used the residuals of this model (CCres in Equation. 4.4) to identify plots that have higher or lower than expected canopy cover for a given TCH. Equation 4.5 was used following Jucker *et al*. (2018a), who carefully compared alternative functional forms.

$$\mathrm{CCres} = \mathrm{CC} - \frac{1}{1+ e^{-\mathrm{dTCH} - \mathrm{f}}} \quad \text{(Eqn. 4.4)}$$

$$\mathrm{ACD} = \mathrm{a}\,\mathrm{TCH}^{\mathrm{b}}\,(1 + \mathrm{c}\,\mathrm{CCres}), \quad \text{(Eqn. 4.5)}$$

where lowercase letters indicate regression coefficients. To aid interpretation, Spearman rank correlation coefficients (*r*) between structural variables and area-based approach metrics were calculated to investigate the relationship of both average tree height and tree density with both TCH and CC LiDAR metrics.

4.3.6 Tree-Centric Approach

As an alternative to area-based approaches, we tested whether ACD could be estimated accurately by summing the biomass of individual tree crowns (ITCs). The *itcSegment* algorithm was used to delineate trees within each of the 27 plots and determine the tree heights and individual crown areas. *itcSegment* is implemented in R and made freely available on CRAN (https://cran.r-project.org/web/packages/itcSegment/index.html). It works by finding local maxima in the raster CHM, regarding these maxima as tree tops, then growing crowns around them by local searching of the raster CHM and point cloud. This approach was initially developed for coniferous forests (Dalponte *et al*., 2014; Dalponte and Coomes, 2016) following the concept of Nyström, *et al*. (2012), and modified in this manuscript to adapt to forests with low variation in height (i.e., oil palm plantations). The tree-centric approach consists of three stages (Dalponte *et al*., 2015): (1) a Guassian low-pass filter to smooth the canopy height model; (2) an iterative search for local maximum in the CHM, which are assumed to represent the tops of tree crown, using a window size that varied with the height of the CHM; we included a weighting exponent in the *itcSegment* function to increase the contrast in the CHM and found this greatly improved the accuracy of segmentation; (3) a region-growing step then searches for crowns around each local maximum, constraining the search with pre-determined crown width and depth information. The *itcSegment* algorithm has been upgraded in R after inclusion of the weighting exponent explained in stage 2.

The next step was to calculate a correction factor to account for the fact that the individual tree heights obtained by the ITC approach overestimated the oil palm tree heights, because large oil palm fronds arch up beyond the meristem at the top of the trunk, which were not accounted

for in field measurements. This correction factor was obtained by fitting a nonlinear regression as follows:

$$\overline{Hc} = a\,\overline{H_{ITC}}^{b} \quad \text{(Eqn. 4. 6)}$$

where $\overline{Hc}$ is the mean field-estimated height within the 27 0.0625 ha plots and $\overline{H_{ITC}}$ is the mean LiDAR-esimated height within the surrounding 1-ha plots, and *a* and *b* are parameters estimated by nonlinear least squares regression. The model was validated using the leave-one-out procedure.

The next step was to estimate individual biomass, by entering $\overline{H_C}$ values into equation 1. We then summed the AGB of segmented trees, and multiplied by a carbon density of 0.47 to obtain ACD estimates as before. The accuracy of the ITC delineation was assessed by comparing the numbers of delineated trees with the numbers observed in the field plots and ACD predicted from the summed individual biomasses.

Goodness of fit of models and the tree-centric approach are compared by reporting the normalised RMSE (%), calculated as $\sqrt{\frac{\sum(y-\hat{y})^2}{n}} \times 100/\bar{y}$, and bias (%) as $\sum(y - \hat{y}) \times 100/(N\bar{y})$, where y are the field data, $\bar{y}$ is the mean, $\hat{y}$ are the model estimates and N is the number of observations (Coomes *et al*., 2017).

4.4 Results

4.4.1 Relating LiDAR Metrics to Oil Palm Plantation Structure

Both LiDAR area-based approach metrics, top of canopy height and canopy cover, are correlated to tree density and average plot tree height (Fig. 4.4 a–d). Canopy cover (CC) at 3 m height was chosen after a comparison of different models that included heights between 1 and 23 metres, to include a few individuals other than oil palm trees within the 1-ha plots. Top of canopy height was more strongly influenced by height, whereas CC at 3 m was more influenced by tree density.

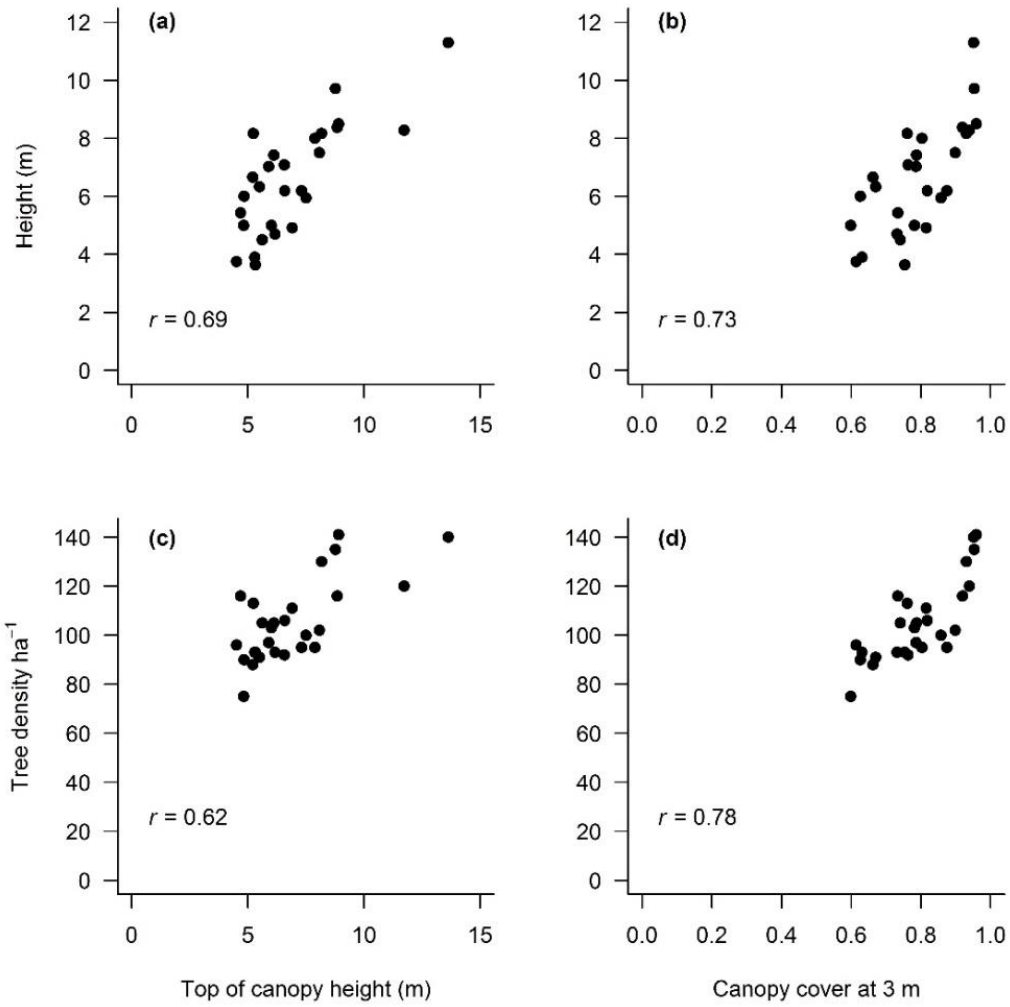

Figure 4.4 | Spearman correlation (*r*) between field-measured average tree height per plot and LiDAR-derived (**a**) top-of-canopy-height (TCH), and (**b**) canopy cover (CC) at 3 m height, as well as between field-measured tree density (#.ha^{-1}) and (**c**) TCH and (**d**) CC.

4.4.2 Area-Based Approaches

The local model obtained by fitting a power-law model to the data available from SAFE oil palm plantations yielded the following relationship between top of canopy height (TCH) and aboveground carbon density (Fig. 4.5a):

$$ACD_{HTC} = 1.494\ TCH^{1.107} \qquad \text{(Eqn. 4.7)}$$

A TCH exponent of just over 1 indicates a near-linear relationship between TCH and carbon density in oil palm plantations, as expected from the straight-line relationship between

individual biomass and height (i.e. Equation 4.1). The relationship between ACD and CC follows instead an exponential relationship (Fig. 4.5b)

$$ACD_{CC} = 22.991\ CC^{2.744} \quad \text{(Eqn. 4.8)}$$

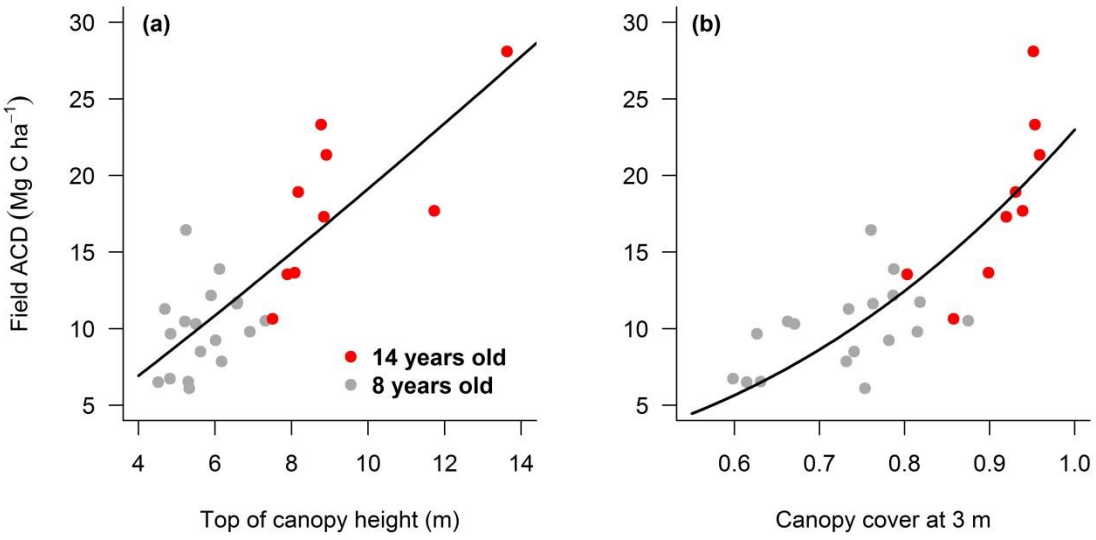

Figure 4.5 | Relationship between aboveground carbon density (ACD) and (**a**) top-of-canopy-height (TCH), and (**b**) canopy cover (CC) at 3 m height per plot for 8-year-old and 14-year-old plantations.

In comparison, when ACD was expressed a function of both TCH and residual CC, we obtained the following model:

$$ACD = 1.31\ TCH^{1.17}\ (1 + 3.52\ CCres) \quad \text{(Eqn. 4.9)}$$

where CC*res* can be obtained by subtracting the actual CC by the model that predicted CC from logistic regression with TCH as the predictor variable:

$$CCres = CC - \frac{1}{1 + e^{0.77\ TCH^{-0.37}}} \quad \text{(Eqn. 4.10)}$$

The model based on TCH generated unbiased ACD predictions with RMSE of 26.3%, whereas the model based on CC showed a bias of 1.2% with similar RMSE of 26.4%, with both models yielding an $R^2 = 0.62$ (Fig. 4.6a–b). The inclusion of both TCH and residual canopy cover into

the model reduced RMSE to 23.9% and improved the strength of relationship to $R^2 = 0.69$ (Fig. 4.6c). The predictions were obtained from the validation datasets using the leave-one-out procedure. Neither approach showed any trend with oil palm plantation age (e.g., plots deviating from the 1:1 line), which indicates that the equations can be applied to plantations of different ages and to faster and slower growing stands of the same age.

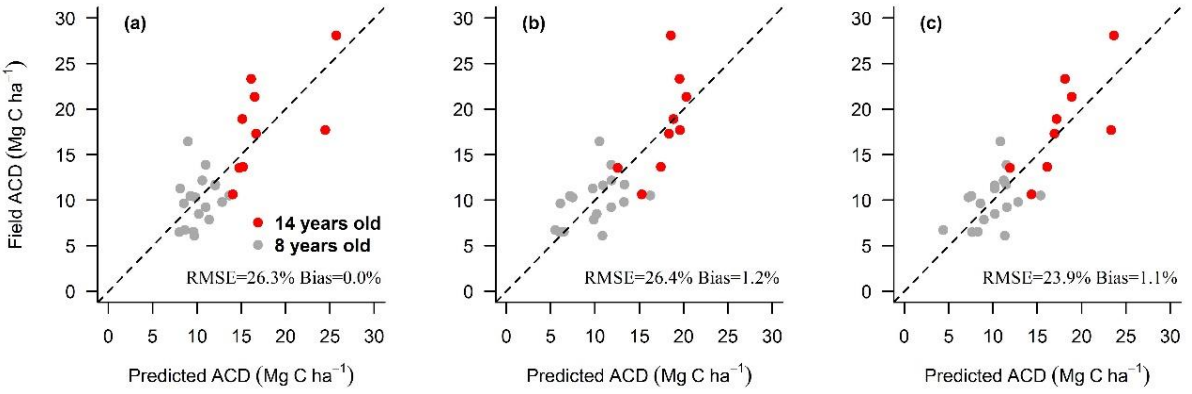

Figure 4.6 | Relationship between aboveground carbon density (ACD) estimated from field data and (**a**) ACD estimated from the leave-one-out cross validated datasets using LiDAR-derived top of canopy height (HTC), (**b**) canopy cover (CC) at 3 m, and (**c**) ACD estimated from TCH and residual CC at 3 m height per plot for 8-year-old and 14-year-old plantations. The 1:1 line is given for reference in both panels (dashed black lines).

4.4.3 Individual Tree Crown Approach

ITCsegment used variable window sizes when searching for local maxima, which avoided omitting small palms when the window was large, or over-segmenting large palms when the window was small (Fig. 4.7a). Heights obtained from the individual tree crown segmentation (H_{ITC}) included the upward pointing fronds of palms. The relationship between stem height and H_{ITC} (Fig. 4.7b) was:

$$Hc = 0.61\ H_{ITC}^{\ 1.02} \qquad \text{(Eqn. 4.11)}$$

This equation was used to predict the tree stem height (Hc) of all trees in the plots, from their segmented heights.

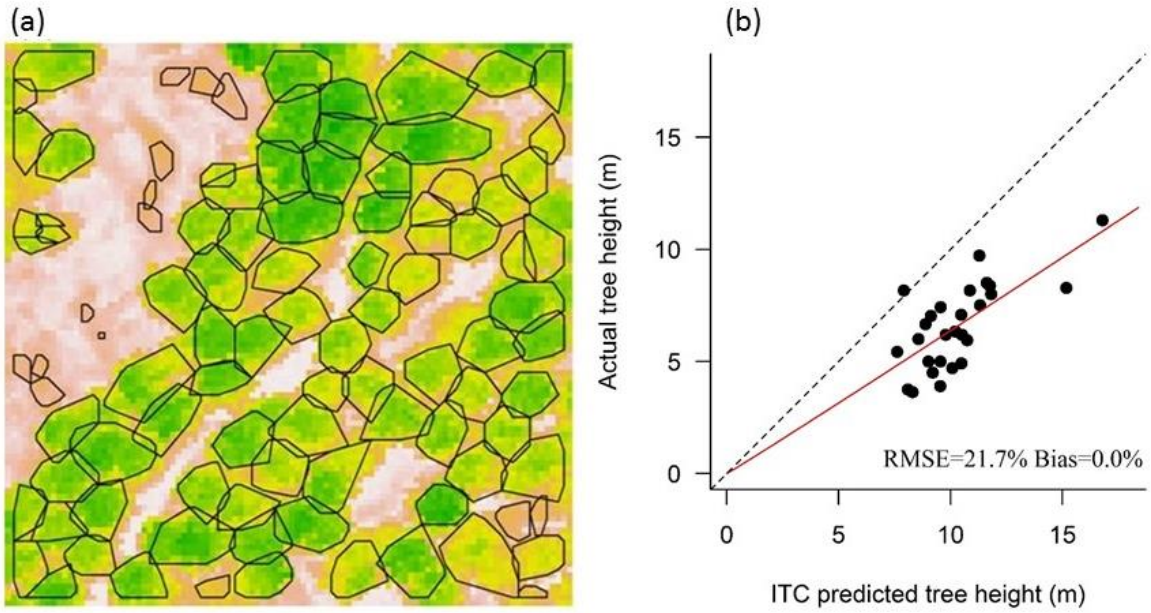

Figure 4.7 | a) Detection of individual tree crowns in a 1-ha plot LiDAR imagery using *itcSegment* (Dalponte and Coomes, 2016) for oil palm plantations; b) The relationship between tree stem height obtained from field data and tree height obtained from the individual tree crown segmentation (H_{ITC}). The regression line fitted to all 27 plots is shown as a red line and the 1:1 line as a black dashed line.

A comparison of the number of delineated trees with the tree density obtained from the Pléiades optical imagery was used to estimate the accuracy of the ITC delineation for all the 1-ha plots (Fig. 4.8a). ACD of individual oil palm trees was summed to estimate plot ACD at the 1-ha plot level (Figure 8b). The ITC approach gave a percentage RMSE of 25.9% and was biased (−11.6%), showing a slight trend from over-estimation of lower carbon density values and under-estimation of higher carbon density values.

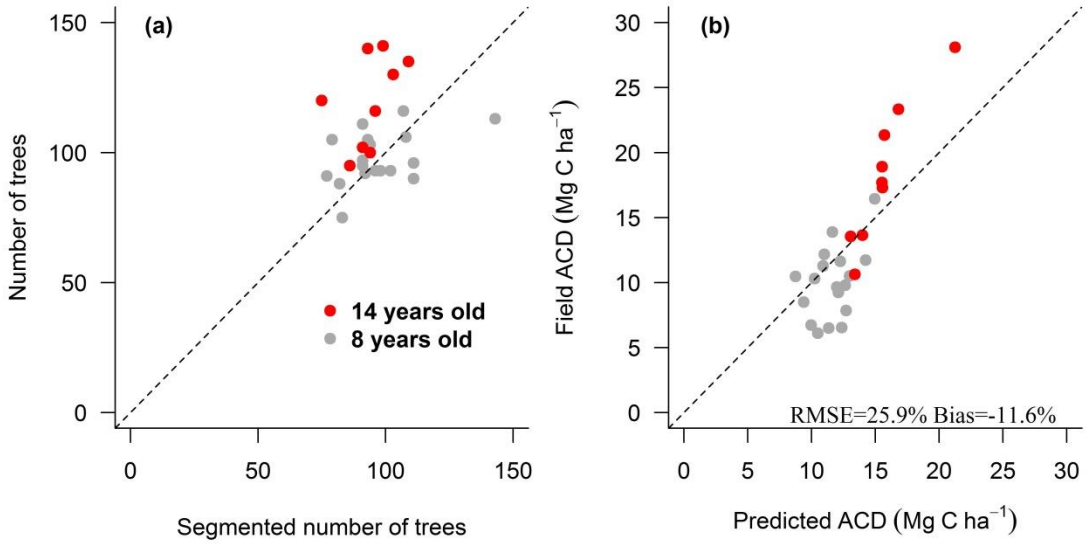

Figure 4.8 | Relationship between (a) the number of trees in the 1-ha plots estimated from Pléiades optical imagery and number of trees obtained from the LiDAR-derived individual tree crown (ITC) segmentation approach, and (b) aboveground carbon density predicted from the ITC approach and ACD estimated from field data for 8-year-old and 14-year-old plantations. The 1:1 line is given for reference in both panels (dashed black lines).

4.5 Discussion

We have demonstrated that the ACD of oil palm plantations can be assessed accurately using airborne LiDAR and can give better results compared to estimates using satellites (Morel *et al*., 2011). Our ACD estimates of 10.0 Mg C ha^{-1} for a 8-year-old plantation and 18.3 Mg C ha^{-1} for a 14-year-old plantation are similar to those reported in previous studies. mean ACD of oil palm in the SAFE landscape was estimated as 17.9 Mg C ha^{-1} by Pfeifer *et al*. (2016) using optical satellite imagery (age of stands not distinguished), while elsewhere in Sabah, the ACD of a 3-year-old oil palm plantation was given as 1.1 Mg C/ha, rising to an average value of 24.4 Mg C ha^{-1} for plantations ranging from 4 to 19 years old (Morel *et al*., 2011).

Area-based approaches yielded more accurate carbon stock predictions in oil palm plantations than the tree-centric approach. ACD predictions were most accurate when incorporating both TCH and canopy cover as predictors (Simonson *et al*., 2016). Power-law modelling incorporates basal area and wood density relating to TCH; however, our function assumes that wood density and basal area are both constant, as the field biomass equation that was used to

predict individual biomass, used tree height only. Coomes *et al*. (2017) found that the crown area of each forest tree scales with its basal area, so the gap fraction at ground level of a plot is negatively related to the basal area of its trees. The authors also showed that incorporating canopy cover in tropical forests into ACD models gave more accurate results, as ACD is more closely related to basal area than to height. However, secondary thickening does not occur in palm trees, with basal area increase instead being due to division and enlargement of parenchyma cells (Mauseth, 2012). Thus, cover fraction is not necessarily correlated to basal area, but more dependent on tree density and height. When incorporating both TCH and CC, the model yielded better results as a result of complementarity, by taking into account the high correlations between tree height and TCH as well as with tree density and CC.

The tree-centric approach was less accurate. It showed a slight tendency to over-estimate the number of trees in younger plantations. A likely reason for this over-segmentation is overlap of palm crowns of similar heights. In mature plantations, crowns were more likely to be connected to other tree crowns, making them difficult to distinguish and resulting in miscounting of trees. Other studies focussing on tropical rainforests have also found the tree-centric approach to perform slightly less well than area-based methods (Coomes *et al*., 2017; Ferraz *et al*., 2016), due to over-segmentation of emergent trees and incomplete detection of sub-canopy trees. Here, the problem is instead the under-segmentation of large crowns, which merge into one another, owing to their similar height.

Although the tree-centric approach gives less accurate results, it can still be advantageous to segment individual trees for precision agriculture (McBratney *et al*., 2005), particularly in oil palm plantations as individual trees are long-lived. Field-based tree counting is labour intensive, and the use of remote-sensing using high-resolution optical imagery from satellites has been suggested as a cost efficient alternative (Jusoff and Pathan, 2009). A semi-automatic technique to count oil palm trees using high-resolution airborne imaging spectrometer data has also been developed (Shafri *et al*., 2011), and LiDAR has been used to detect and classify oil palm diseases (Khosrokhani *et al*., 2016). The detection of diseases, such as the Ganoderma basal stem rot, using airborne spectral imagery (Shafri and Hamdan, 2009) and space-borne multispectral sensors (Santoso *et al*., 2011) has also been demonstrated.

The Roundtable on Sustainable Palm Oil, the major accreditation body for sustainable palm oil production, recognises the importance of developing approaches for growers to monitor

emissions across their estates. However, it has been recognised that emission cannot be monitored completely, or accurately, using current methodologies (RSPO, 2013). Studies indicate that remote sensing missions should estimate carbon with an error within 20% of field estimates (Houghton *et al*., 2009; Hall *et al*., 2011). Both area-based and individual tree-centric approaches offer reliable opportunities to map oil palm plantation ACD, within acceptable standards of estimation. High-resolution LiDAR techniques are a reliable tool to collect reference data, in order to decrease the uncertainty associated with satellite-based mapping projects. It is through the integration of optical and samples of LiDAR data, based upon the above findings, that measures in support of carbon sequestration programs may be generated.

4.5.1 Conclusions

Area-based modelling proved more effective at mapping ACD in oil palm plantations than a more sophisticated tree-centric approach. Using both canopy cover and top-of-canopy height in the model generated the most accurate ACD predictions. Canopy cover is related primarily to tree density and secondarily to tree height, so provides complementary information to TCH and improves accuracy. The tree-centric approach underestimated the density of trees, particularly in older plantations, because tree crowns were overlapping and our segmentation algorithm recognised overlapping crowns as a single tree. Nevertheless, the tree-centric approach may prove useful in the future for detecting individual trees and for monitoring growth and foliar properties.

4.6 Authors' Contributions

Study design: David Coomes, Rob Ewers, Ed Turner. *Data collection*: David Coomes, Rob Ewers, Ed Turner. *Data analysis*: Matheus Nunes. *Manuscript writing*: Matheus Nunes with support from all the co-authors.

Chapter 5 | Extensive leaf loss of tropical forests during an El Niño, with fragmented edges, primary forests and hilltops most affected

5.1 Abstract

Droughts associated with El Niño Southern Oscillation (ENSO) events can lead to leaf loss, tree mortality and lower productivity in tropical rain forests, but what remains unclear is how and why drought impacts vary across tropical landscapes. Here, we use repeat airborne LiDAR surveys conducted before and after the strong ENSO event of 2015-16 in Malaysian Borneo to produce high-resolution maps of canopy height change across 25,000 ha of a human-modified tropical landscape which encompasses the world's largest forest fragmentation experiment. We hypothesise that forest fragmented communities and those on ridge-tops would be most affected by the ENSO, whereas mature forests in damp valley bottoms would be more resilient. We found that following the El Niño canopy profiles increased 0.19 - 0.23 m, however there was a strong environmental filter on the vegetation response to the El Niño event. As predicted, forests near fragment edges and tall forests (i.e. primary or slightly logged forests) were particularly susceptible to the El Niño – with canopy height decreasing by 0.4 - 0.6 m within 450 m from the edges, and canopy losses of 0.1 - 0.2 m of forests > 20 m in canopy height. Topography also had a significant effect on forest growth, with those on hilltops virtually presenting no growth (0 - 0.2 m). Long-term tree census and leaf area index data revealed that these changes in canopy height were primarily driven by leaf shedding rather than tree aboveground biomass (AGB) change, which is consistent with a short-term physiological response owing to increased atmospheric water pressure deficit. The El Niño did not affect negatively AGB, which kept positive change rates after two years following up the climatic event. By mapping landscape-scale variation in forest responses to microclimate and regional climate variations, our study demonstrates that primary forests are more susceptible to extreme climatic events whereas secondary forests can be resilient even under high temperatures and atmospheric dryness of the understory.

5.2 Introduction

El Niño is a natural phenomenon that creates periods of water shortage in regions where water is typically plentiful. The Southern Oscillations responsible for El Niño events have occurred for at least 130,000 years (Tudhop et al., 2001), suggesting ample opportunity for natural selection of trees capable of tolerating irregular drought events, which occur at frequencies far greater than their lifespans (Harrison, 2000; Detto et al., 2018). However, there is concern that anthropogenic climate change is increasing the frequency and intensity of El Niño events (Thirumalai et al., 2017,Wang et al., 2017), which has the potential to shift tropical forests from net carbon sinks to sources due to increased tree mortality and decreased productivity during drought (Gatti et al., 2014; Qie et al., 2017; Zuleta et al., 2017; Greenwood et al., 2017; Mitchard, 2018). In particular, increased air temperatures cause greater evaporative demand, resulting in greater water stress even if rainfall patterns remain unchanged (Weiss et al., 2009; Clark et al., 2010; Allen et al., 2015). There is mounting evidence that drought events in a warming world are having catastrophic effects on forests in many regions of the world (Asner et al., 2016; Liu et al., 2013; Williams et al., 2010; Williams et al., 2013). However, we still have a poor understanding of how tropical forests in different regions are responding to climate change (Huntingford et al., 2013), particularly because rainforest species vary in resilience (Nepstad et al., 2002; Doughty et al., 2015; Santos et al, 2018) and rising CO_2 concentrations may allow trees to use water more efficiently (Norby et al., 2005). Stomatal regulation and plant physiological response strongly regulate evapotranspiration, and responses to drought may vary from leaf shedding (Wolfe et al.,2016), decreased productivity (Coomes and Grubb, 2000; Phillips et al., 2009) to widespread death of trees (Phillips et al., 2009; Saatchi et al., 2013). Understanding how tropical forests respond to extreme drought events has therefore emerged as a key priority if we are to forecast the impacts of climate change on the terrestrial carbon cycle (Mitchard 2018; McDowell et al. 2018), given that anthropogenic warming will emerge sooner in the low latitudes (Thirumalai et al., 2017).

A key challenge to predicting the impacts of drought on tropical forest carbon cycling is that we lack a quantitative understanding of how responses to drought vary across landscapes and why. For instance, anthropogenic disturbance such as fragmentation and selective logging can have significant effects on forest responses to drought (Huang and Asner, 2010; Baccini et al., 2017; Putz et al., 2012; Qie et al., 2017; Brinck et al., 2017), although these human-modified landscapes have received much less attention than intact forests – even though they are the new

norm (Malhi et al., 2014). Although logged forests are reported to have more accelerated woody growth rates (McMahon et al., 2010; Pretzsch et al., 2014; Riutta et al., 2018), the dynamics of secondary forests are also being impacted by droughts associated with changing climate (Anderson-Teixeira et al., 2013; Uriarte et al., 2016). These disturbed forests can be vulnerable to global warming because such changes increase evapotranspiration, leading to depleted soil moisture and creating stresses for drought-sensitive plants (Laurance 2004). Conversely, higher competition for water in forests with high aboveground biomass can have a strong influence on the response to drought (Young et al., 2017). Local topography also modulates soil and air moisture conditions, thereby impacting on population-level responses to drought (Slik, 2004; Itoh et al., 2012; Zellweger et al., 2013; Méndez-Toribio et al., 2017; Jucker et al., 2018b). Response of vegetation to drought associated with topographic variation is dependent on the tolerance of species, and forests can be more (Itoh et al., 2012) or less (Slik 2004) prone to mortality in wetter areas of the landscape. This tolerance is mediated by species-specific traits that induce enormous variation from leaf turgor loss point (Maréchaux et al.,2015), leaf shedding to refilling cavitated xylem (Nepstad et al., 2002; Doughty et al., 2015; Santos et al, 2018). However, the role of topography and forest disturbance in shaping canopy dynamics during an El Niño event has not been explored spatially because the scales of variability from local to regional levels are difficult to measure.

Here we investigated the immediate effects of El Niño (i.e. high temperatures and droughts leading to higher evaporative demand) on human-modified tropical forests in Borneo using repeat-LiDAR surveys across 250 km^2. The surveys fell immediately before and after two back-to-back El Niño droughts in 2015 and 2016, which were particularly severe due to the exacerbating effects of global warming (Thirumalai et al., 2017). By combining LiDAR-derived maps of canopy height change and local topography with field measurements of tree demography and leaf dynamics time-series across the world's largest forest fragmentation experiment, we tested whether: 1) El Niño would impact forest canopies through aboveground biomass change or leaf shedding; 2) the effects of drought would be greatest near forest edges and in logged forest; 3) valleys and low-lying areas would be less affected. The extreme droughts led by high temperatures in 2015 and 2016 owing to global warming exacerbating the El Niño effects in Southeast Asia, in combination with spatially continuous high-resolution canopy change, microclimatic and topographic data documenting regional forest processes, make the region an ideal natural experimental target for examining the immediate influence of extreme climatic events on forest canopies with unprecedented detail.

5.3 Material and methods

5.3.1 Study site and El Niño event

The study is located in Sabah, Malaysian Borneo, within a region dominated by logged forests and oil palm plantations (4 38' N to 4 46' N, 116 57' to 117 42' E). Few regions have seen such rapid and extensive transformation as Borneo, where 163,000 km^2 (30%) of forest cover was lost between 1973 and 2010 (Gaveau et al., 2014). By 2009, 28% of the original forest area of Sabah and Sarawak had been converted to plantations, predominantly oil palm, and 72% of the remaining forest area had been selectively logged (Bryan et al., 2013), radically altering forest composition and structure (Shima et al., 2018). The study area also encompasses the world's largest forest fragmentation experiment, the Stability of Altered Forest Ecosystems (SAFE) Project, located in an area gazetted for conversion to oil palm: as the plantations are established, patches of logged forests are being protected as part of an experiment seeking to establish the consequences of fragmentation on biodiversity and ecosystem functioning (Ewers et al., 2011). The SAFE Project site connects a 2200 ha of a lightly disturbed Virgin Jungle Reserve (VJR) forest to a large area of degraded forest (over 1 million ha), most of which has been through one to three rotations of selective logging. Logging intensity varies greatly over small scales due to differences in topography, proximity to roads and quality of the timber, which has created a complex mosaic of heavily to moderately logged sites (Pfeifer et al., 2016; Riutta et al, 2018). The forest modification gradient reproduces the real-world pattern of habitat conversion in Borneo, ensuring that phenomena observed in the study should be directly pertinent to policy issues in the region.

Eastern Sabah typically has an aseasonal climate. We used monthly mean precipitation (mm hour-1) data for the SAFE region estimated by the Tropical Rainfall Measuring Mission (TRMM, 3B43 version 7). Between January 2000 and December 2014, the average annual rainfall (± standard error) was 2,827± 350 mm. However, the region experienced severe droughts between January 2015 and April 2016 linked to El Niño, with average monthly rainfall of 169 ± 61 mm compared with the long-term average of 235 ± 61 mm. Exceptionally high temperatures observed in April 2016 were the result of El Niño combined with global warming (Thirumalai et al., 2017).

5.3.2 Airborne laser scanning: data acquisition, fusion and height change estimation

The first LiDAR data were acquired in November 2014 using a Leica ALS50-II LiDAR sensor flown by NERC's Airborne Research Facility. Data acquisition parameters are described in detail in Jucker *et al*. (2018a). The second LiDAR survey was conducted by the Carnegie Airborne Observatory-3 (CAO; Asner *et al*., 2012a) in April 2016. The juxtaposed area with repeat LiDAR flights were 24,120 ha. Data acquisition parameters for the second flight are described in detail in Asner *et al*., 2018. Sensors of both flights record full waveform information, but for the purposes of this study the data were discretised, with up to four returns recorded per pulse. Average pulse density of the first flight was 7.3 m^{-2} with some pulse density reaching values near 0 m^{-2}, whereas settings of the second flight were selected to achieve a minimum pulse density of 1.14 pulses m^{-2}.

We used the LAStools (rapidlasso, GmbH; Gilching, Germany) suite of computational tools to identify ground points and interpolate ground and upper canopy returns into 2 m resolution maps of bare-earth ground elevation (DEM) and top-of-canopy height above ground (TCH) for each flight line d the LAStools (rapidlasso, GmbH; Gilching, Germany) suite of computational tools to identify ground points and interpolate ground and upper canopy returns into 2 m resolution maps of bare-earth ground elevation (DEM) and top-of-canopy height above ground (TCH) for each flight (Figure 5.1a).

All further processing was undertaken using LAStools software (rapidlasso GmbH, Germany). To minimize errors in the fusion of both datasets, a common digital terrain model (DTM) at 1 m resolution was created using a combination of ground returns from both surveys. Using a TIN-densifying algorithm available in "lasground" tool, ALS returns were classified as ground and non-ground, and their heights above ground were calculated by subtracting the elevation of the resulting DTM underneath each of them. Then a canopy height model (CHM) representing the height of vegetation was generated separately for each survey, following the methodology outlined by Khosravipour *et al*. (2014), and top-of-canopy height aboveground (TCH) was initially calculated as the mean CHM at 2 m resolution. From the two LiDAR measurements of TCH obtained in 2014 and 2016, namely hereafter as TCH before (TCH_i) and TCH after (TCH_f) the El Niño, TCH change (TCH_{Change}) at each 2 × 2 m cell over the wider SAFE landscape was calculated as $TCH_f - TCH_i$ (Figure 5.1c)

Since ALS estimates of TCH increase asymptotically with pulse density (Silva *et al*., 2017), biases arising from differences in pulse density were removed using the approach of Roussel *et al*. (2017), as explained in supplementary information (S1). Variance of (TCH_{Change}can be overestimated owing to artefacts of repeat LiDAR data such as wind direction and within-canopy variation. TCH map was then resampled until resampling would no longer affect variance (See Supplementary Information). We found that 30 m resolution is the sample size that TCH_{Change} distribution is no longer affected by pixel size. A small number of outliers that may have resulted from anomalies in the processing of the DTM and TCH or small misalignments were still detected, and thus we trimmed 1% of the maximum positive change and 1% of the maximum negative change with the intention to eliminate unrealistic values of TCH change.

5.3.3 Mapping topography and distances from edge

A map of topographic position index (TPI) was generated from the combined LiDAR-derived DTM (Figure 5.1b). TPI describes the height of a pixel relative to the surrounding landscape and ranges from negative where the terrain is concave (i.e. valleys) to positive where it is convex (i.e. ridges). TPI was calculated by first coarsening the resolution of the DTM to 10 m by spatial averaging, then point mean values were extracted at 1 ha as in Jucker *et al*., 2018b.

Satellite imagery was used to classify land use, and calculate distance from edges. Earth Imaging data from the Pléiades satellite constellation (EADS Astrium), acquired over the SAFE landscape in June 2016, were classified visually to define boundaries between forest and plantations. Pléiades data comprise a 0.5-m resolution panchromatic band, and four spectral bands (blue, green, red, and near infrared). The panchromatic band has sufficiently high resolution to distinguish forests, oil palm plantations and clear-cut logging. Oil palm plantations did not expand between both flight times, however recently clear-cut areas between flights were easily identified by their large drops in canopy height and near-zero height in 2016. Care was taken to avoid considering the forest edges that were recently created by clear-cut logging into the analysis. Pixels within 200 m of the clear-cut areas were then removed from the analysis as they could be a source for disturbance during the survey. Distance of each pixel to these boundaries (D_{Edge}) was finally calculated using the gDistance function from the rgeos package in R, with values ranging from 0 to 4000 m distance.

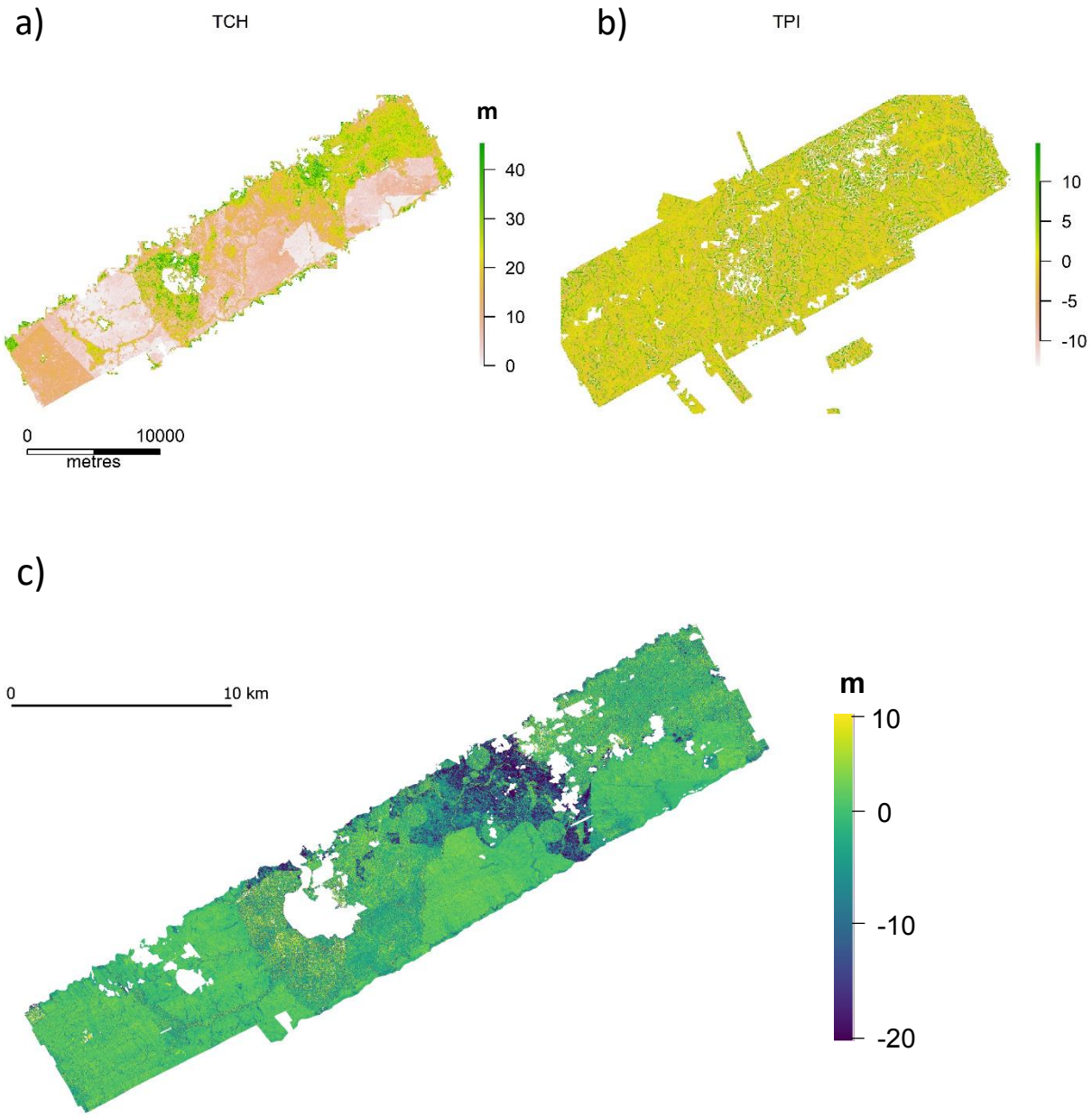

Figure 5.1 | Variation in a) top-of-canopy height (TCH), b) topographic position index (TPI) and c) TCH change across the Stability of Altered of Altered Forest Ecosystems (SAFE) landscape at 2 x 2.

5.3.4 Field data used to elucidate mechanisms

Canopy height loss recorded by LiDAR could be a response to leaf loss, branch loss or tree death, while height gain could arise from leaf gain or upward stem growth. We used field data from 38 permanent plots established through the SAFE project (each 25 x 25 m in size) to assess which factors were driving the changes observed by LiDAR. The centre of each plot

was geolocated using hand-held Garmin GPS device, and mean top-of-canopy height observed by LiDAR for each plot was used for bivariate comparison with aboveground biomass (AGB) growth, AGB mortality, AGB change, crown area weighted height and field microclimatic variables.

Growth, death and biomass change: Estimates of canopy height and aboveground carbon density were made in the permanent forest plots in 2013, 2014, 2015, 2016 and 2017 (Jucker et al., 2018a). Stem diameters at 1.3 m height (*DBH*), or immediately above buttresses, of all trees > 10 cm *DBH* were measured in these plots. We excluded trees exhibiting extreme diameter growth, defined as trunks where *DBH* increased by ≥ 5 cm yr^{-1} or that shrank by ≥ 12 *s*, where *s* is the standard deviation of the *DBH* measurement error, $s = 0.9036 + 0.006214\ DBH$ (see Condit et al., 2004; Condit et al., 2006; Stephenson et al., 2014); outliers of these magnitudes were almost certainly due to recording errors. An *H-DBH* allometric equation was locally calibrated to estimate total tree height (*H*) for individuals with no height measurement in the field (Eq. S2; see Supplementary Information). Aboveground carbon density in these plots was estimated using the BIOMASS package in R, which draws on global databases of wood density and allometry to makes its estimates, and accounts for uncertainty associated with both field measurement errors and uncertainty in allometric models (Réjou-Méchain et al., 2017). We firstly estimated aboveground biomass of individual trees (in Mg) using Chave et al's (2014) pantropical biomass equation: $AGB = 0.0673 \times (D \times H \times D^2)^{0.976}$. The *WD* was either attributed to an individual at a species, genus, family or stand level. Given data from two censuses, annual productivity was calculated as the *AGB* growth of all stems present in both censuses, annual mortality was the *AGB* lost in dead trees, and annual *AGB* change was the net gain all corrected for a one-year period. We then used a non-parametric bias-corrected and accelerated bootstrapping to generate 95% confidence intervals (resampling plots 999 times with replacement).

Canopy height growth: We apply a crown-area weighted height suited for LiDAR applications (Pang *et al*., 2008), where the height of each individual tree is weighted by the projected crown area, to compare field and LiDAR-based top-of-canopy heights. Since the upper canopy surface measured by LiDAR consists primarily of the tallest dominant and codominant trees, we are then able to minimise the influence of smaller stems that are incorrectly included as dominant or codominant stems. We first fitted allometric relationships between *DBH* and crown area using non-linear least-squares regression (Eq. S2; see Supplementary Information) and the

crown area of all trees with missing crown information was then estimated from their *DBH* values. The height of each tree was weighted by its proportional contribution to total crown area to calculate mean TCH as in Kent *et al*. (2015).

Canopy openness: Hemispherical photographs were taken at 2 different heights (ca 1 and 2 m) at 17 locations on each plot on a yearly basis using Sigma 4.5 mm f/2.8 EX DC HSM circular fisheye lens. The photos were then adjusted in Adobe Photoshop CC 2018, classified in *ImageJ* 1.51j8 (sky 0, vegetation 1) using Auto Threshold and IsoData methods, and converted to binary bmp files. The R package *cimesr* was used to calculate: 1) total gap which is unweighted canopy openness, and 2) weighted canopy openness for zenith angles 60° and 90°. When computing canopy openness, 40 zenith bands and 150 sectors were used; more details on calculation can be found in *cimesr* package documentation.

Microclimate: Air temperature (T, in °C) and relative humidity (RH, in %) were measured across a network of 113 permanent forest plots (each 25 × 25 m in size) established through the SAFE project (see Jucker *et al*., 2018c). These plots also include all the plots where tree measurements were conducted. Suspended Hygrochron iButton loggers (Maxim Integrated, USA) at a height of 1.5 m above the ground and shielded from direct solar radiation were used to record hourly T and RH readings in each plot (accurate to ± 0.5 °C and ± 5 %, respectively). Microclimate data were collected between May 2013 and May 2016, resulting in a total of 953,789 coupled T and RH readings. However, only measurements from January 2014 to December 2014 prior to the start of El Niño-induced droughts were used to investigate whether extreme events have exacerbated effects on forests that usually reach higher temperatures and lower RH (see Thirumalai *et al*., 2017). From the hourly temperature records we calculated mean annual temperature (T_{mean}), mean maximum daily temperature (T_{dmax}) and maximum annual temperature (T_{max}), variables directly related to biological activity across a range of taxonomic groups of tropical forests (Clarke, 2017). We used the microclimate data to characterize atmospheric water balance by estimating Vapour-Pressure Deficit (VPD, in hPa). VPD is the difference between the saturation water vapour pressure (e_s) and the actual water vapour pressure (e), or atmospheric dryness. Given that $RH = e/e_s \times 100$, VPD can be expressed as $[(100 - RH/100)] \times e_s$, where e_s is derived from T using Bolton's (1980) equation: $e_s = 6.112 \times e^{17.67 \times T/[T+243.5]}$. Having estimated VPD for each coupled hourly observation of T and RH, we then calculated annual mean VPD (VPD_{mean}), mean daily maximum VPD (VPD_{dmax}) and maximum annual VPD (VPD_{max}) for each study plot.

5.3.5 Landscape drivers of canopy height change during drought

ΔTCH was modelled as a non-linear function of D_{Edge}, TPI and TCH_i. After comparing various alternative models (using AIC) the following was selected:

$$\Delta\mathrm{TCH}_i = \beta_0 + \beta_1 TPI_i + \beta_2 TCH_{i_i} + \beta_3 \, \mathrm{e}^{-\beta_4 * D_{Edge_i}} + \varepsilon_i, \qquad \text{(Eqn. 5.1)}$$

where β_0 to β_4 are the model parameters and ε_i is the normally-distributed residual error. The model was fitted using the nlme R package (Pinheiro et al, 2016) and only variables with P-value ≤ 0.05 were selected. We recognise that spatial autocorrelation could result in a slight underestimation of the true uncertainty in the fitted parameter values. A spatial correlation structure was first generated using the function *corSpatial* in R with a randomised sample of 3000 pixels to investigate whether $\Delta\mathrm{TCH}_i$in was spatially correlated. Then we replicated the model 1000 times to obtain the mean and 95% confidence interval of the model parameters.

5.4 Results

5.4.1 Canopy height loss driven by leaf shedding and lower productivity

Local average maximum daily temperature and average maximum daily Vapour-Pressure Deficit (VPD), in other words the difference between how much moisture the air can hold before becoming saturated and the amount of moisture actually present in the air) obtained from a network of permanent forest plots between 08 May 2013 and 03 August 2017 indicate the increased temperature and atmospheric dryness in the region during the second LiDAR flight and marking the end of the 2015/2016 El Niño (Figure 5.2).

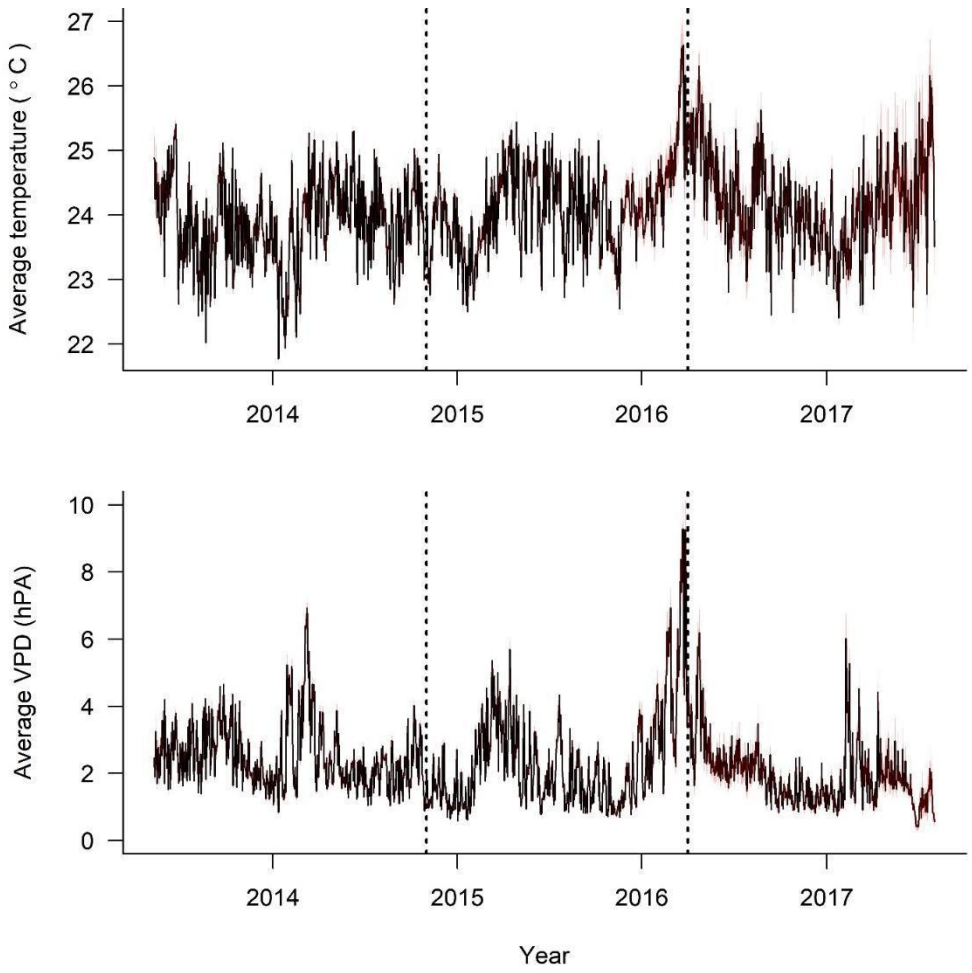

Figure 5.2 | Local average daily temperature and average daily Vapour-Pressure Deficit (VPD). Air temperature (in °C) and relative humidity (RH, in %) were measured across a network of 129 permanent forest plots (each 25 × 25 m in size) between 08 May 2013 and 03 August 2017. We used the microclimate data to characterize atmospheric water balance by estimating VPD (in hPa). VPD, or atmospheric dryness, is the difference between the saturation water vapour pressure and the actual water vapour pressure – in other words the difference between how much moisture the air can hold before becoming saturated and the amount of moisture actually present in the air. Dashed vertical lines represent the LiDAR surveys in November 2014 and April 2016.

Top-of-canopy height increased 0.19 – 0. 23 m (95% confidence interval from bootstrapping) during the El Niño event on Borneo. Variation in top-of-canopy height can be an artefact of leaf shedding or flushing, as well as variation in aboveground biomass as a result of mortality and woody growth. Overall, there was no evidence that AGB change was negatively affected by El Niño (Figure 5.3). Long-term measurements between 2011 and 2018 revealed annual

AGB change rates of 1.0 – 5.1 Mg ha^{-1} year^{-1} in December 2015 and 0.7 – 4.1 Mg ha^{-1} year^{-1} after the El Nino in September 2016, similar to the annual AGB change rates observed immediately in November 2014 of -0.7 – 4.7 Mg ha^{-1} year^{-1}. Two plot networks of tree measurements in early 2018 revealed higher annual AGB change rates post-El Niño of 2.0 – 6.1 and 5.8 – 12.5 Mg ha^{-1} year^{-1}, which indicate that mortality did not increase as a response to the climatic event.

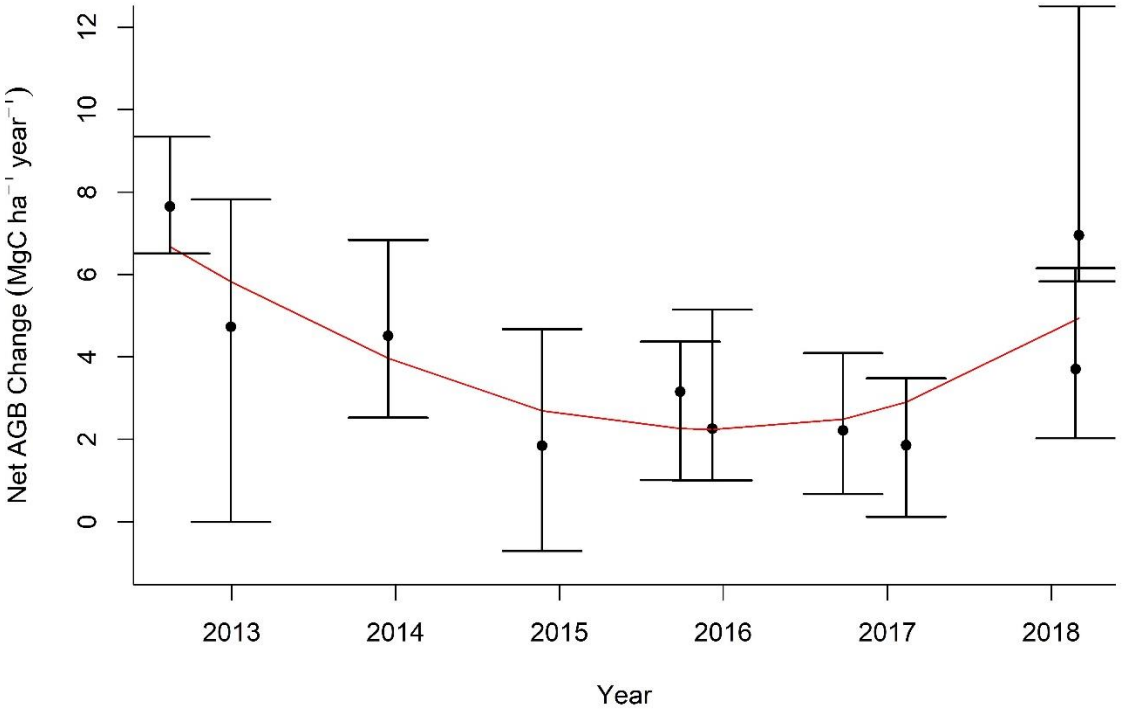

Figure 5.3 | Net aboveground biomass (AGB) change estimated from a plot network of 38 small plots of 625 m^2 (red dots) and 4 large plots of 1 ha (black dots) in a human modified landscape in Borneo. Median net AGB changes are corrected to express annual variation monitored between July 2011 and March 2018, including an El Niño event shown in yellow that occurred in the region between Jan 2016 with its peak in April 2016. Bars represent non-parametric bias-corrected and accelerated bootstrapping to generate 95% confidence intervals and the solid red line denotes a cubic smoothing spline. Different letters represent significant differences at α = 0.05 using the nonparametric Wilcoxon test.

We assessed the impact of the El Nino on canopy openness and found significant effects on plots that were slightly logged or with no logging history only (Figure 5.4). Canopy openness early 2017 are similar to canopy openness before the El Niño event.

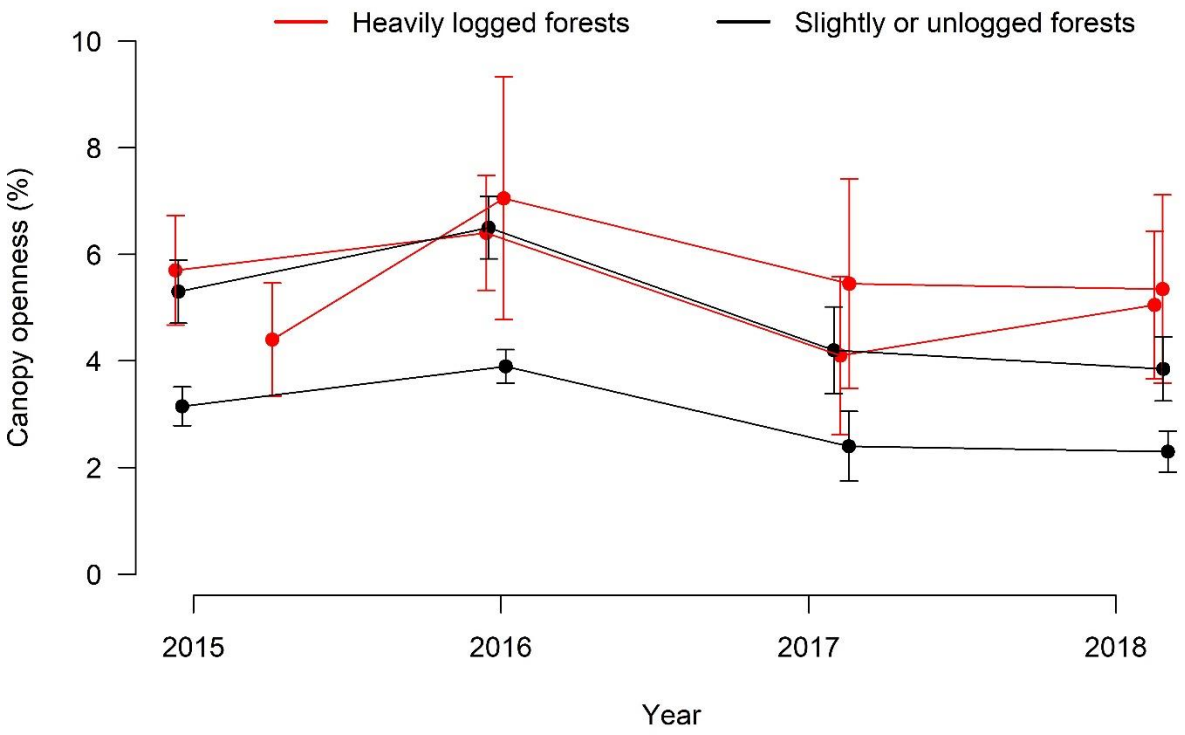

Figure 5.4 | Changes in canopy openness measured from hemiphotos between December 2014 and March 2018 within 38 25 x 25 m plots across 4 fragments. Heavily logged forests (red) are characterized by shorter top-of-canopy values than slightly or unlogged forests (black). Values are median and 95% confidence interval bars.

From the 38 permanent forest plots used to estimate AGB change, only 27 were under both flight paths (Figure 5.5). Even though both flights swept across all the plots, clouds affected data availability. The repeat LiDAR survey was able to capture spatial differences among plots in canopy openness and AGB change.

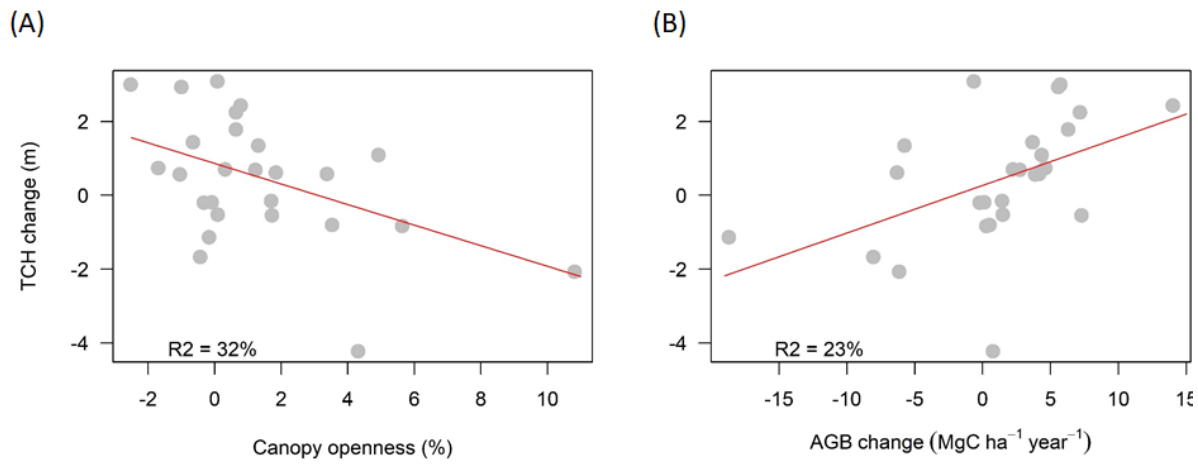

Figure 5.5 | Relationship between LiDAR-estimated top-of-canopy (TCH) change and field-based annual aboveground (a) change and (b) canopy openness from 27 permanent plots. Field-estimated carbon dynamics rates and canopy openness were measured between January 2015 and January 2016 whereas LiDAR-based carbon change was measured between November 2014 and April 2016.

Oil palm plantations recorded a mean height growth of 0.9 m which corresponds to an aboveground carbon stock gain of 2.2 Mg C ha-1 per year. This indicates that the LiDAR measurements are reliable and not biased by modifications in sensors and flight specifications over the study period (see Supplementary Information for more details).

5.4.2 Effects of drought on fragmented logged forests

Bivariate relationships suggest canopy height change was related to forest structure, edge effects and variation in topography (Fig. 5.6). Short regenerating forests (i.e. recently heavily logged forests) within average canopy height > 20 m showed loss in canopy height, whilst there was small positive gain in the canopy height of regenerating forests. Forests close to edges were greatly affected on average within approximately 800 metres from plantations, with permanent losses regardless of edge effects shaped by forest structure and topography. Forests associated with bottom-lying had values of gain in height, while hilltops were associated with reductions of canopy height.

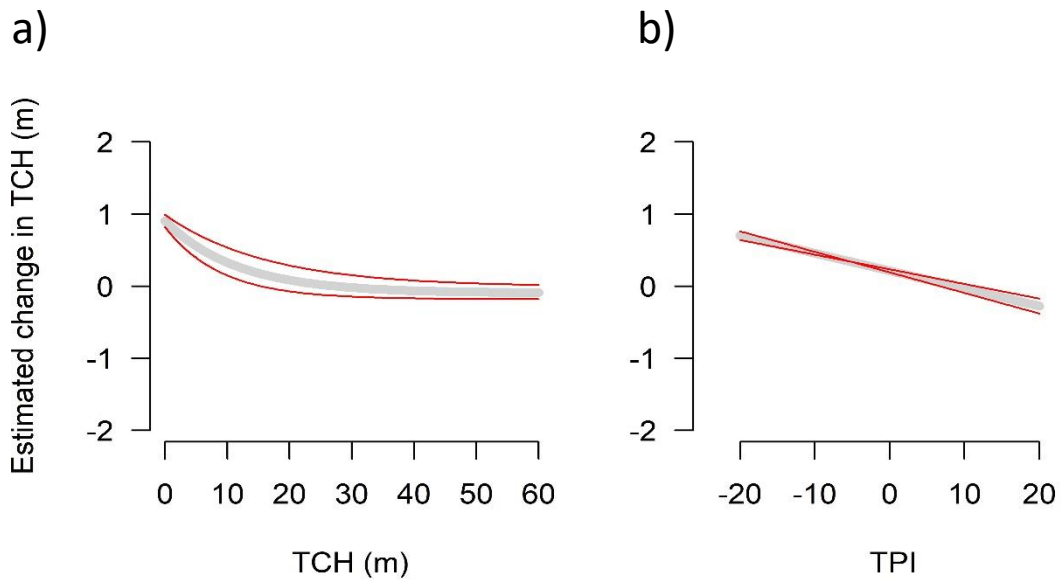

Figure 5.6 | Predicted top-of-canopy height (TCH) change (grey lines) and 95% confidence interval (red lines) as a function of (a) initial top-of-canopy height (TCH) measured from LiDAR immediately before the onset of the El Niño event and (b) Topographic Position Index (TPI) denoting negative values associated with valleys and positive values corresponding to hilltop areas.

A 1000-times iteration of a nonlinear multiple regression modelling confirms an asymptotic edge effect with significant effects of topography and successional stage on the response of vegetation to the El Niño, producing the following relationship:

$$\Delta\mathrm{TCH} = 1.0998 - 0.0308\,TPI - 0.0442\,TCH_i - 1.6105\mathrm{e}^{-(0.0032)*D_{Edge}}, \quad \text{(Eqn. 5.4)}$$

Predictions from this model are shown in Figure 5.7. Successional stage had a strong influence on canopy structure change. Forests within 450 m from edges were negatively affected during the El Nino with a significant decrease in canopy height. Short regenerating forests distant from edges (i.e. oil palm plantations, logging stations) in damp valley areas had particularly high increase in canopy height, whereas tall forests on hilltops were negatively affected with loss in canopy height.

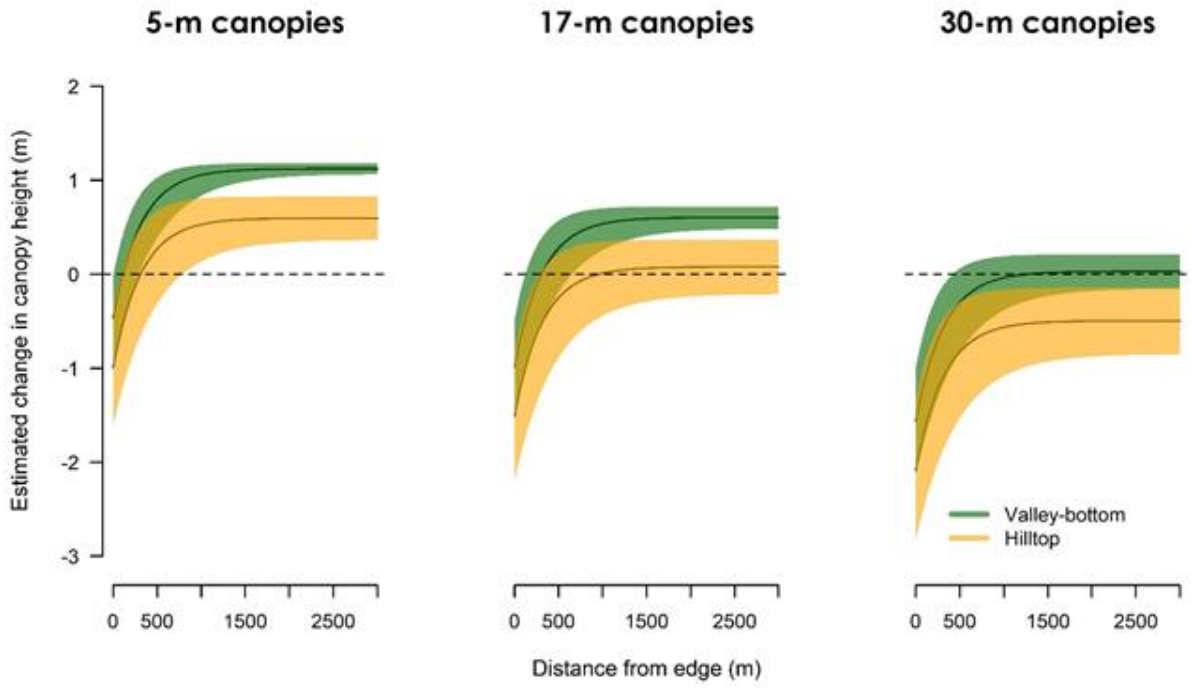

Figure 5.7 | Change in canopy height in relation to forest height, distance from edge (m) and topographic position, predicted by nonlinear modelling. Short, medium and tall forests were 5 m, 17 m and 30 m in height, corresponding with the a) 10th, b) 50th and c) 90th quantiles of Top-of-canopy height. Valley-bottom and hilltop curves correspond with TPI values of -8.6 and 9.3, respectively, from the 10^{th} and 90^{th} quantiles.

5.5 Discussion

Repeat-survey LiDAR provided high-resolution maps of canopy height change over 300 km^2 of forests and plantations, detecting strong environmental controls over leaf shedding and aboveground carbon accumulation in lowland rainforests during an El Niño drought. Ground data demonstrates that loss in canopy height change measured by LiDAR was primarily the result of higher canopy openness during the El Niño and lower aboveground biomass change rates. Canopy height change was highly variable across these human modified landscapes, being strongly influenced by logging history and fragmentation. Growth estimate of 1.2 m in oil palm plantations is consistent with the published literature (Morel *et al*., 2011; Nunes *et al*., 2017b). Although oil palm exhibits some definite symptoms of water stress during the dry season, there is no visible wilting because of the nature of the fronds (fibrous, thick hypodermis and well-developed cuticle) (Rees, 1961). Furthermore, the less dense canopies in oil palm plantations than tropical forests transpire less water (Hardwick *et al*., 2015), so are expected to

be less affected by short-term drought. Distance from edge also had strong effects, extending 450 metres into the interior. Ignoring the exacerbated edge effects under changing climate circumstances would substantially underestimate the impacts of El Niño on disturbed forests, with implications for forest policy and management.

5.5.1 ENSO drought effects on Bornean forests

The time series of LAI measurements indicate that forests responded to drought by shedding leaves, while forest inventory dataset indicates a reduction in productivity without any indication of increased mortality. Leaf abscission is a well-known response to drought (Tyree *et al*., 1993; Wolfe *et al*.,2016). When soil water and plant water transport are non-limiting, transpiration is a function of the radiation and vapour pressure deficit which controls atmospheric demand (Monteith, 1965). The diel transpiration of a leaf is approximately linearly related to radiation or VPD – whichever is more limiting – until maximum hydraulic conductivity occurs and saturation of transpiration is reached (Oren *et al*., 1999). Reducing leaf area is therefore an efficient way to control canopy water loss of an entire tree, while maintaining sufficient water supply to the remaining leaves to attain high levels of photosynthesis per unit of leaf area, albeit at the loss of whole tree productivity (Coomes and Grubb, 2000). Shedding of leaves has been observed as a response to both intense short and long period droughts in the north of Borneo (Ichie et al., 2004) and most trees flush new young leaves with the end of drought and increase in rainfall (Itioca and Yamauti, 2003). Manoli et al. (2018) recreated dry-season greening in the Amazon using an eco-hydrological model, providing further support for the idea that leaf development and synchronized dry season litterfall and dry conditions are in agreement with evolutionary strategies aimed at increasing the efficiency of photosynthesis and water consumption during periods of abundant light but potentially low water availability. We observed the greening with both ground-based sensor in the early part of the el Niño in Chapter 3, quite possibly because plants were not initially droughted despite increased evaporative demand, but then towards its climax in April 2016 forest greenness reduced, presumably because of leaf shedding in response to water availability.

Our analyses suggest that rainforest trees may be resilient during El Niño droughts, showing no indication of increased mortality. Previous studies in tropical forests have shown that droughts result in branch dieback and elevated tree mortality (Saatchi *et al*., 2013) and

mortality of large trees can remain elevated for several years after the drought (Phillips *et al*., 2009). The recovery of canopy trees after drought events is a slow process and may take long to reach the pre-drought state (Condit *et al*., 1995; Nakagawa *et al*., 2000). Tropical forests contain plant species with widely varying resource acquisition and reproductive strategies, which are associated with different phenological responses to seasonal cycles (Detto *et al*., 2018). Similar AGB rates during El Nino to the preceding year revealed that the climate event immediately affected only leaf demography, and higher AGB change rates post-El Nino suggests that the canopy recovery (observed by canopy openness time-series) acted positively upon woody growth rates. Our study shows that trees responded to drought by shedding leaves, but our approach was unable to distinguish variability in resilience among species. Anthropogenic global warming is increasing the severity of ENSO droughts in Southeast Asia, because evaporative demand increases exponentially with temperature (Thirumalai *et al*., 2017), and we do not currently know whether species resilient to drought will be pushed beyond their physiological limits as the climate warms.

5.5.2 Edge forests are more vulnerable to ENSO

Forest fragmentation results in an increased proportion of the remaining forest being located in close proximity to the forest edge (Saunders *et al*., 1991). While the majority of these edge effects are thought to extend no further than 1 km (Murcia, 1995), some may extend as far as 5–10 km into forest areas (Curran *et al*., 1999). Our results are consistent with studies showing desiccation patterns during dry seasons in fragmented forests with different levels of disturbance (Laurance and Williamson, 2002). The extent, magnitude and progression of edge effects on dry-season canopy water appeared to differ between the moderately and heavily fragmented landscapes. The heavily fragmented or heavily logged landscapes suffered a greater penetration of canopy desiccation associated with higher temperatures which increased vapour-pressure deficit, up to 1.5 km from edges, whereas in late-successional fragmented forests desiccation penetrated only 300 – 400 m into the forest interior. Forest edges affect microclimate (increasing wind speed to 400 m from the edge; Laurance *et al*., 2002), increase plant desiccation (up to 2.7 km from the edge; Briant *et al*., 2010) and affect phenology and tree recruitment (up to 5–10 km; Curran *et al*., 1999). Trees on forest edges have been found to transpire more than those in forest interiors, but this pattern appears to be influenced by the level of edge exposure and species-specific levels of stomatal resistance to water loss (Giambelluca *et al*., 2003; Herbst *et al*., 2007).

5.5.3 Microtopography buffering ENSO

Soil nutrients and water availability become increasingly limiting on ridges and at higher elevations within the landscape (Werner and Homeier, 2015), whereas low-lying, alluvial valleys are more productive (Banin *et al*., 2014) and exhibit high turnover rates (Stephenson *et al*., 2005; Russo *et al*., 2008). Our results suggest that small-scale variation in topography contributes to landscape-scale variation in both water deficit and temperature, which in turn affect the degree of canopy loss associated with leaf shedding and decreased productivity. Areas associated with high water availability may buffer the impacts of El Niño on forest canopy loss. Although we have measured water deficit of the air only, forests in valleys and possibly associated with less dry soils lost fewer leaves than on ridges in the forest interior, corroborating another study in Borneo where the author found less carbon loss associated with lower mortality in humid soils during a previous drought caused by El Niño (Slik 2004). Fine-scale topographic variation amplifies El Niño independent of logging intensity or fragmentation, suggesting that canopy sensitivity is largely associated with local fine-scale processes that differentiate water availability among habitats, which, in turn, may determine the forest dynamics at the landscape scale (Valencia *et al*. 2009, Gonzalez-Akre *et al*. 2016, Levine *et al*. 2016). One clear implication of these results is that data on canopy turnover should always be accompanied by information on the relative topographic position of trees, in order to enable scaling up to the landscape scale.

5.6 Authors' Contributions

Study design: David Coomes , Gregory Asner. *Data collection*: David Coomes, Gregory Asner, Martin Svátek, Jakub Kvasnica, Sabine Both, Dafydd Elias David, Terhi Riutta, Yadvinder Malhi. LiDAR *data processing*: Tommaso Jucker, Nicholas Vaughn, Tom Swinfield, Rubén Valbuena. *Data analysis*: Matheus Nunes. *Manuscript writing*: Matheus Nunes with support from all the co-authors.

Chapter 6 | General discussion and conclusion

The aim of this thesis was to investigate the effects of El Niño on forests at species, community and landscape levels. I have shown the power of field spectroscopy to estimate traits (Chapter 2) and used it to demonstrate how spectroscopy can estimate the El Niño effects on trees (Chapter 3). My results reveal the influences of El Niño on leaf traits, and the coupled relationship between traits and leaf spectra. I demonstrated how we can use LiDAR to map aboveground carbon in oil palm plantations (Chapter 4). I then investigated canopy structural dynamics using repeat LiDAR surveys to map the environmental filters that affect canopy structural change during El Niño events (Chapter 5). My results also reveal the links between canopy structural change and the microclimate of the forest understory.

1) How well can the traits of tropical forest trees be predicted remotely (**Chapters 3, 4, 5**)?
2) Did the 2015/2016 El Niño event affect leaf traits of old-growth tropical forests (**Chapter 3**)?
3) What are the environmental controls on canopy structural change of tropical forests during El Niño (**Chapter 5**)?

In this final chapter I return to these questions and critically evaluate how the work presented in this thesis has addressed them.

6.1 How well can the traits of tropical forest trees be predicted remotely

6.1.1 Field spectroscopy as tools to investigate leaf trait variation

In **Chapter 2** and **3**, I identify the spectral regions in which different leaf traits have strong absorption features, working with both temperate and tropical species. As expected, the visible region was the most useful for predicting pigments (Curran *et al*., 1991, Sims and Gamon, 2002), whereas the most other traits had strong absorption features in the infra-red region

(Serbin *et al*., 2014). The spectral regions selected by our partial-least-square regression models match the locations of known spectral absorption features related to proteins, starch, lignin, cellulose, hemicellulose and leaf water content (Knipling 1970; Curran 1989; Elvidge 1990; Fourty and Baret 1998; Kokaly *et al*. 2009) demonstrating that PLSR approaches deliver reliable predictions. PLSR proved successful at predicting variation in LMA, phenolics, N, water content and pigments of temperate trees on different soil types and tropical trees affected by El Niño.

As discussed in **Chapter 2**, some of the most accurately predicted traits (e.g. potassium and silicon) have no absorption features in the visible-to-near-infrared (VSWIR), but were instead estimated indirectly via constellation effects, an artefact of covariance with traits that do exhibit absorption features. For example, **Chapters 2** and **3** confirm that LMA is consistently among the most accurately predicted traits using spectroscopy, despite the fact that LMA is measured indirectly via its close coupling with water content and leaf structural traits (Asner and Martin 2008; Serbin *et al*. 2014; Chavana-Bryant *et al*. 2016). The relative high precision of predictions of K, Fe and B concentrations in temperate species and Mg concentrations in tropical species may arise from the integration of information from several leaf traits that co-vary with these metal concentrations. In contrast, I show that leaf P concentrations are not closely predicted by spectroscopy in either temperate or tropical forests. P absorption features associated with RNA and DNA lie in the ultraviolet (e.g. Tataurov *et al*. 2008) and phosphates in the longwave infrared, but there are no pronounced absorption features in the VSWIR region (Homolová *et al*. 2013), and covariance with other traits is not strong enough, making constellation effects unreliable. **Chapter 2** initially identifies a problem with estimating traits indirectly. There were strong differences in foliar concentrations of rock-derived mineral nutrients between soil types, but these soil effects were poorly predicted using PLSR, because the concentrations of rock-derived mineral are estimated indirectly via co-variance with defence and structural traits that were barely affected by soil type. In **Chapter 3,** I show that the traits which responded to El Niño - phenolics, pigments and δ^{13}C – could all be detected using field spectroscopy. This is because phenolics and pigments have known absorption features in the range of wavelengths measured (Curran *et al*., 1991; Kokaly and Skidmore, 2015). The relationship between δ^{13}C and spectral reflectance is not direct, given that δ^{13}C is present in only minute quantities in leaves, but appear to be driven indirectly by the covariance between δ^{13}C and phenolics. Our analyses of leaf spectra based on field spectroscopy have

important implications for remote sensing of forest canopies using airborne or spaceborne spectrometers. Large areas of earth are being mapped with airborne spectrometers (e.g. Asner *et al*., 2017), but some of the traits mapped by these surveys are indirectly predicted, and the accuracy of those predictions depend critically on whether covariance among traits remains consistent along environmental gradients. For example, I found that changes in water use efficiency (i.e. δ^{13} C) over the El Niño in Sabah could be predicted reliably from field spectrometry because phenolics concentrations co-varied with δ^{13} C.

Time series of spectral data that capture long-term and seasonal changes in plant community functioning have the potential to transform our understanding of ecosystem processes (Schweiger *et al*., 2018). To our knowledge, **Chapter 3** is the first study to measure leaf traits and spectral reflectance during and after an El Niño event. Field spectroscopy was able to detect changes in pigment concentrations over the course of the El Niño event. Leaf-level increases in chlorophyll observed during the El Niño in Sabah (Chapter 3) provides a new perspective on a longstanding argument in the remote sensing literature about "green-up" during dry seasons in Amazonia (Huete *et al*., 2006; Saleska *et al*., 2007; *cf*. Samanta *et al*., 2010). Those critical of the "green-up" hypothesis argue that it is an artefact of sun-sensor geometry (Morton *et al*., 2014). Ground-based spectral data in this study suggest canopy-level greening in response to the initial phase of the El Niño drought, similar to those observed in several studies and attributed to greater irradiance when cloud cover is reduced and/or to leaf demography (Nemani et al.. 2003, Huete et al., 2006; Wu et al., 2016). Manoli et al. (2018) recreated dry-season greening in the Amazon using an eco-hydrological model, providing further support for the idea that leaf development and synchronized dry season litterfall and dry conditions are in agreement with evolutionary strategies aimed at increasing the efficiency of photosynthesis and water consumption during periods of abundant light but potentially low water availability. We observed the greening with ground-based sensor in the early part of the el Niño, quite possibly because plants were not initially droughted despite increased evaporative demand.

In our analysis we have analysed the spectral information at specific wavelengths within broad regions of the electromagnetic spectrum, i.e., visible, near infrared and shortwave infrared regions of the spectrum. Future work will examine changes in spectral response associated with specific absorption and reflectance features within each spectra. This will likely yield better predictive and explanatory models of changing leaf traits with hyperspectral remote sensing in an era when airborne spectrometers are mapping large areas of the Earth (e.g. Asner et al.,

2017) and new spaceborne hyperspectral missions (e.g. ESA's EnMap) are being developed, thus paving the way for changing leaf and canopy traits to be observed at landscape-scales. The implication of this study thus extends beyond the Borneo region and suggests that remote sensing-based observations will soon enable vegetation and ecosystem function, and their responses to short-term climate changes, to be characterised at the global scale. Providing evidence that plant strategies during short-term climate change can be accurately predicted using spectrometers paves the way for new research on tropical forest responses to a changing climate using sensors in space.

6.1.2 LiDAR to quantify aboveground carbon density of oil palm plantations

LiDAR is known to be able to quantify forest structure and forest properties like canopy cover and gap fraction, however it remains uncertain how aboveground carbon density (ACD) in oil palm plantations can be quantified from LiDAR. In **Chapter 4** we tested a tree-centric and area-based approaches to predict ACD. The area-based approach that incorporates both top-of-canopy height and canopy cover yielded more accurate ACD predictions. We demonstrated that canopy cover is correlated to palm tree density and improved ACD predictions of oil palm plantations. We also showed that the tree-centric approach was less accurate. It showed a slight tendency to under-estimate the number of trees in mature plantations given that overlapped crowns in mature plantations make it more difficult to distinguish palm crowns of similar heights. Other studies focussing on tropical rainforests have also found the tree-centric approach to perform slightly less well than area-based methods (Coomes *et al*., 2017; Ferraz *et al*., 2016), due to over-segmentation of emergent trees and incomplete detection of sub-canopy trees.

Although the tree-centric approach gives less accurate results, it can still be advantageous to segment individual trees for precision agriculture (McBratney *et al*., 2005), particularly in oil palm plantations as individual trees are long-lived. Field-based tree counting is labour intensive, and the use of remote-sensing using high-resolution optical imagery from satellites has been suggested as a cost efficient alternative (Jusoff and Pathan, 2009). **Chapter 4** demonstrates the potential of the tree-centric approach based on two plantation ages, but identifies under-segmentation of adult palm trees, a problem that can be persistent with plantation age. Testing a large range of oil palm plantations age may indicate which ages are more sensitive to segmentation errors using the tree-centric approach. The potential for this

approach will also increase as its methodology improves; I have modified the *itcSegment* algorithm in R to adapt to forests with low variation in height such as palm plantations, but further improvements to reduce uncertainties in segmentation could generate better results.

6.1.3 Repeat-LidAR for canopy structure dynamics

Increased availability of repeat-measures data from LiDAR provide opportunities to measure ecosystem dynamics (Dubaya *et al*., 2010; Réjou-Méchain *et al*., 2015). Decreasing acquisition costs and standardised processing pipelines are stimulating many new applications of these data (Schimel *et al*., 2015). Despite these advances in the use of LiDAR, assessing dynamics using multi-temporal measurements is constrained by field data availability and differences in sensor specification (Zhao *et al*.,2018). This limitation is more severe in the tropics, given the challenges of long-term *in situ* observations (Schimel *et al*., 2015).

In **Chapter 5** I demonstrate that repeat-LiDAR surveys in combination with field measurements can detect the effects of environmental change on forest structure dynamics and leaf shedding. LiDAR provided spatially detailed measurements of canopy height change by recording the return-time of reflected laser pulses. Variation in leaf and branch structure influences light energy reflection, transmission and absorption within canopies (Hyer and Goetz, 2004), thereby pulse penetration may represent naturally occurring variability in canopy structure and the associate effects of environment. Differences in top-of-canopy penetration depth can be a combination of species-specific differences in canopy architecture and leaf condition (Wasser *et al*., 2013). For example, LiDAR measurements can be used to classify deciduous species in North American forests during leaf-off events (Brandtberg, 2007), and repeat measurements detect the El Niño impacts on leaf and branch turnover in the Amazon forest (Leitold *et al*., 2018). Nonetheless, closed canopy can affect beam penetration and be misinterpreted as growth when actually there was none (Dubayah *et al*., 2010). Thus, the use of field data is key to separating the effects of aboveground biomass change on canopy height change from the effects of leaf shedding. By disentangling the woody biomass change and leaf shedding on canopy structure, I then show in **Chapter 5** that repeat-LiDAR can be used to detect the effects of vegetation structural characteristics and micro-topography on canopy structure dynamics.

A key challenge in repeat-LiDAR measurements can be the differences in LiDAR settings. One potential solution to minimise the effects of difference in flight settings on forest estimates is to assess the effects that LiDAR acquisition parameters have on the structure of the point cloud, and hence on metrics and model predictions (Roussel *et al*., 2017). We have accounted only for pulse density effects on model prediction, given that point density has received more attention in the literature (Gobakken and Næsset, 2008; Jakubowski *et al*., 2013). Differences in flight altitude can also have effects on top-of-canopy height change estimations, given that emitted light energy will attenuate and spread as it travels towards the earth's surface and through the canopy (Goodwin *et al*., 2006). However, removing potential systematic biases arising from differences in altitude cannot be overcome by increased sampling. Any potential effects of differences in altitude would be modelled by incorporating the known effect of altitude on the vegetation, but it is beyond our scope here.

6.2 What environmental factors influence canopy structural change during El Niño?

Trees possess regulatory mechanisms to reduce water loss and maintain functional plant-water relations when water supply is limited (Hartmann, 2010). Plant responses to El Niño-induced droughts include stomatal closure in the short-term (Farquhar and Sharkey, 1982), morphological acclimatisation such as leaf shedding at the medium-term (Bréda *et al*., 2006) and long-term adaptations such as cavitation resistant xylems and thick scherophyll leaves (Chaves *et al*., 2003). Net carbon assimilation is reduced with stomatal closure and leaf shedding due to lower photosynthetic carbon gain at the plant level (Hartmann, 2010). If trees are unable to tolerate drought through one or more of these mechanisms, mortality can occur, years to decades after drought events (Bigler *et al*., 2007; Phillips *et al*., 2009). In Chapter 5, I demonstrate that during the 2015/2016 El Niño there was an increase in canopy height across most of a human-modified landscape in Borneo. I show that the most likely explanation for changes in height change were leaf area and aboveground biomass change. Biomass productivity can increase during El Niño events, when reduced cloud cover increases photosynthetically active radiation, however when soil moisture is low, productivity may decline (Brando *et al*., 2008).

Nevertheless, canopy structural changes in response to El Niño varied across the landscape. **Chapter 5** reveals the strong influence of the vegetation structure and topography on leaf area and aboveground biomass change. Our results demonstrate that the tallest canopies (> 20

metres in height) were the most affected by El Niño and depending on topography reduced in canopy height. Our results provide new insights on the effects of climatic events on tropical forests. Under severe droughts associated with climate change, fragmented and primary forests may be under greater risk. Considering that extreme high temperatures were a product of both natural and anthropogenic causes, the repeat-LiDAR surveys over the world's largest forest fragmentation experiment is a testbed to investigate the forest responses to drought and how degraded and primary forests will respond to warming. With increasing vapour-pressure deficit and temperatures predicted for the rest of the 21st century, in response to business-as-usual greenhouse-gas emissions scenarios, negative effects on degraded tropical forests are highly likely. This may mean that primary and fragmented forests will gain relative importance as drought intensifies in the coming decades. My work highlights the complex interactions between climate and land-use change on forest functioning.

6.3 Did the 2015/2016 El Niño event affect leaf traits of old-growth tropical forests?

In **Chapter 3**, I show that leaves of old-growth tropical trees responded to the 2015/2016 Nino, and plant traits in intact forests can rapidly acclimate to climatic events. The repeated measurements indicate that forests responded to the El Niño event by investing in pigments and phenolics, and by enhancing leaf-level water use efficiency. Pigment concentrations were about a third higher during the El Niño event than afterwards, which suggests that trees responded to having more light by upregulating photosynthetic processes. Greater foliar chlorophyll concentrations ensures that more photosynthetically active radiation is utilised for electron transport (Poorter et al., 2009). Increased light availability during the relative dry phase of the El Niño cycle can result in high rates of photosynthesis (Guan et al., 2015). However, it remains unclear whether higher rates of photosynthesis occur in Sabah, as N and P concentrations are similar during and after the El Niño, suggesting that the total concentration of leaf proteins (including Rubisco) remain unchanged (Evans, 1989); this is a topic in need of further research. Carotenoids protect leaves from photoinhibition (i.e. damage caused by solar radiation when supply outstrips demand) by releasing excess energy as heat via the xanthophyll cycle (Ustin et al., 2009). The ratio of carotenoids to chlorophyll remains similar between surveys, suggesting leaves retain similar commitment to protection against photoinhibition.

The rapid shift in water-use efficiency (suggested using δ^{13} C values) indicates the ability of plants to adapt to these short-term climatic variation, but also may indicate the prospect that

more frequent droughts could increase selection towards greater intrinsic water-use efficiency (Cernusak *et al*., 2009). Higher phenolics concentration in leaves during El Niño also indicates a mechanism of leaf protection, given that solar UV-B radiation induces a variety of acclimation responses, which typically include accumulation of phenolic compounds that serve as "sunscreens" or UV filters (Caldwell *et al*., 2003). In general, our results indicate that plants of intact forests shifted leaf traits to acclimate to higher irradiance.

Nevertheless, shedding of leaves has been observed as a response to both intense short and long period droughts in the north of Borneo (Ichie et al., 2004) and most trees flush new young leaves with the end of drought and increase in rainfall (Itioca and Yamauti, 2003). This is also evidenced in **Chapter 5**. If leaf loss was greater in the period running up to the first field campaign, and if new leaves were flushed almost immediately, then we could have inadvertently sampled younger leaves in the first campaign which are known to have higher concentrations of photosynthetic pigments (Doughty and Goulden, 2008; Hilker et al., 2017). Recent studies have demonstrated strong relationships of leaf traits and spectra with leaf age (Chavana-Bryant et al., 2017; Wu et al., 2017). By selecting what appeared to be mature leaves on each branch we attempted to minimise any effects of leaf turnover, but leaf age was not determined. Here, an opportunity of combining LiDAR and trait measurements and foliar spectroscopy could give rise to better understanding whether leaf shedding and flushing related to extreme climatic events affect leaf quality with its associated impacts on foliar traits.

References

Adams, H.D., Guardiola-Claramonte, M., Barron-Gafford, G.A., Villegas, J.C., Breshears, D.D., Zou, C.B., *et al*. (2009). Temperature sensitivity of drought-induced tree mortality portends increased regional die-off under global-change-type drought. *Proceedings of the National Academy of Sciences*, 116, 7063–7066.

Adler, P.B., Salguero-Gomez, R., Compagnoni, A., Hsu, J.S., Ray-Mukherjee, J., Mbeau-Ache, C., *et al*. (2014). Functional traits explain variation in plant life history strategies. *Proceedings of the National Academy of Sciences*, 111, 740–745.

Aerts, R. & Chapin, F.S. (1999). The mineral nutrition of wild plants revisited: a re-evaluation of processes and patterns. *Advances in Ecological Research*, 30, 1–67.

Albert, C.H., Grassein, F., Schurr, F.M., Vieilledent, G. & Violle, C. (2011). When and how should intraspecific variability be considered in trait-based plant ecology? *Perspectives in Plant Ecology, Evolution and Systematics*, 13, 217–225.

Allen, C.D., Breshears, D.D. & McDowell, N.G. (2015). On underestimation of global vulnerability to tree mortality and forest die-off from hotter drought in the Anthropocene. *Ecosphere*, 6, 1–55.

Allen, C.D., Macalady, A.K., Chenchouni, H., Bachelet, D., McDowell, N., Vennetier, M., *et al*. (2010). A global overview of drought and heat-induced tree mortality reveals emerging climate change risks for forests. *Forest Ecology and Management*, 259, 660–684.

Anderson, M.J. (2001). A new method for non-parametric multivariate analysis of variance. *Austral Ecology*, 26, 32–46.

Anderson-Teixeira, K.J., Miller, A.D., Mohan, J.E., Hudiburg, T.W., Duval, B.D. & DeLucia, E.H. (2013). Altered dynamics of forest recovery under a changing climate. *Global Change Biology*, 19, 2001–2021.

Asner, G.P., Martin, R.E., Knapp, D.E., Tupayachi, R., Anderson, C.B., Sinca, F., *et al*. (2017). Airborne laser-guided imaging spectroscopy to map forest trait diversity and guide conservation. *Science*, 355, 385–389.

Asner, G.P., Nepstad, D., Cardinot, G. & Ray, D. (2004). Drought stress and carbon uptake in an Amazon forest measured with spaceborne imaging spectroscopy. *Proceedings of the National Academy of Sciences*, 101, 6039–6044.

Asner, G.P., Powell, G.V.N., Mascaro, J., Knapp, D.E., Clark, J.K., Jacobson, J., *et al*. (2010). High-resolution forest carbon stocks and emissions in the Amazon. *Proceedings of the National Academy of Sciences*, 107, 16738–16742.

Asner, G.P., Anderson, C.B., Martin, R.E., Tupayachi, R., Knapp, D.E. & Sinca, F. (2015). Landscape biogeochemistry reflected in shifting distributions of chemical traits in the Amazon forest canopy. *Nature Geoscience*, 8, 567–573.

Asner, G.P., Brodrick, P.G., Anderson, C.B., Vaughn, N., Knapp, D.E. & Martin, R.E. (2016). Progressive forest canopy water loss during the 2012–2015 California drought. *Proceedings of the National Academy of Sciences*, 113, E249–E255.

Asner, G.P., Brodrick, P.G., Philipson, C., Vaughn, N.R., Martin, R.E., Knapp, D.E., *et al*. (2018). Mapped aboveground carbon stocks to advance forest conservation and recovery in Malaysian Borneo. *Biological Conservation*, 217, 289–310.

Asner, G.P., Knapp, D.E., Boardman, J., Green, R.O., Kennedy-Bowdoin, T., Eastwood, M., *et al*. (2012a). Carnegie Airborne Observatory-2: increasing science data dimensionality via high-fidelity multi-sensor fusion. *Remote Sensing of Environment*, 124, 454–465.

Asner, G.P. & Martin, R.E. (2008). Spectral and chemical analysis of tropical forests: scaling from leaf to canopy levels. *Remote Sensing of Environment*, 112, 3958–3970.

Asner, G.P. & Martin, R.E. (2009). Airborne spectranomics: mapping canopy chemical and taxonomic diversity in tropical forests. *Frontiers in Ecology and the Environment*, 7, 269–276.

Asner, G.P. & Martin, R.E. (2011). Canopy phylogenetic, chemical and spectral assembly in a lowland Amazonian forest. *New Phytologist*, 189, 999–1012.

Asner, G.P. & Martin, R.E. (2016a). Convergent elevation trends in canopy chemical traits of tropical forests. *Global Change Biology*, 22, 2216–2227.

Asner, G.P. & Martin, R.E. (2016b). Spectranomics: emerging science and conservation opportunities at the interface of biodiversity and remote sensing. *Global Ecology and Conservation*, 8, 212–219.

Asner, G.P., Martin, R.E., Carranza-Jiménez, L., Sinca, F., Tupayachi, R., Anderson, C.B., *et al*. (2014a). Functional and biological diversity of foliar spectra in tree canopies throughout the Andes to Amazon region. *New Phytologist*, 204, 127–139.

Asner, G.P., Martin, R.E., Knapp, D.E., Tupayachi, R., Anderson, C., Carranza, L., *et al*. (2011a). Spectroscopy of canopy chemicals in humid tropical forests. *Remote Sensing of Environment*, 115, 3587–3598.

Asner, G.P., Martin, R.E. & Suhaili, A. Bin. (2012b). Sources of Canopy Chemical and Spectral Diversity in Lowland Bornean Forest. *Ecosystems*, 15, 504–517.

Asner, G.P., Martin, R.E., Tupayachi, R., Emerson, R., Martinez, P., Sinca, F., *et al*. (2011b). Taxonomy and remote sensing of leaf mass per area (LMA) in humid tropical forests. *Ecological Applications*, 21, 85–98.

Asner, G.P. & Mascaro, J. (2014). Mapping tropical forest carbon: calibrating plot estimates to a simple LiDAR metric. *Remote Sensing of Environment*, 140, 614–624.

Asner, G.P., Martin, R.E., Tupayachi, R., Anderson, C.B., Sinca, F., Carranza-Jiménez, L., *et al*. (2014b). Amazonian functional diversity from forest canopy chemical assembly. *Proceedings of the National Academy of Sciences*, 111, 5604–9.

Asner, G.P. (2014). A Chemical-Evolutionary Basis for Remote Sensing of Tropical Forest Diversity. In: *Forests and Global Change*. Cambridge University Press, Cambridge, p. 462.

Aubin, I., Ouellette, M.H., Legendre, P., Messier, C. & Bouchard, A. (2009). Comparison of two plant functional approaches to evaluate natural restoration along an old-field - deciduous forest chronosequence. *Journal of Vegetation Science*, 20, 185–198.

Baccini, A., Walker, W., Carvalho, L., Farina, M., Sulla-Menashe, D. & Houghton, R.A. (2017). Tropical forests are a net carbon source based on aboveground measurements of gain and loss. *Science*, 358, 230–234.

Bala, G., Caldeira, K., Wickett, M., Phillips, T.J., Lobell, D.B., Delire, C., *et al*. (2007). Combined climate and carbon-cycle effects of large-scale deforestation. *Proceedings of the National Academy of Sciences*, 104, 6550–6555.

Banin, L., Lewis, S.L., Lopez-Gonzalez, G., Baker, T.R., Quesada, C.A., Chao, K.J., *et al*. (2014). Tropical forest wood production: a cross-continental comparison. *Journal of Ecology*, 102, 1025–1037.

Bartlett, M.K., Scoffoni, C. & Sack, L. (2012). The determinants of leaf turgor loss point and prediction of drought tolerance of species and biomes: A global meta-analysis. *Ecology Letters*, 15, 393–405.

Bazzaz, F. & Pickett, S. (2016). Physiological Ecology of Tropical Succession: a Comparative Review. *Annual Review of Ecology and Systematics*, 11, 287–310.

Berry, N.J., Phillips, O.L., Lewis, S.L., Hill, J.K., Edwards, D.P., Tawatao, N.B., *et al*. (2010). The high value of logged tropical forests: Lessons from northern Borneo. *Biodiversity and Conservation*, 19, 985–997.

Bigler, C., Gavin, D.G., Gunning, C. & Veblen, T.T. (2007). Drought induces lagged tree mortality in a subalpine forest in the Rocky Mountains. *Oikos*, 116, 1983–1994.

Blanc, L., Echard, M., Herault, B., Bonal, D., Marcon, E., Chave, J., *et al*. (2009). Dynamics of aboveground carbon stocks in a selectively logged tropical forest. *Ecological Applications*, 19, 1397–1404.

Blonder, B., Both, S., Coomes, D.A., Elias, D., Jucker, T., Kvasnica, J., *et al*. (2018). Extreme and Highly Heterogeneous Microclimates in Selectively Logged Tropical Forests. *Frontiers in Forests and Global Change*, 1.

Bloom, A.J., Chapin, F.S. & Mooney, H.A. (1985). Resource Limitation in Plants-An Economic Analogy. *Annual Review of Ecology and Systematics*, 16, 363–392.

Boege, K. & Dirzo, R. (2004). Intraspecific variation in growth, defense and herbivory in *Dialium guianense* (Caesalpiniaceae) mediated by edaphic heterogeneity. *Plant Ecology*, 175, 59–69.

Bolster, K., Martin, M. & Aber, J. (1996). Determination of carbon fraction and nitrogen concentration in tree foliage by near infrared reflectances: a comparison of statistical methods. *Canadian Journal of Forest Research*, 26, 590–600.

Bolton, D. (1980). The Computation of Equivalent Potential Temperature. *Monthly Weather Review*, 108, 1046–1053.

Both, S., Riutta, T., Paine, C.E.T., Elias, D.M.O., Cruz, R.S., Jain, A., *et al*. (2018). Logging and soil nutrients independently explain plant trait expression in tropical forests. *New Phytologist*. https://doi.org/10.1111/nph.15444

Brando, P.M., Nepstad, D.C., Davidson, E.A., Trumbore, S.E., Ray, D. & Camargo, P. (2008). Drought effects on litterfall, wood production and belowground carbon cycling in an Amazon forest: Results of a throughfall reduction experiment. *Philosophical Transactions of the Royal Society B: Biological Sciences*, 363, 1839–1848.

Brandtberg, T. (2007). Classifying individual tree species under leaf-off and leaf-on conditions using airborne LiDAR. *ISPRS Journal of Photogrammetry and Remote Sensing*, 61, 325–340.

Bréda, N., Huc, R., Granier, A. & Dreyer, E. (2006). Temperate forest trees and stands under severe drought: a review of ecophysiological responses, adaptation processes and long-term consequences. *Annals of Forest Science*, 63, 625–644.

Breiman, L., Friedman, J.H., Olshen, R.A. & Stone, C.J. (2017). *Classification and regression trees*. Routledge.

Breshears, D.D., Myers, O.B., Meyer, C.W., Barnes, F.J., Zou, C.B., Allen, C.D., *et al*. (2009). Research communications research communications Tree die-off in response to global change-type drought: Mortality insights from a decade of plant water potential measurements. *Frontiers in Ecology and the Environment*, 7, 185–189.

Briant, G., Gond, V. & Laurance, S.G.W. (2010). Habitat fragmentation and the desiccation of forest canopies: a case study from eastern Amazonia. *Biological Conservation*, 143, 2763–2769.

Brinck, K., Fischer, R., Groeneveld, J., Lehmann, S., Dantas De Paula, M., Pütz, S., *et al*. (2017). High resolution analysis of tropical forest fragmentation and its impact on the global carbon cycle. *Nature Communications*, 8, e14855.

Broadley, M.R., White, P.J., Hammond, J.P., Zelko, I. & Lux, A. (2007). Zinc in plants: Tansley review. *New Phytologist*, 146, 185–205.

Bryan, J.E., Shearman, P.L., Asner, G.P., Knapp, D.E., Aoro, G. & Lokes, B. (2013). Extreme differences in forest degradation in Borneo: comparing practices in Sarawak, Sabah, and Brunei. *PLoS ONE*, 8, e69679.

Buchmann, N., Kao, W.Y. & Ehleringer, J. (1997). Influence of stand structure on carbon-13 of vegetation, soils, and canopy air within deciduous and evergreen forests in Utah, United States. *Oecologia*, 110, 109–119.

Cai, W., Wang, G., Santoso, A., Mcphaden, M.J., Wu, L., Jin, F.F., *et al*. (2015). Increased frequency of extreme La Niña events under greenhouse warming. *Nature Climate Change*, 5, 132–137.

Caldwell, M.M., Bornman, J.F., Ballaré, C.L., Flint, S.D. & Kulandaivelu, G. (2007). Terrestrial ecosystems, increased solar ultraviolet radiation, and interactions with other climate change factors. *Photochemical and Photobiological Sciences*, 6, 252–266.

Cane, M.A. (2005). The evolution of El Niño, past and future. *Earth and Planetary Science Letters*, 230, 227–240.

Cao, L., Coops, N.C., Innes, J.L., Sheppard, S.R.J., Fu, L., Ruan, H., *et al*. (2016). Estimation of forest biomass dynamics in subtropical forests using multi-temporal airborne LiDAR data. *Remote Sensing of Environment*, 178, 158–171.

Carlson, K.M., Curran, L.M., Ratnasari, D., Pittman, A.M., Soares-Filho, B.S., Asner, G.P., *et al*. (2012). Committed carbon emissions, deforestation, and community land conversion from oil palm plantation expansion in West Kalimantan, Indonesia. *Proceedings of the National Academy of Sciences*, 109, 7559–7564.

Carter, P.W. & Porter, J.D. (1991). Probing of π conjugation in trans-polyacetylene using near-infrared photoluminescence spectroscopy. *Physical Review B*, 43, 144–178.

Cernusak, L.A., Tcherkez, G., Keitel, C., Cornwell, W.K., Santiago, L.S., Knohl, A., *et al*. (2009). Why are non-photosynthetic tissues generally 13C enriched compared with leaves in C3 plants? Review and synthesis of current hypotheses. *Functional Plant Biology*, 36, 199–213.

Chaplin-Kramer, R., Ramler, I., Sharp, R., Haddad, N.M., Gerber, J.S., West, P.C., *et al*. (2015). Degradation in carbon stocks near tropical forest edges. *Nature Communications*, 6, e10158.

Chavana-Bryant, C., Malhi, Y., Wu, J., Asner, G.P., Anastasiou, A., Enquist, B.J., *et al*. (2017). Leaf aging of Amazonian canopy trees as revealed by spectral and physiochemical measurements. *New Phytologist*, 214, 1049–1063.

Chave, J., Réjou-Méchain, M., Búrquez, A., Chidumayo, E., Colgan, M.S., Delitti, W.B.C., *et al*. (2014). Improved allometric models to estimate the aboveground biomass of tropical trees. *Global Change Biology*, 20, 3177–3190.

Chaves, M.M., Maroco, J.P. & Pereira, J.S. (2003). Understanding plant responses to drought - From genes to the whole plant. *Functional Plant Biology*, 30, 239–264.

Chen, J.M., Black, T.A. & Adams, R.S. (1991). Evaluation of hemispherical photography for determining plant area index and geometry of a forest stand. *Agricultural and Forest Meteorology*, 56, 129–143.

Chen, J.M. & Cihlar, J. (1995). Plant canopy gap-size analysis theory for improving optical measurements of leaf-area index. *Applied Optics*, 34, 6211–6222.

Chen, Q., Vaglio Laurin, G. & Valentini, R. (2015). Uncertainty of remotely sensed aboveground biomass over an African tropical forest: Propagating errors from trees to plots to pixels. *Remote Sensing of Environment*, 160, 134–143.

Chen, S., Hong, X., Harris, C.J. & Sharkey, P.M. (2004). Sparse modeling using orthogonal forward regression with press statistic and regularization. *IEEE Transactions on Systems, Man, and Cybernetics, Part B: Cybernetics*, 34, 898–911.

Clark, D.B., Clark, D.A. & Oberbauer, S.F. (2010). Annual wood production in a tropical rain forest in NE Costa Rica linked to climatic variation but not to increasing CO_2. *Global Change Biology*, 16, 747–759.

Clarke, A. (2017). *Principles of thermal ecology: Temperature, energy and life*. Oxford University Press.

Classen, A.T., Hart, S.C., Whitman, T.G., Cobb, N.S. & Koch, G.W. (2005). Insect infestations linked to shifts in microclimate. *Soil Science Society of America Journal*, 69, 2049–2057.

Coley, P.D. (1983). Herbivory and defensive characteristics of tree species in a lowland tropical forest. *Ecological Monographs*, 53, 209–234.

Coley, P.D. (1987). Interspecific variation in plant anti-herbivore properties: the role of habitat quality and rate of disturbance. *New Phytologist*, 106, 251–263.

Coley, P.D. & Kursar, T.A. (2014). On tropical forests and their pests. *Science*, 343, 35–36.

Colledge, F. (2017). *Summary of the 2015/2016 El Niño wet and dry season climatology for: Ethiopia, Ghana, Malawi, Colombia, Papua New Guinea and Indonesia*.

Condit, R., Engelbrecht, B.M.J., Pino, D., Perez, R. & Turner, B.L. (2013). Species distributions in response to individual soil nutrients and seasonal drought across a community of tropical trees. *Proceedings of the National Academy of Sciences*. https://doi.org/10.1073/pnas.1218042110

Condit, R., Aguilar, S., Hernandez, A., Perez, R., Lao, S., Angehr, G., *et al*. (2004). Tropical forest dynamics across a rainfall gradient and the impact of an El Niño dry season. *Journal of Tropical Ecology*, 20, 51–72.

Condit, R., Ashton, P., Bunyavejchewin, S., Dattaraja, H.S., Davies, S., Esufali, S., *et al*. (2006). The importance of demographic niches to tree diversity. *Science*, 313, 98–101.

Condit, R., Hubbell, S.P. & Foster, R.B. (1995). Mortality rates of 205 neotropical tree and shrub species and the impact of a severe drought. *Ecological Monographs*, 65, 419–439.

Coomes, D.A., Allen, R.B., Scott, N.A., Goulding, C. & Beets, P. (2002). Designing systems to monitor carbon stocks in forests and shrublands. *Forest Ecology and Management*, 164, 89–108.

Coomes, D.A., Dalponte, M., Jucker, T., Asner, G.P., Banin, L.F., Burslem, D.F.R.P.R.P., *et al*. (2017). Area-based vs tree-centric approaches to mapping forest carbon in Southeast Asian forests with airborne laser scanning data. *Remote Sensing of Environment*, 194, 77–88.

Coomes, D.A. & Grubb, P.J. (2000). Impacts of root competition in forests and woodlands: a theoretical framework and review of experiments. *Ecological Monographs*, 70, 171–207.

Couture, J.J., Serbin, S.P. & Townsend, P.A. (2013). Spectroscopic sensitivity of real-time, rapidly induced phytochemical change in response to damage. *New Phytologist*, 198, 311–319.

Curran, L.M., Caniago, I., Paoli, G.D., Astianti, D., Kusneti, M., Leighton, M., *et al*. (1999). Impact of El Niño and logging on canopy tree recruitment in Borneo. *Science*, 286, 2184–2188.

Curran, L.M., Trigg, S.N., McDonald, A.K., Astiani, D., Hardiono, Y.M., Siregar, P., *et al*. (2004). Lowland Forest Loss in Protected Areas of Indonesian Borneo. *Science*, 303, 1000–1003.

Curran, P.J. (1989). Remote sensing of foliar chemistry. *Remote Sensing of Environment*, 30, 271–278.

Curran, P.J., Dungan, J.L., Macler, B.A. & Plummer, S.E. (1991). The effect of a red leaf pigment on the relationship between red edge and chlorophyll concentration. *Remote Sensing of Environment*, 35, 69–76.

Dalponte, M. (2017). itcSegment: individual Tree Crowns Segmentation. R package version 0.8

Dalponte, M. & Coomes, D.A. (2016). Tree-centric mapping of forest carbon density from airborne laser scanning and hyperspectral data. *Methods in Ecology and Evolution*, 7, 1236–1245.

Dalponte, M., Ørka, H.O., Ene, L.T., Gobakken, T. & Næsset, E. (2014). Tree crown delineation and tree species classification in boreal forests using hyperspectral and ALS data. *Remote Sensing of Environment*, 140, 306–317.

Dalponte, M., Reyes, F., Kandare, K. & Gianelle, D. (2015). Delination of Individual Tree Crowns from ALS and Hyperspectral data: a comparison among four methods. *European Journal of Remote Sensing*, 48, 365–382.

Dana Chadwick, K. & Asner, G.P. (2016). Organismic-scale remote sensing of canopy foliar traits in lowland tropical forests. *Remote Sensing*, 8, 87.

Dassot, M., Constant, T. & Fournier, M. (2011). The use of terrestrial LiDAR technology in forest science: Application fields, benefits and challenges. *Annals of Forest Science*, 68, 959–974.

Davenport, D.W., Breshears, D.D., Wilcox, B.P. & Allen, C.D. (1998). Sustainability of pinon-juniper ecosystems: a unifying perspective of soil erosion thresholds. *Journal of Range Management*, 51, 231–240.

Davey, M.P., Harmens, H., Ashenden, T.W., Edwards, R. & Baxter, R. (2007). Species-specific effects of elevated CO_2 on resource allocation in *Plantago maritima* and *Armeria maritima*. *Biochemical Systematics and Ecology*, 35, 121–129.

De Frenne, P., Rodriguez-Sanchez, F., Coomes, D.A., Baeten, L., Verstraeten, G., Vellend, M., *et al*. (2013). Microclimate moderates plant responses to macroclimate warming. *Proceedings of the National Academy of Sciences*, 110, 18561–18565.

Detto, M., Muller-Landau, H.C., Mascaro, J. & Asner, G.P. (2013). Hydrological networks and associated topographic variation as templates for the spatial organization of tropical forest vegetation. *PLoS ONE*, 8, e76296.

Detto, M., Wright, S.J., Calderón, O. & Muller-Landau, H.C. (2018). Resource acquisition and reproductive strategies of tropical forest in response to the El Niño-Southern Oscillation. *Nature Communications*, 9, e913.

Díaz, S., Kattge, J., Cornelissen, J.H.C., Wright, I.J., Lavorel, S., Dray, S., *et al*. (2016). The global spectrum of plant form and function. *Nature*, 529, 167–171.

Donohue, K., Dorn, L., Griffith, C. & Kim, E. (2005). Environmental and genetic influences on the germination of *Arabidopsis thallana* in the field. *Evolution*, 59, 740–757.

dos Santos, U.M., de Carvalho Gonçalves, J.F. & Feldpausch, T.R. (2006). Growth, leaf nutrient concentration and photosynthetic nutrient use efficiency in tropical tree species planted in degraded areas in central Amazonia. *Forest Ecology and Management*, 226, 299–309.

Doughty, C.E., Asner, G.P. & Martin, R.E. (2011). Predicting tropical plant physiology from leaf and canopy spectroscopy. *Oecologia*, 165, 289–299.

Doughty, C.E., Metcalfe, D.B., Girardin, C.A.J., Amézquita, F.F., Cabrera, D.G., Huasco, W.H., *et al*. (2015). Drought impact on forest carbon dynamics and fluxes in Amazonia. *Nature*, 519, 78–82.

Doughty, C.E., Santos-Andrade, P.E., Goldsmith, G.R., Blonder, B., Shenkin, A., Bentley, L.P., *et al*. (2017). Can leaf spectroscopy predict leaf and forest traits along a peruvian tropical forest elevation gradient? *Journal of Geophysical Research: Biogeosciences*, 122, 2952–2965.

Doughty, C.E., Santos-Andrade, P.E., Shenkin, A., Goldsmith, G.R., Bentley, L.P., Blonder, B., *et al*. (2018). Tropical forest leaves may darken in response to climate change. *Nature Ecology and Evolution*, 2, 1918–1924.

Douglas, I. (1999). Hydrological investigations of forest disturbance and land cover impacts in South-East Asia: a review. *Philosophical Transactions of the Royal Society B: Biological Sciences*, 354, 1725–1738.

Dubayah, R.O., Sheldon, S.L., Clark, D.B., Hofton, M.A., Blair, J.B., Hurtt, G.C., *et al*. (2010). Estimation of tropical forest height and biomass dynamics using LiDAR remote sensing at la Selva, Costa Rica. *Journal of Geophysical Research: Biogeosciences*, 115, 1–17.

Duncanson, L.I., Dubayah, R.O., Cook, B.D., Rosette, J. & Parker, G. (2015). The importance of spatial detail: assessing the utility of individual crown information and scaling approaches for LiDAR-based biomass density estimation. *Remote Sensing of Environment*, 168, 102–112.

Elvidge, C.D. (1990). Reflectance characteristics of dry plant materials. *International Journal of Remote Sensing*, 11, 1775–1795.

Elvidge, C.D. (1990). Visible and near infrared reflectance characteristics of dry plant materials. *International Journal of Remote Sensing*, 11, 1775–1795.

Englhart, S., Jubanski, J. & Siegert, F. (2013). Quantifying dynamics in tropical peat swamp forest biomass with multi-temporal LiDAR datasets. *Remote Sensing*, 5, 2368–2388.

Ewers, R.M., Didham, R.K., Fahrig, L., Ferraz, G., Hector, A., Holt, R.D., *et al*. (2011). A large-scale forest fragmentation experiment: the Stability of Altered Forest Ecosystems Project. *Philosophical Transactions of the Royal Society B: Biological Sciences*, 366, 3292–3302.

Eysn, L., Hollaus, M., Lindberg, E., Berger, F., Monnet, J.M., Dalponte, M., *et al*. (2015). A benchmark of LiDAR-based single tree detection methods using heterogeneous forest data from the Alpine Space. *Forests*, 6, 1721–1747.

FAO. (2016). *FAOSTAT Gateway [WWW Document]. 2014*. Available at: http://faostat3.fao.org/faostat-gateway/go/to/home/E. Last accessed 15 June 2017.

Farquhar, G.D., Ehleringer, J.R. & Hubick, K.T. (1989). Carbon isotope discrimination and photosynthesis. *Annual Review of Plant Physiology and Plant Molecular Biology*, 40, 503–537.

Farquhar, G.D. & Sharkey, T.D. (1982). Stomatal conductance and photosynthesis. *Annual Review of Plant Physiology*, 33, 317–345.

Fauset, S., Baker, T.R., Lewis, S.L., Feldpausch, T.R., Affum-Baffoe, K., Foli, E.G., *et al*. (2012). Drought-induced shifts in the floristic and functional composition of tropical forests in Ghana. *Ecology Letters*, 15, 1120–1129.

Feilhauer, H., Asner, G.P., Martin, R.E. & Schmidtlein, S. (2010). Brightness-normalized Partial Least Squares Regression for hyperspectral data. *Journal of Quantitative Spectroscopy and Radiative Transfer*, 111, 1947–1957.

Feret, J.B. & Asner, G.P. (2013). Tree species discrimination in tropical forests using airborne imaging spectroscopy. *IEEE Transactions on Geoscience and Remote Sensing*, 51, 73–84.

Ferraz, A., Saatchi, S., Mallet, C. & Meyer, V. (2016). LiDAR detection of individual tree size in tropical forests. *Remote Sensing of Environment*, 183, 318–333.

Field, C.B., Chapin III, F.S., Matson, P.A. & Mooney, H.A. (1992). Responses of terrestrial ecosystems to the changing atmosphere: a resource-based approach. *Annual Review of Ecology and Systematics*, 23, 201–235.

Field, R.D., Van Der Werf, G.R. & Shen, S.S.P. (2009). Human amplification of drought-induced biomass burning in Indonesia since 1960. *Nature Geoscience*, 2, 185–188.

Fine, P.V.A., Miller, Z.J., Mesones, I., Irazuzta, S., Appel, H.M., Stevens, M.H.H., *et al*. (2006). The growth-defense trade-off and habitat specialization by plants in Amazonian forests. *Ecology*, 87, 150–162.

Fitzherbert, E.B., Struebig, M.J., Morel, A., Danielsen, F., Brühl, C.A., Donald, P.F., *et al*. (2008). How will oil palm expansion affect biodiversity? *Trends in Ecology and Evolution*, 23, 538–545.

Foley, J.A., Ramankutty, N., Brauman, K.A., Cassidy, E.S., Gerber, J.S., Johnston, M., *et al*. (2011). Solutions for a cultivated planet. *Nature*, 478, 337–342.

Fortunel, C., Garnier, E., Joffre, R., Kazakou, E., Quested, H., Grigulis, K., *et al*. (2009). Leaf traits capture the effects of land use changes and climate on litter decomposability of grasslands across Europe. *Ecology*, 90, 598–611.

Fourty, T.H. & Baret, F. (1998). On spectral estimates of fresh leaf biochemistry. *International Journal of Remote Sensing*, 19, 1283–1297.

Fox, J.E.D. (1972). The natural vegetation of the Sabah and natural regeneration of the Dipterocarp Forests. University of Wales, Bangor.

Frey, S.J.K., Hadley, A.S., Johnson, S.L., Schulze, M., Jones, J.A. & Betts, M.G. (2016). Spatial models reveal the microclimatic buffering capacity of old-growth forests. *Science Advances*, 2, e1501392.

Fry, E.L., Power, S.A. & Manning, P. (2014). Trait-based classification and manipulation of plant functional groups for biodiversity-ecosystem function experiments. *Journal of Vegetation Science*, 25, 248–261.

Funk, J., Larson, J., Ames, G., Butterfield, B., J., C.-B., Firn, J., *et al*. (2016). Revisiting the Holy Grail: using plant functional traits to predict ecological processes. *Biological Reviews*, 92, 1156–1173.

Galvez-Sola, L., García-Sánchez, F., Pérez-Pérez, J.G., Gimeno, V., Navarro, J.M., Moral, R., *et al*. (2015). Rapid estimation of nutritional elements on citrus leaves by near infrared reflectance spectroscopy. *Frontiers in plant science*, 6, e571.

Gatti, L. V., Gloor, M., Miller, J.B., Doughty, C.E., Malhi, Y., Domingues, L.G., *et al*. (2014). Drought sensitivity of Amazonian carbon balance revealed by atmospheric measurements. *Nature*, 506, 76–80.

Gaveau, D.L.A., Sheil, D., Husnayaen, Salim, M.A., Arjasakusuma, S., Ancrenaz, M., *et al*. (2016). Rapid conversions and avoided deforestation: examining four decades of industrial plantation expansion in Borneo. *Scientific Reports*, 6.

Gaveau, D.L.A., Sloan, S., Molidena, E., Yaen, H., Sheil, D., Abram, N.K., *et al*. (2014). Four decades of forest persistence, clearance and logging on Borneo. *PLoS ONE*, 9, e101654.

Genty, B., Briantais, J.-M. & Baker, N.R. (1989). The relationship between the quantum yield of photosynthetic electron transport and quenching of chlorophyll fluorescence. *Biochimica et Biophysica Acta (BBA) - General Subjects*, 990, 87–92.

Gerke, J. (1992). Orthophosphate and organic phosphate in the soil solution of four sandy soils in relation to pH-evidence for humic-FE-(AL-) phosphate complexes. *Communications in Soil Science and Plant Analysis*, 23, 601–612.

Giambelluca, T.W., Ziegler, A.D., Nullet, M.A., Truong, D.M. & Tran, L.T. (2003). Transpiration in a small tropical forest patch. *Agricultural and Forest Meteorology*, 117, 1–22.

Gillespie, T.W., Brock, J. & Wright, C.W. (2004). Prospects for quantifying structure, floristic composition and species richness of tropical forests. *International Journal of Remote Sensing*, 25, 707–715.

Gillon, D., Houssard, C. & Joffre, R. (1999). Using near-infrared reflectance spectroscopy to predict carbon, nitrogen and phosphorus content in heterogeneous plant material. *Oecologia*, 118, 173–182.

Girardin, C.A.J., Malhi, Y., Aragão, L.E.O.C., Mamani, M., Huaraca Huasco, W., Durand, L., *et al*. (2010). Net primary productivity allocation and cycling of carbon along a tropical forest elevational transect in the Peruvian Andes. *Global Change Biology*, 16, 3176–3192.

Gitelson, A.A., Viña, A., Ciganda, V., Rundquist, D.C. & Arkebauer, T.J. (2005). Remote estimation of canopy chlorophyll content in crops. *Geophysical Research Letters*, 32, 1–4.

Giusti, M.M., Rodríguez-Saona, L.E. & Wrolstad, R.E. (1999). Molar absorptivity and color characteristics of acylated and non- acylated pelargonidin-based anthocyanins. *Journal of Agricultural and Food Chemistry*, 47, 4631–4637.

Gobakken, T. & Næsset, E. (2008). Assessing effects of laser point density, ground sampling intensity, and field sample plot size on biophysical stand properties derived from airborne laser scanner data. *Canadian Journal of Forest Research*, 38, 1095–1109.

Gobakken, T., Naesset, E., Nelson, R., Bollandss, O.M., Gregoire, T.G., Stahl, G., *et al*. (2012). Estimating biomass in Hedmark County, Norway using national forest inventory field plots and airborne laser scanning. *Remote Sensing of Environment*, 123, 443–456.

Goetz, S.J., Bond-Lamberty, B., Law, B.E., Hicke, J.A., Huang, C., Houghton, R.A., *et al*. (2012). Observations and assessment of forest carbon dynamics following disturbance in North America. *Journal of Geophysical Research: Biogeosciences*, 117, 1–17.

González del Pliego, P., Scheffers, B.R., Basham, E.W., Woodcock, P., Wheeler, C., Gilroy, J.J., *et al*. (2016). Thermally buffered microhabitats recovery in tropical secondary forests following land abandonment. *Biological Conservation*, 201, 385–395.

Gonzalez-Akre, E., Meakem, V., Eng, C.Y., Tepley, A.J., Bourg, N.A., McShea, W., *et al*. (2016). Patterns of tree mortality in a temperate deciduous forest derived from a large forest dynamics plot. *Ecosphere*, 7, e01595.

Goodwin, N.R., Coops, N.C. & Culvenor, D.S. (2006). Assessment of forest structure with airborne LiDAR and the effects of platform altitude. *Remote Sensing of Environment*, 103, 140–152.

Grace, J.B., Michael Anderson, T., Han, O. & Scheiner, S.M. (2010). On the specification of structural equation models for ecological systems. *Ecological Monographs*, 80, 67–87.

Graham, M.H. (2003). Confronting multicollinearity in ecological multiple regression. *Ecology*, 84, 2809–2815.

Greegor, D.H. (2011). Ecology from Space: Biologists need to be involved today in planning. *Ecology*, 36, 429–432.

Green, J.L., Bohannan, B.J.M. & Whitaker, R.J. (2008). Microbial biogeography: from taxonomy to traits. *Science*, 320, 1039–1043.

Greenwood, S., Ruiz-Benito, P., Martínez-Vilalta, J., Lloret, F., Kitzberger, T., Allen, C.D., *et al*. (2017). Tree mortality across biomes is promoted by drought intensity, lower wood density and higher specific leaf area. *Ecology Letters*, 20, 539–553.

Grime, J.P., Brown, V.K., Thompson, K., Masters, G.J., Hillier, S.H., Clarke, I.P., *et al*. (2000). The response of two contrasting limestone grasslands to simulated climate change. *Science (New York, N.Y.)*, 289, 762–765.

Grime, J.P.P., Thompson, K., Hunt, R., Hodgson, J.G.G., Cornelissen, J.H.C.H.C., Rorison, I.H.H., *et al*. (1997). Integrated screening validates primary axes of specialisation in plants. *Oikos*, 79, 259–281.

Guan, K., Pan, M., Li, H., Wolf, A., Wu, J., Medvigy, D., *et al*. (2015). Photosynthetic seasonality of global tropical forests constrained by hydroclimate. *Nature Geoscience*, 8, 284–289.

Guanter, L., Kaufmann, H., Segl, K., Foerster, S., Rogass, C., Chabrillat, S., *et al*. (2015). The EnMAP spaceborne imaging spectroscopy mission for earth observation. *Remote Sensing*, 7, 8830–8857.

Gunes, A., Inal, A., Bagci, E.G., Coban, S. & Sahin, O. (2007). Silicon increases boron tolerance and reduces oxidative damage of wheat grown in soil with excess boron. *Biologia Plantarum*, 51, 571–574.

Gutiérrez-Vélez, V.H. & DeFries, R. (2013). Annual multi-resolution detection of land cover conversion to oil palm in the Peruvian Amazon. *Remote Sensing of Environment*, 129, 154–167.

Haaland, D.M. & Thomas, E. V. (1988). Partial least-squares methods for spectral analyses. 1. Relation to other quantitative calibration methods and the extraction of qualitative information. *Analytical Chemistry*, 60, 1193–1202.

Haines-Young, R., Barr, C.J., Firbank, L.G., Furse, M., Howard, D.C., McGowan, G., *et al*. (2003). Changing landscapes, habitats and vegetation diversity across Great Britain. *Journal of Environmental Management*, 67, 267–281.

Hall, F.G., Bergen, K., Blair, J.B., Dubayah, R., Houghton, R., Hurtt, G., *et al*. (2011). Characterizing 3D vegetation structure from space: Mission requirements. *Remote Sensing of Environment*, 115, 2753–2775.

Hall, R.B.; Mc Nabb Jr., H.S.; Maynard, C.A., Green, T.L. (1979). Toward Development of Optimal Alnus glutinosa Symbioses, 140, 120–126.

Hansen, M.C., Potapov, P. V., Moore, R., Hancher, M., Turubanova, S.A., Tyukavina, A., *et al*. (2013). High-resolution global maps of 21st-century forest cover change. *Science*, 342, 850–853.

Hardwick, S.R., Toumi, R., Pfeifer, M., Turner, E.C., Nilus, R. & Ewers, R.M. (2015). The relationship between leaf area index and microclimate in tropical forest and oil palm plantation: Forest disturbance drives changes in microclimate. *Agricultural and Forest Meteorology*, 201, 187–195.

Harrison, R.D. (2000). Repercussions of El Niño: Drought causes extinction and the breakdown of mutualism in Borneo. *Proceedings of the Royal Society B: Biological Sciences*, 267, 911–915.

Hartmann, H. (2011). Will a 385 million year-struggle for light become a struggle for water and for carbon? - How trees may cope with more frequent climate change-type drought events. *Global Change Biology*, 17, 642–655.

Hautier, Y., Tilman, D., Isbell, F., Seabloom, E.W., Borer, E.T. & Reich, P.B. (2015). Anthropogenic environmental changes affect ecosystem stability via biodiversity. *Science*, 348, 336–340.

Herbst, M., Roberts, J.M., Rosier, P.T.W. & Gowing, D.J. (2007). Seasonal and interannual variability of canopy transpiration of a hedgerow in southern England. *Tree Physiology*, 27, 321–333.

Hikosaka, K. (2004). Interspecific difference in the photosynthesis-nitrogen relationship: Patterns, physiological causes, and ecological importance. *Journal of Plant Research*, 117, 481–494.

Hillier, S.H., Walton, D.W.H. & Wells, D.A. (1990). *Calcareous grasslands: Ecology and management*. Huntingdon.

Hodson, M.J., White, P.J., Mead, A. & Broadley, M.R. (2005). Phylogenetic variation in the silicon composition of plants. *Annals of Botany*, 96, 1027–1046.

Hofmann, R.W., Campbell, B.D., Bloor, S.J., Swinny, E.E., Markham, K.R., Ryan, K.G., *et al*. (2003). Responses to UV-B radiation in *Trifolium repens* L. - Physiological links to plant productivity and water availability. *Plant, Cell and Environment*, 26, 603–612.

Homolová, L., Malenovský, Z., Clevers, J.G.P.W., García-Santos, G. & Schaepman, M.E. (2013). Review of optical-based remote sensing for plant trait mapping. *Ecological Complexity*, 15, 1–16.

Houghton, R.A., Hall, F. & Goetz, S.J. (2009). Importance of biomass in the global carbon cycle. *Journal of Geophysical Research: Biogeosciences*, 114, 1–13.

Huang, M. & Asner, G.P. (2010). Long-term carbon loss and recovery following selective logging in Amazon forests. *Global Biogeochemical Cycles*, 24, 1–15.

Huete, A.R., Didan, K., Shimabukuro, Y.E., Ratana, P., Saleska, S.R., Hutyra, L.R., *et al*. (2006). Amazon rainforests green-up with sunlight in dry season. *Geophysical Research Letters*, 33, L06405/1-L06405/4.

Hughes, R.F., Archer, S.R., Asner, G.P., Wessman, C.A., McMurtry, C., Nelson, J., *et al*. (2006). Changes in aboveground primary production and carbon and nitrogen pools accompanying woody plant encroachment in a temperate Savannah. *Global Change Biology*, 12, 1733–1747.

Hyde, P., Nelson, R., Kimes, D. & Levine, E. (2007). Exploring LiDAR-RaDAR synergy-predicting aboveground biomass in a Southwestern ponderosa pine forest using LiDAR, SAR and InSAR. *Remote Sensing of Environment*, 106, 28–38.

Hyer, E.J. & Goetz, S.J. (2004). Comparison and sensitivity analysis of instruments and radiometric methods for LAI estimation: Assessments from a boreal forest site. *Agricultural and Forest Meteorology*, 122, 157–174.

Hyyppä, J., Kelle, O., Lehikoinen, M. & Inkinen, M. (2001). A segmentation-based method to retrieve stem volume estimates from 3-D tree height models produced by laser scanners. *IEEE Transactions on Geoscience and Remote Sensing*, 39, 969–975.

Inanaga, S., Okasaka, A. & Tanaka, S. (1995). Does silicon exist in association with organic compounds in rice plant? *Soil Science & Plant Nutrition*, 41, 111–117.

Isbell, F., Craven, D., Connolly, J., Loreau, M., Schmid, B., Beierkuhnlein, C., *et al*. (2015). Biodiversity increases the resistance of ecosystem productivity to climate extremes. *Nature*, 526, 574–577.

Ishii, H.T., Tanabe, S.I. & Hiura, T. (2004). Exploring the relationships among canopy structure, stand productivity, and biodiversity of temperate forest ecosystems. *Forest Science*, 50, 342–355.

Itoh, A., Nanami, S., Harata, T., Ohkubo, T., Tan, S., Chong, L., *et al*. (2012). The effect of habitat association and edaphic conditions on tree mortality during El Niño-induced drought in a Bornean Dipterocarp forest. *Biotropica*, 44, 606–617.

Izaguirre, M.M., Mazza, C.A., Biondini, M., Baldwin, I.T. & Ballare, C.L. (2006). Remote sensing of future competitors: Impacts on plant defenses. *Proceedings of the National Academy of Sciences*, 103, 7170–7174.

Jakubowski, M.K., Guo, Q. & Kelly, M. (2013). Trade-offs between LiDAR pulse density and forest measurement accuracy. *Remote Sensing of Environment*, 130, 245–253.

Jetz, W., Cavender-Bares, J., Pavlick, R., Schimel, D., Davis, F.W., Asner, G.P., *et al*. (2016). Monitoring plant functional diversity from space. *Nature Plants*, 2, 16024.

Jonckheere, I., Nackaerts, K., Muys, B. & Coppin, P. (2005). Assessment of automatic gap fraction estimation of forests from digital hemispherical photography. *Agricultural and Forest Meteorology*, 132, 96–114.

Jucker, T., Asner, G.P., Dalponte, M., Brodrick, P.G., Philipson, C.D., Vaughn, N.R., *et al*. (2018a). Estimating aboveground carbon density and its uncertainty in Borneo's structurally complex tropical forests using airborne laser scanning. *Biogeosciences*, 15, 3811–3830.

Jucker, T., Bongalov, B., Burslem, D.F.R.P., Nilus, R., Dalponte, M., Lewis, S.L., *et al*. (2018b). Topography shapes the structure, composition and function of tropical forest landscapes. *Ecology Letters*, 21, 989–1000.

Jucker, T., Caspersen, J., Chave, J., Antin, C., Barbier, N., Bongers, F., *et al*. (2016). Allometric equations for integrating remote sensing imagery into forest monitoring programmes. *Global Change Biology*, 23, 177–190.

Jucker, T., Hardwick, S.R., Both, S., Elias, D.M.O., Ewers, R.M., Milodowski, D.T., *et al*. (2018c). Canopy structure and topography jointly constrain the microclimate of human-modified tropical landscapes. *Global Change Biology*, 24, 5243–5258.

Jusoff, K. & Pathan, M. (2009). Mapping of individual oil palm trees using airborne hyperspectral sensing: an overview. *Applied Physics Research*, 1, 15–30.

Katz, J.J., Dougherty, R.C. & Boucher, L.J. (1966). *Infrared and nuclear magnetic resonance spectroscopy of chlorophyll*. New York.

Kellner, J.R., Clark, D.B. & Hubbell, S.P. (2009). Pervasive canopy dynamics produce short-term stability in a tropical rain forest landscape. *Ecology Letters*, 12, 155–164.

Kent, R., Lindsell, J.A., Laurin, G.V., Valentini, R. & Coomes, D.A. (2015). Airborne LiDAR detects selectively logged tropical forest even in an advanced stage of recovery. *Remote Sensing*, 7, 8348–8367.

Khosravipour, A., Skidmore, A.K., Isenburg, M., Wang, T. & Hussin, Y.A. (2014). Generating pit-free canopy height models from airborne LiDAR. *Photogrammetric Engineering & Remote Sensing*, 80, 863–872.

Khosrokhani, M., Khairunniza-Bejo, S. & Pradhan, B. (2016). Geospatial technologies for detection and monitoring of *Ganoderma* basal stem rot infection in oil palm plantations: a review on sensors and techniques. *Geocarto International*, 6049, 1–17.

Kleinebecker, T., Schmidt R., S., Fritz, C., Smolders J. P., A. & Hölzel, N. (2009). Prediction of δ13C and δ15N in plant tissues with near-infrared reflectance spectroscopy. *New Phytologist*, 184, 732–739.

Knipling, E.B. (1970). Physical and physiological basis for the reflectance of visible and near-infrared radiation from vegetation. *Remote Sensing of Environment*, 1, 155–159.

Koh, L.P., Miettinen, J., Liew, S.C. & Ghazoul, J. (2011). Remotely sensed evidence of tropical peatland conversion to oil palm. *Proceedings of the National Academy of Sciences*, 108, 5127–5132.

Koh, L.P. & Wilcove, D.S. (2008). Is oil palm agriculture really destroying tropical biodiversity? *Conservation Letters*, 1, 60–64.

Koh, L.P. & Wilcove, D.S. (2007). Cashing in palm oil for conservation. *Nature*, 448, 993–994.

Kokaly, R.F., Asner, G.P., Ollinger, S. V., Martin, M.E. & Wessman, C.A. (2009). Characterizing canopy biochemistry from imaging spectroscopy and its application to ecosystem studies. *Remote Sensing of Environment*, 113, 78–91.

Kokaly, R.F. & Skidmore, A.K. (2015). Plant phenolics and absorption features in vegetation reflectance spectra near 1.66 μm. *International Journal of Applied Earth Observation and Geoinformation*, 43, 55–83.

Kooperman, G.J., Chen, Y., Hoffman, F.M., Koven, C.D., Lindsay, K., Pritchard, M.S., *et al*. (2018). Forest response to rising CO_2 drives zonally asymmetric rainfall change over tropical land. *Nature Climate Change*, 8, 434–440.

Koricheva, J., Larsson, S., Haukioja, E. & Keinanen, M. (1998). Regulation plant secondary metabolism by resource availability: Hypothesis testing by means of meta-analysis. *Oikos*, 83, 212–226.

Kretsch, J.L. (2000). Shuttle Radar Topography Mission Overview. In: *Proceedings - Applied Imagery Pattern Recognition Workshop*. p. 276.

Kumar, L., Schmidt, K., Dury, S. & Skidmore, A. (2002). Imaging Spectrometry and Vegetation Science. In: *Imaging Spectrometry*. pp. 111–156.

Lambers, H. & Poorter, H. (1992). Inherent variation in growth rate between higher plants: a search for physiological causes and ecological consequences. *Advances in Ecological Research*.

Lamont, B.B., Groom, P.K. & Cowling, R.M. (2002). High leaf mass per area of related species assemblages may reflect low rainfall and carbon isotope discrimination rather than low phosphorus and nitrogen concentrations. *Functional Ecology*, 16, 403–412.

Lasky, J.R., Uriarte, M., Boukili, V.K., Erickson, D.L., John Kress, W. & Chazdon, R.L. (2014). The relationship between tree biodiversity and biomass dynamics changes with tropical forest succession. *Ecology Letters*, 17, 1158–1167.

Laurance, W.F. & Bruce Williamson, G. (2001). Positive feedbacks among forest fragmentation, drought, and climate change in the Amazon. *Conservation Biology*, 15, 1529–1535.

Laurance, W.F., Camargo, J.L.C., Luizão, R.C.C., Laurance, S.G., Pimm, S.L., Bruna, E.M., *et al*. (2011). The fate of Amazonian forest fragments: a 32-year investigation. *Biological Conservation*, 144, 56–67.

Laurance, W.F., Lovejoy, T.E., Vasconcelos, H.L., Bruna, E.M., Didham, R.K., Stouffer, P.C., *et al*. (2002). Ecosystem decay of Amazonian forest fragments: a 22-year investigation. *Conservation Biology*, 16, 605–618.

Laurance, W.F., Nascimento, H.E.M., Laurance, S.G., Andrade, A.C., Fearnside, P.M., Ribeiro, J.E.L., *et al*. (2006). Rain forest fragmentation and the proliferation of successional trees. *Ecology*, 87, 469–482.

Law, C. & Exley, C. (2011). New insight into silica deposition in horsetail (*Equisetum arvense*). *BMC plant biology*, 11, 112.

Leblanc, S.G. (2002). Correction to the plant canopy gap-size analysis theory used by the Tracing Radiation and Architecture of Canopies instrument. *Applied Optics*, 41, 7667–7670.

Lebrija-Trejos, E., Pérez-García, E.A., Meave, J.A., Poorter, L. & Bongers, F. (2011). Environmental changes during secondary succession in a tropical dry forest in Mexico. *Journal of Tropical Ecology*, 27, 477–489.

Lefsky, M.A., Cohen, W.B., Parker, G.G. & Harding, D.J. (2002). LiDAR remote sensing for ecosystem studies. *BioScience*, 52, 19–30.

Leitold, V., Morton, D.C., Longo, M., Dos-Santos, M.N., Keller, M. & Scaranello, M. (2018). El Niño drought increased canopy turnover in Amazon forests. *New Phytologist*, 219, 959–971.

Levine, C.R., Krivak-Tetley, F., van Doorn, N.S., Ansley, J.-A.S. & Battles, J.J. (2016). Long-term demographic trends in a fire-suppressed mixed-conifer forest. *Canadian Journal of Forest Research*, 46, 745–752.

Lichtenthaler, H.K. (1987). Chlorophylls and carotenoids: Pigments of photosynthetic biomembranes. *Methods in Enzymology*, 148, 350–382.

Lim, K., Treitz, P., Wulder, M., St-Onge, B. & Flood, M. (2003). LiDAR remote sensing of forest structure. *Progress in Physical Geography*, 27, 88–106.

Lindenmayer, D.B., Laurance, W.F. & Franklin, J.F. (2012). Ecology: Global decline in large old trees. *Science*, 338, 1305–1306.

Liu, H., Park Williams, A., Allen, C.D., Guo, D., Wu, X., Anenkhonov, O.A., *et al*. (2013). Rapid warming accelerates tree growth decline in semi-arid forests of Inner Asia. *Global Change Biology*, 19, 2500–2510.

Lohbeck, M., Poorter, L., Lebrija-Trejos, E., Nez-Ramos, M.M., Meave, J.A., Paz, H., *et al*. (2013). Successional changes in functional composition contrast for dry and wet tropical forest. *Ecology*, 94, 1211–1216.

Lopes, A. V., Chiang, J.C.H., Thompson, S.A. & Dracup, J.A. (2016). Trend and uncertainty in spatial-temporal patterns of hydrological droughts in the Amazon basin. *Geophysical Research Letters*, 43, 3307–3316.

Ma, J.F. & Yamaji, N. (2006). Silicon uptake and accumulation in higher plants. *Trends in Plant Science*, 11, 392–397.

MacGillivray, C.W., Grime, J.P. & The Integrated Screening Programme (Isp) Team. (1995). Testing predictions of the resistance and resilience of vegetation subjected to extreme events. *Functional Ecology*, 9, 640–649.

MacKinnon, K., Hatta, G., Halim, H. & Mangalik, A. (1996). *The ecology of Kalimantan*. *Oxford University Press*.

Malhi, Y., Aragao, L.E.O.C., Galbraith, D., Huntingford, C., Fisher, R., Zelazowski, P., *et al*. (2009). Exploring the likelihood and mechanism of a climate-change-induced dieback of the Amazon rainforest. *Proceedings of the National Academy of Sciences*, 106, 20610–20615.

Manoli, G., Meijide, A., Huth, N., Knohl, A., Kosugi, Y., Burlando, P., *et al*. (2018). Ecohydrological changes after tropical forest conversion to oil palm. *Environmental Research Letters*, 13, 064035.

Mansori, M., Chernane, H., Latique, S., Benaliat, A., Hsissou, D. & El Kaoua, M. (2015). Seaweed extract effect on water deficit and antioxidative mechanisms in bean plants (*Phaseolus vulgaris* L.). *Journal of Applied Phycology*, 27, 1689–1698.

Maréchaux, I., Bartlett, M.K., Sack, L., Baraloto, C., Engel, J., Joetzjer, E., *et al*. (2015). Drought tolerance as predicted by leaf water potential at turgor loss point varies strongly across species within an Amazonian forest. *Functional Ecology*, 29, 1268–1277.

Marschner, H. (1995). Functions of Mineral Nutrients: Macronutrients. In: *Mineral Nutrition of Higher Plants*. pp. 229–312.

Marschner, M. (2012). *Mineral nutrition of higher plants*. *Marschner's mineral nutrition of higher plants: Third Edition*.

Marten, G.C., Halgerson, J.L. & Cherney, J.H. (1983). Quality prediction of small grain forages by near infrared reflectance spectroscopy. *Crop Science*, 23, 94–96.

Martin, A.R. & Thomas, S.C. (2011). A reassessment of carbon content in tropical trees. *PLoS ONE*, 6, e23533.

Marvin, D.C., Asner, G.P., Knapp, D.E., Anderson, C.B., Martin, R.E., Sinca, F., *et al*. (2014). Amazonian landscapes and the bias in field studies of forest structure and biomass. *Proceedings of the National Academy of Sciences*, 111, E5224–E5232.

Mauseth, J.D. (2012). *Botany*. Jones & Bartlett Publishers.

McAlpine, C.A., Johnson, A., Salazar, A., Syktus, J., Wilson, K., Meijaard, E., *et al*. (2018). Forest loss and Borneo's climate. *Environmental Research Letters*, 13, e044009.

McBratney, A., Whelan, B., Ancev, T. & Bouma, J. (2005). Future Directions of Precision Agriculture. *Precision Agriculture*, 6, 7–23.

McDowell, N., Pockman, W.T., Allen, C.D., Breshears, D.D., Cobb, N., Kolb, T., *et al*. (2008). Mechanisms of plant survival and mortality during drought: why do some plants survive while others succumb to drought? *New Phytologist*, 178, 719–739.

McGill, B.J., Enquist, B.J., Weiher, E. & Westoby, M. (2006). Rebuilding community ecology from functional traits. *Trends in Ecology and Evolution*, 21, 178–185.

Mcmahon, S.M., Parker, G.G. & Miller, D.R. (2010). Evidence for a recent increase in forest growth. *Proceedings of the National Academy of Sciences*, 107, 3611–3615.

McPhaden, M.J., Zebiak, S.E. & Glantz, M.H. (2006). ENSO as an integrating concept in earth science. *Science*, 314, 1740–1745.

Méndez-Toribio, M., Ibarra-Manríquez, G., Navarrete-Segueda, A. & Paz, H. (2017). Topographic position, but not slope aspect, drives the dominance of functional strategies of tropical dry forest trees. *Environmental Research Letters*, 12, 085002.

Meyer, V., Saatchi, S.S., Chave, J., Dalling, J.W., Bohlman, S., Fricker, G.A., *et al*. (2013). Detecting tropical forest biomass dynamics from repeated airborne LiDAR measurements. *Biogeosciences*, 10, 5421–5438.

Miettinen, J., Shi, C. & Liew, S.C. (2011). Deforestation rates in insular Southeast Asia between 2000 and 2010. *Global Change Biology*, 17, 2261–2270.

Milton, E.J. (1987). Review article: Principles of field spectroscopy. *International Journal of Remote Sensing*, 8, 1807–1827.

Milton, K. & Dintzis, F.R. (1981). Nitrogen-to-protein conversion factors for tropical plant-samples. *Biotropica*, 13, 177–181.

Misra, A. & Tyler, G. (2000). Effects of soil moisture on soil solution chemistry, biomass production, and shoot nutrients in two native grasses on a calcareous soil. *Communications in Soil Science and Plant Analysis*, 31, 37–41.

Mitchard, E.T.A. (2018). The tropical forest carbon cycle and climate change. *Nature*, 559, 527–534.

Mithöfer, A. & Boland, W. (2012). Plant defense against herbivores: chemical aspects. *Annual Review of Plant Biology*, 63, 431–450.

Monteith, J.L. (1965). Evaporation and environment. *Symposia of the Society for Experimental Biology*, 19, 4.

Morel, A.C., Saatchi, S.S., Malhi, Y., Berry, N.J., Banin, L., Burslem, D., *et al*. (2011). Estimating aboveground biomass in forest and oil palm plantation in Sabah, Malaysian Borneo using ALOS PALSAR data. *Forest Ecology and Management*, 262, 1786–1798.

Morton, D.C., Nagol, J., Carabajal, C.C., Rosette, J., Palace, M., Cook, B.D., *et al*. (2014). Amazon forests maintain consistent canopy structure and greenness during the dry season. *Nature*, 506, 221–224.

MPOB. (2016). *Oil palm planted area 2016*. Available at: http://bepi.mpob.gov.my/index.php/en/statistics/area/176-area-2016/790-oil-palm-planted-area-as-at-dec-2016.html. Last accessed 15 June 2017.

Murcia, C. (1995). Edge effects in fragmented forests: Implications for conservation. *Trends in Ecology & Evolution*, 10, 58–62.

Nakagawa, M., Tanaka, K., Nakashizuka, T., Ohkubo, T., Kato, T., Maeda, T., *et al*. (2000). Impact of severe drought associated with the 1997-1998 El Niño in a tropical forest in Sarawak. *Journal of Tropical Ecology*, 16, 355–367.

Neelin, J.D., Battisti, D.S., Hirst, A.C., Jin, F.-F., Wakata, Y., Yamagata, T., *et al*. (1998). ENSO theory. *Journal of Geophysical Research: Oceans*, 103, 14261–14290.

Nelson, R.F., Hyde, P., Johnson, P., Emessiene, B., Imhoff, M.L., Campbell, R., *et al*. (2007). Investigating RaDAR-LiDAR synergy in a North Carolina pine forest. *Remote Sensing of Environment*, 110, 98–108.

Nemani, R.R., Keeling, C.D., Hashimoto, H., Jolly, W.M., Piper, S.C., Tucker, C.J., *et al*. (2003). Climate-driven increases in global terrestrial net primary production from 1982 to 1999. *Science*, 300, 1560–1563.

Nepstad, D.C. (2002). The effects of partial throughfall exclusion on canopy processes, aboveground production, and biogeochemistry of an Amazon forest. *Journal of Geophysical Research*, 107, 1–18.

Newbery, D.M., Campbell, E.J.F., Lee, Y.F., Ridsdale, C.E. & Still, M.J. (1992). Primary lowland dipterocarp forest at Danum Valley, Sabah, Malaysia: Structure, relative abundance and family composition. *Philosophical Transactions - Royal Society of London, B*, 335, 341–356.

Newbold, T., Hudson, L.N., Hill, S.L.L., Contu, S., Lysenko, I., Senior, R.A., *et al*. (2015). Global effects of land use on local terrestrial biodiversity. *Nature*, 520, 45–50.

Nguyen, H.T., Hutyra, L.R., Hardiman, B.S. & Raciti, S.M. (2016). Characterizing forest structure variations across an intact tropical peat dome using field samplings and airborne LiDAR. *Ecological Applications*, 26, 587–601.

Niinemets, Ü. (2001). Global-scale climatic controls of leaf dry mass per area, density, and thickness in trees and shrubs. *Ecology*, 82, 453–469.

Niklas, K.J., Owens, T., Reich, P.B. & Cobb, E.D. (2005). Nitrogen/phosphorus leaf stoichiometry and the scaling of plant growth. *Ecology Letters*, 8, 636–642.

Norby, R.J., DeLucia, E.H., Gielen, B., Calfapietra, C., Giardina, C.P., King, J.S., *et al*. (2005). Forest response to elevated CO_2 is conserved across a broad range of productivity. *Proceedings of the National Academy of Sciences*, 102, 18052–18056.

Numata, I., Cochrane, M.A., Souza, C.M. & Sales, M.H. (2011). Carbon emissions from deforestation and forest fragmentation in the Brazilian Amazon. *Environmental Research Letters*, 6, 1–7.

Nunes, M.H., Davey, M.P. & Coomes, D.A. (2017a). On the challenges of using field spectroscopy to measure the impact of soil type on leaf traits. *Biogeosciences*, 14, 3371–3385.

Nunes, M.H., Ewers, R.M., Turner, E.C. & Coomes, D.A. (2017b). Mapping aboveground carbon in oil palm plantations using LiDAR: a comparison of tree-centric versus area-based approaches. *Remote Sensing*, 9, 816.

Nyström, M., Holmgren, J. & Olsson, H. (2012). Prediction of tree biomass in the forest-tundra ecotone using airborne laser scanning. *Remote Sensing of Environment*, 123, 271–279.

O'Brien, M.J., Reynolds, G., Ong, R. & Hector, A. (2017). Resistance of tropical seedlings to drought is mediated by neighbourhood diversity. *Nature Ecology & Evolution*, 1, 1643–1648.

Odum, H.T. (1983). *Systems ecology: an introduction*. United States.

Okuda, T., Suzuki, M., Adachi, N., Quah, E.S., Hussein, N.A. & Manokaran, N. (2003). Effect of selective logging on canopy and stand structure and tree species composition in a lowland dipterocarp forest in peninsular Malaysia. *Forest Ecology and Management*, 175, 297–320.

Oleksyn, J., Reich, P.B., Zytkowiak, R., Karolewski, P. & Tjoelker, M.G. (2002). Needle nutrients in geographically diverse *Pinus sylvestris* L. populations. *Annals of Forest Science*, 59, 1–18.

Olsson, L.C., Veit, M., Weissenböck, G. & Bornman, J.F. (1998). Differential flavonoid response to enhanced UV-B radiation in *Brassica napus*. *Phytochemistry*, 49, 1021–1028.

Oren, R. & Pataki, D.E. (2001). Transpiration in response to variation in microclimate and soil moisture in Southeastern deciduous forests. *Oecologia*, 127, 549–559.

Pan, Y., Birdsey, R.A., Fang, J., Houghton, R., Kauppi, P.E., Kurz, W.A., *et al*. (2011). A large and persistent carbon sink in the world's forests. *Science*, 333, 988–993.

Pang, Y., Lefsky, M., Andersen, H.E., Miller, M.E. & Sherrill, K. (2008). Validation of the ICEsat vegetation product using crown-area-weighted mean height derived using crown delineation with discrete return LiDAR data. *Canadian Journal of Remote Sensing*, 34, 471–484.

Patra, P.K., Crisp, D., Kaiser, J.W., Wunch, D., Saeki, T., Ichii, K., *et al*. (2017). The Orbiting Carbon Observatory (OCO-2) tracks 2-3 peta-gram increase in carbon release to the atmosphere during the 2014-2016 El Niño. *Scientific Reports*, 7.

Pau, G., Fuchs, F., Sklyar, O., Boutros, M. & Huber, W. (2010). EBImage-an R package for image processing with applications to cellular phenotypes. *Bioinformatics*, 26, 979–981.

Pavlis, N.K., Holmes, S.A., Kenyon, S.C. & Factor, J.K. (2013). Erratum: Correction to the development and evaluation of the earth gravitational model 2008 (EGM2008). *Journal of Geophysical Research: Solid Earth*, 118, 2633–2633.

Pérez-Harguindeguy, N., Díaz, S., Garnier, E., Lavorel, S., Poorter, H., Jaureguiberry, P., *et al*. (2013). New handbook for standardised measurement of plant functional traits worldwide. *Australian Journal of Botany*, 61, 167–234.

Perry, C.C. & Keeling-Tucker, T. (2003). Model studies of colloidal silica precipitation using biosilica extracts from Equisetum telmateia. *Colloid and Polymer Science*, 281, 652–664.

Petisco, C., Garcia-Criado, B., Mediavilla, S., Vazquez De Aldana, B.R., Zabalgogeazcoa, I., Garcia-Ciudad, A., *et al*. (2006). Near-infrared reflectance spectroscopy as a fast and non-destructive tool to predict foliar organic constituents of several woody species. *Analytical and Bioanalytical Chemistry*, 386, 1823–1833.

Pfeifer, M., Kor, L., Nilus, R., Turner, E., Cusack, J., Lysenko, I., *et al*. (2016). Mapping the structure of Borneo's tropical forests across a degradation gradient. *Remote Sensing of Environment*, 176, 84–97.

Phillips, O.L., Aragão, L.E.O.C., Lewis, S.L., Fisher, J.B., Lloyd, J., López-González, G., *et al*. (2009). Drought sensitivity of the amazon rainforest. *Science*, 323, 1344–1347.

Pillar, V.D., Sosinski, E.E. & Lepš, J. (2003). An improved method for searching plant functional types by numerical analysis. *Journal of Vegetation Science*, 14, 323–332.

Pinheiro, J., Bates, D., DebRoy, S. & Sarkar, D. (2007). nlme: Linear and Nonlinear Mixed Effects Models. *R Development Core Team*.

Pirker, J., Mosnier, A., Kraxner, F., Havlík, P. & Obersteiner, M. (2016). What are the limits to oil palm expansion? *Global Environmental Change*, 40, 73–81.

Poorter, H., Niinemets, Ü., Poorter, L., Wright, I.J. & Villar, R. (2009). Causes and consequences of variation in leaf mass per area (LMA): a meta-analysis. *New Phytologist*, 182, 565–588.

Poorter, L. & Bongers, F. (2006). Leaf traits are good predictors of plant performance across 53 rain forest species. *Ecology*, 87, 1733–1743.

Potter, C.S., Davidson, E.A., Klooster, S.A., Nepstad, D.C., De Negreiros, G.H. & Brooks, V. (1998). Regional application of an ecosystem production model for studies of biogeochemistry in Brazilian Amazonia. *Global Change Biology*, 4, 315–333.

Pretzsch, H., Biber, P., Schütze, G., Uhl, E. & Rötzer, T. (2014). Forest stand growth dynamics in Central Europe have accelerated since 1870. *Nature Communications*, 5, e4967.

Putz, F.E., Zuidema, P.A., Synnott, T., Peña-Claros, M., Pinard, M.A., Sheil, D., *et al*. (2012). Sustaining conservation values in selectively logged tropical forests: the attained and the attainable. *Conservation Letters*, 5, 296–303.

Qie, L., Lewis, S.L., Sullivan, M.J.P., Lopez-Gonzalez, G., Pickavance, G.C., Sunderland, T., *et al*. (2017). Long-term carbon sink in Borneo's forests halted by drought and vulnerable to edge effects. *Nature Communications*, 8.

Rees, A.R. (1961). Midday closure of stomata in the oil palm *Elaeis guineensis*. Jacq. *Journal of Experimental Botany*, 12, 129–146.

Reich, P.B. (2012). Key canopy traits drive forest productivity. *Proceedings of the Royal Society B: Biological Sciences*, 279, 2128–2134.

Reich, P.B. (2014). The world-wide "fast-slow" plant economics spectrum: a traits manifesto. *Journal of Ecology*, 102, 275–301.

Réjou-Méchain, M., Tanguy, A., Piponiot, C., Chave, J. & Hérault, B. (2017). biomass: an r package for estimating above-ground biomass and its uncertainty in tropical forests. *Methods in Ecology and Evolution*, 8, 1163–1167.

Réjou-Méchain, M., Tymen, B., Blanc, L., Fauset, S., Feldpausch, T.R., Monteagudo, A., *et al*. (2015). Using repeated small-footprint LiDAR acquisitions to infer spatial and

temporal variations of a high-biomass Neotropical forest. *Remote Sensing of Environment*, 169, 93–101.

Reynolds, G., Payne, J., Sinun, W., Mosigil, G. & Walsh, R.P.D.D. (2011). Changes in forest land use and management in Sabah, Malaysian Borneo, 1990-2010, with a focus on the Danum Valley region. *Philosophical Transactions of the Royal Society B: Biological Sciences*, 366, 3168–3176.

Richardson, A.D. & Reeves III, J.B. (2005). Quantitative reflectance spectroscopy as an alternative to traditional wet lab analysis of foliar chemistry: Near-infrared and mid-infrared calibrations compared. *Canadian Journal of Forest Research*, 35, 1122–1130.

Ridler, T.W. Calvard, S. (1978). Picture thresholding using iterative selection methods. *IEEE Transactions on Systems, Man and Cybernetics*, 19, 41–47.

Riutta, T., Malhi, Y., Kho, L.K., Marthews, T.R., Huaraca Huasco, W., Khoo, M.S., *et al*. (2018). Logging disturbance shifts net primary productivity and its allocation in Bornean tropical forests. *Global Change Biology*, 24, 2913–2928.

Rosseel, Y. (2012). lavaan: An R Package for Structural Equation Modeling. *Journal of Statistical Software*, 48, 1–36.

Roussel, J.R., Caspersen, J., Béland, M., Thomas, S. & Achim, A. (2017). Removing bias from LiDAR-based estimates of canopy height: accounting for the effects of pulse density and footprint size. *Remote Sensing of Environment*, 198, 1–16.

RSPO. (2013). *Adoption of Principles and Criteria*. Available at: https://www.rspo.org/file/revisedPandC2013.pdf. Last accessed 15 June 2017.

Russo, S.E., Brown, P., Tan, S. & Davies, S.J. (2008). Interspecific demographic trade-offs and soil-related habitat associations of tree species along resource gradients. *Journal of Ecology*, 96, 192–203.

Saatchi, S., Asefi-Najafabady, S., Malhi, Y., Aragao, L.E.O.C., Anderson, L.O., Myneni, R.B., *et al*. (2013). Persistent effects of a severe drought on Amazonian forest canopy. *Proceedings of the National Academy of Sciences*, 110, 565–570.

Sakschewski, B., Von Bloh, W., Boit, A., Poorter, L., Peña-Claros, M., Heinke, J., *et al*. (2016). Resilience of Amazon forests emerges from plant trait diversity. *Nature Climate Change*, 6, 1032–1036.

Sala, O.E., Chapin, F.S., Armesto, J.J., Berlow, E., Bloomfield, J., Dirzo, R., *et al*. (2000). Global biodiversity scenarios for the year 2100. *Science*, 287, 1770–1774.

Saleska, S.R., Didan, K., Huete, A.R. & Da Rocha, H.R. (2007). Amazon forests green-up during 2005 drought. *Science*, 318, 612–612.

Samanta, A., Ganguly, S., Hashimoto, H., Devadiga, S., Vermote, E., Knyazikhin, Y., *et al*. (2010). Amazon forests did not green-up during the 2005 drought. *Geophysical Research Letters*, 37, 1–5.

Santos, V.A.H.F. dos, Ferreira, M.J., Rodrigues, J.V.F.C., Garcia, M.N., Ceron, J.V.B., Nelson, B.W., *et al*. (2018). Causes of reduced leaf-level photosynthesis during strong El Niño drought in a Central Amazon forest. *Global Change Biology*, 24, 4266–4279.

Santoso, H., Gunawan, T., Jatmiko, R.H., Darmosarkoro, W. & Minasny, B. (2011). Mapping and identifying basal stem rot disease in oil palms in North Sumatra with QuickBird imagery. *Precision Agriculture*, 12, 233–248.

Sardans, J. & Peñuelas, J. (2004). Increasing drought decreases phosphorus availability in an evergreen Mediterranean forest. *Plant and Soil*, 267, 367–377.

Saunders, D.A., Hobbs, R.J. & Margules, C.R. (1991). Biological consequences of ecosystem fragmentation: a review. *Conservation Biology*, 5, 18–32.

Sayer, J., Ghazoul, J., Nelson, P. & Klintuni Boedhihartono, A. (2012). Oil palm expansion transforms tropical landscapes and livelihoods. *Global Food Security*, 1, 114–119.

Schachtman, D.P., Reid, R.J. & Ayling, S.M. (1998). Phosphorus uptake by plants: from soil to cell. *Plant Physiology*, 116, 447–453.

Scheffers, B.R., Evans, T.A., Williams, S.E. & Edwards, D.P. (2014). Microhabitats in the tropics buffer temperature in a globally coherent manner. *Biology Letters*, 10, e20140819.

Schimel, D., Pavlick, R., Fisher, J.B., Asner, G.P., Saatchi, S., Townsend, P., *et al*. (2015). Observing terrestrial ecosystems and the carbon cycle from space. *Global Change Biology*, 21, 1762–1776.

Schlesinger, W.H. & Jasechko, S. (2014). Transpiration in the global water cycle. *Agricultural and Forest Meteorology*, 189, 115–117.

Schwarz, K. (1973). A bound form of silicon in glycosaminoglycans and polyuronides. *Proceedings of the National Academy of Sciences*, 70, 1608–1612.

Schweiger, A.K., Cavender-Bares, J., Townsend, P.A., Hobbie, S.E., Madritch, M.D., Wang, R., *et al*. (2018). Plant spectral diversity integrates functional and phylogenetic components of biodiversity and predicts ecosystem function. *Nature Ecology and Evolution*, 2, 976–982.

Serbin, S.P., Singh, A., McNeil, B.E., Kingdon, C.C. & Townsend, P.A. (2014). Spectroscopic determination of leaf morphological and biochemical traits for northern temperate and boreal tree species. *Ecological Applications*, 24, 1651–1669.

Shafri, H. Z. M., Hamdan, N. (2009). Hyperspectral imagery for mapping disease infection in oil palm plantation. *American Journal of Applied Sciences*, 6, 1031–1035.

Shafri, H.Z.M., Hamdan, N. & Saripan, M.I. (2011). Semi-automatic detection and counting of oil palm trees from high spatial resolution airborne imagery. *International Journal of Remote Sensing*, 32, 2095–2115.

Sheil, D., Casson, A., Meijaard, E., Van Noordwijk, M., Gaskell, J., Sunderland-Groves, J., *et al*. (2009). *The impacts and opportunities of oil palm in Southeast Asia*. Bogor, Indonesia: Center for International Forestry Research.

Shima, K., Yamada, T., Okuda, T., Fletcher, C. & Kassim, A.R. (2018). Dynamics of tree species diversity in unlogged and selectively logged Malaysian forests. *Scientific Reports*, 8, e1024.

Shugart, H.H., Asner, G.P., Fischer, R., Huth, A., Knapp, N., Le Toan, T., *et al*. (2015). Computer and remote-sensing infrastructure to enhance large-scale testing of individual-based forest models. *Frontiers in Ecology and the Environment*, 13, 503–511.

Siegert, F., Ruecker, G., Hinrichs, A. & Hoffmann, A.A. (2001). Increased damage from fires in logged forests during droughts caused by El Niño. *Nature*, 414, 437–440.

Silva, C.A., Hudak, A.T., Vierling, L.A., Klauberg, C., Garcia, M., Ferraz, A., *et al*. (2017). Impacts of airborne LiDAR pulse density on estimating biomass stocks and changes in a selectively logged tropical forest. *Remote Sensing*, 9, 1068.

Simonson, W., Ruiz-Benito, P., Valladares, F. & Coomes, D. (2016). Modelling above-ground carbon dynamics using multi-temporal airborne LiDAR: Insights from a Mediterranean woodland. *Biogeosciences*, 13, 961–973.

Simonson, W., Allen, H. & Coomes, D. (2018). Effect of tree phenology on LiDAR measurement of Mediterranean forest structure. *Remote Sensing*, 10, 659.

Sims, D.A. & Gamon, J.A. (2002). Relationships between leaf pigment content and spectral reflectance across a wide range of species, leaf structures and developmental stages. *Remote Sensing of Environment*, 81, 337–354.

Slaton, M.R., Hunt, E.R. & Smith, W.K. (2001). Estimating near-infrared leaf reflectance from leaf structural characteristics. *American Journal of Botany*, 88, 278–284.

Slik, J.W.F., Arroyo-Rodríguez, V., Aiba, S.-I., Alvarez-Loayza, P., Alves, L.F., Ashton, P., *et al*. (2015). An estimate of the number of tropical tree species. *Proceedings of the National Academy of Sciences*, 112, 7472–7477.

Slik, J.W.F. (2004). El Niño droughts and their effects on tree species composition and diversity in tropical rain forests. *Oecologia*, 141, 114–120.

Smart, S.M., Clarke, R.T., van de Poll, H.M., Robertson, E.J., Shield, E.R., Bunce, R.G.H., *et al*. (2003). National-scale vegetation change across Britain; an analysis of sample-based surveillance data from the Countryside Surveys of 1990 and 1998. *Journal of Environmental Management*, 67, 239–254.

Smis, A., Ancin Murguzur, F.J., Struyf, E., Soininen, E.M., Herranz Jusdado, J.G., Meire, P., *et al*. (2014). Determination of plant silicon content with near infrared reflectance spectroscopy. *Frontiers in plant science*, 5, 1–9.

Sodhi, N.S., Koh, L.P., Brook, B.W. & Ng, P.K.L. (2004). Southeast Asian biodiversity: an impending disaster. *Trends in Ecology and Evolution*, 19, 654–660.

Stephenson, N.L., Das, A.J., Condit, R., Russo, S.E., Baker, P.J., Beckman, N.G., *et al*. (2014). Rate of tree carbon accumulation increases continuously with tree size. *Nature*, 507, 90–93.

Stephenson, N.L. & Van Mantgem, P.J. (2005). Forest turnover rates follow global and regional patterns of productivity. *Ecology Letters*, 8, 524–531.

Sullivan, M.J.P., Talbot, J., Lewis, S.L., Phillips, O.L., Qie, L., Begne, S.K., *et al*. (2017). Diversity and carbon storage across the tropical forest biome. *Scientific Reports*, 7.

Sultan, S.E. (2001). Phenotypic plasticity for fitness components in *Polygonum* species of contrasting ecological breadth. *Ecology*, 82, 328–343.

Sultan, S.E. & Spencer, H.G. (2002). Metapopulation structure favors plasticity over local adaptation. *The American Naturalist*, 160, 271–283.

Swaty, R.L., Deckert, R.J., Whitham, T.G. & Gehring, C.A. (2004). Ectomycorrhizal abundance and community composition shifts with drought: Predictions from tree rings. *Ecology*, 85, 1072–1084.

Tataurov, A. V., You, Y. & Owczarzy, R. (2008). Predicting ultraviolet spectrum of single stranded and double stranded deoxyribonucleic acids. *Biophysical Chemistry*, 133, 66–70.

Tattini, M., Galardi, C., Pinelli, P., Massai, R., Remorini, D. & Agati, G. (2004). Differential accumulation of flavonoids and hydroxycinnamates in leaves of *Ligustrum vulgare* under excess light and drought stress. *New Phytologist*, 163, 547–561.

Tattini, M., Guidi, L., Morassi-Bonzi, L., Pinelli, P., Remorini, D., Degl'Innocenti, E., *et al*. (2005). On the role of flavonoids in the integrated mechanisms of response of *Ligustrum vulgare* and *Phillyrea latifolia* to high solar radiation. *New Phytologist*, 167, 457–470.

Team, R.C. (2014). R: A language and environment for statistical computing. R Foundation for Statistical Computing, Vienna, Austria. URL http://www. R-project. org.

Tegelberg, R., Julkunen-Tiitto, R. & Aphalo, P.J. (2004). Red:far-red light ratio and UV-B radiation: their effects on leaf phenolics and growth of silver birch seedlings. *Plant, Cell and Environment*, 27, 1005–1013.

The R Core Team. (2018). R: A language and environment for statistical computing. *R Foundation for Statistical Computing, Vienna, Austria. URL http://www.R-project.org/*.

Thenkabail, P.S., Stucky, N., Griscom, B.W., Ashton, M.S., Diels, J., van der Meer, B., *et al*. (2004). Biomass estimations and carbon stock calculations in the oil palm plantations of African derived Savannas using IKONOS data. *International Journal of Remote Sensing*, 25, 5447–5472.

Thirumalai, K., DInezio, P.N., Okumura, Y. & Deser, C. (2017). Extreme temperatures in Southeast Asia caused by El Niño and worsened by global warming. *Nature Communications*, 8, e15531.

Tian, H., Melillo, J.M., Kicklighter, D.W., David McGuire, A., Helfrich, J.V.K., Moore, B., *et al*. (1998). Effect of interannual climate variability on carbon storage in Amazonian ecosystems. *Nature*, 396, 664–667.

Trenberth, K.E. & Stepaniak, D.P. (2001). Indices of El Niño evolution. *Journal of Climate*, 14, 1697–1701.

Tripathi, D.K., Kumar, R., Chauhan, D.K., Rai, A.K. & Bicanic, D. (2011). Laser-induced breakdown spectroscopy for the study of the pattern of silicon deposition in leaves of Saccharum species. *Instrumentation Science & Technology*, 39, 510–521.

Tucker, C.J. (1980). Remote sensing of leaf water content in the near infrared. *Remote Sensing of Environment*, 10, 23–32.

Tudhope, A.W., Chilcott, C.P., McCulloch, M.T., Cook, E.R., Chappell, J., Ellam, R.M., *et al*. (2001). Variability in the El Niño-Southern Oscillation through a glacial-interglacial cycle. *Science*, 291, 1511–1517.

Turnbull, M.H., Griffin, K.L., Fyllas, N.M., Lloyd, J., Meir, P. & Atkin, O.K. (2016). Separating species and environmental determinants of leaf functional traits in temperate rainforest plants along a soil-development chronosequence. *Functional Plant Biology*, 43, 751–765.

Tyler, G. (2002). Phosphorus fractions in grassland soils. *Chemosphere*, 48, 343–349.

Tyree, M.T., Cochard, H., Cruiziat, P., Sinclair, B. & Ameglio, T. (1993). Drought-induced leaf shedding in walnut: Evidence for vulnerability segmentation. *Plant, Cell & Environment*, 16, 879–882.

UNFCCC. (2015). *Intended nationally determined contribution of the government of Malaysia*. Available at: https://www4.unfccc.int/sites/submissions/INDC/Published%20Documents/Malaysia/1/INDC%20Malaysia%20Final%2027%20November%202015%20Revised%20Final%20UNFCCC.pdf. Last accessed 15 June 2017.

Uriarte, M., Lasky, J.R., Boukili, V.K. & Chazdon, R.L. (2016). A trait-mediated, neighbourhood approach to quantify climate impacts on successional dynamics of tropical rainforests. *Functional Ecology*, 30, 157–167.

Ustin, S.L., Gitelson, A.A., Jacquemoud, S.S., Schaepman, M., Asner, G.P., Gamon, J.A., *et al*. (2009). Retrieval of foliar information about plant pigment systems from high resolution spectroscopy. *Remote Sensing of Environment*, 113, 67–77.

Ustin, S.L., Roberts, D.A., Gamon, J.A., Asner, G.P. & Green, R.O. (2004). Using Imaging Spectroscopy to Study Ecosystem Processes and Properties. *BioScience*, 54, 523–534.

Ustin, S.L., Roberts, D.A., Pinzón, J., Jacquemoud, S., Gardner, M., Scheer, G., *et al*. (1998). Estimating canopy water content of chaparral shrubs using optical methods. *Remote Sensing of Environment*, 65, 280–291.

Valencia, R., Condit, R., Muller-Landau, H.C., Hernandez, C. & Navarrete, H. (2009). Dissecting biomass dynamics in a large Amazonian forest plot. *Journal of Tropical Ecology*, 25, 473–482.

Vallano, D.M. & Sparks, J.P. (2013). Foliar δ15N is affected by foliar nitrogen uptake, soil nitrogen, and mycorrhizae along a nitrogen deposition gradient. *Oecologia*, 172, 47–58.

van den Berg, R. a, Hoefsloot, H.C.J., Westerhuis, J. a, Smilde, A.K. & van der Werf, M.J. (2006). Centering, scaling, and transformations: improving the biological information content of metabolomics data. *BMC genomics*, 7, 142.

van der Werf, G.R., Morton, D.C., DeFries, R.S., Olivier, J.G.J., Kasibhatla, P.S., Jackson, R.B., *et al*. (2009). CO_2 emissions from forest loss. *Nature Geoscience*, 2, 737–738.

Van Soest, P.J. (1982). *Nutritional ecology of the ruminants*. Cornell University Press.

Vaughn, N.R., Asner, G.P. & Giardina, C.P. (2015). Long-term fragmentation effects on the distribution and dynamics of canopy gaps in a tropical montane forest. *Ecosphere*, 6, 1–15.

Vellend, M. (2010). Conceptual synthesis in community ecology. *The Quarterly review of biology*, 85, 183–206.

Vickers, C.E., Gershenzon, J., Lerdau, M.T. & Loreto, F. (2009). A unified mechanism of action for volatile isoprenoids in plant abiotic stress. *Nature Chemical Biology*, 5, 283–291.

Vierling, K.T., Vierling, L.A., Gould, W.A., Martinuzzi, S. & Clawges, R.M. (2008). LiDAR: shedding new light on habitat characterization and modeling. *Frontiers in Ecology and the Environment*, 6, 90–98.

Violle, C., Enquist, B.J., McGill, B.J., Jiang, L., Albert, C.H., Hulshof, C., *et al*. (2012). The return of the variance: Intraspecific variability in community ecology. *Trends in Ecology and Evolution*, 27, 244–252.

Wang, G., Cai, W., Gan, B., Wu, L., Santoso, A., Lin, X., *et al*. (2017). Continued increase of extreme El Niño frequency long after 1.5 C warming stabilization. *Nature Climate Change*, 7, 568–572.

Wasser, L., Day, R., Chasmer, L. & Taylor, A. (2013). Influence of vegetation structure on LiDAR-derived canopy height and fractional cover in forested riparian buffers during leaf-off and leaf-on conditions. *PLoS ONE*, 8, e54776.

Welles, J.M. & Norman, J.M. (1991). Instrument for indirect measurement of canopy architecture. *Agronomy Journal*, 83, 818–825.

Werk, K.S. & Ehleringer, J. (1986). Field water relations of a compass plant, *Lactuca serriola* L. *Plant, Cell & Environment*, 9, 681–683.

Werner, F.A. & Homeier, J. (2015). Is tropical montane forest heterogeneity promoted by a resource-driven feedback cycle? Evidence from nutrient relations, herbivory and litter decomposition along a topographical gradient. *Functional Ecology*, 29, 430–440.

Wessman, C.A., Aber, J.D., Peterson, D.L. & Melillo, J.M. (1988). Foliar analysis using near infrared reflectance spectroscopy. *Canadian Journal of Forest Research*, 18, 6–11.

Westoby, M., Falster, D.S., Moles, A.T., Vesk, P.A. & Wright, I.J. (2002). Plant ecological strategies: some leading dimensions of variation between species. *Annual Review of Ecology and Systematics*, 33, 125–159.

Wilcox, B.P., Breshears, D.D. & Allen, C.D. (2003). Ecohydrology of a resource-conserving semiarid woodland: Effects of scale and disturbance. *Ecological Monographs*, 73, 223–239.

Williams, A.P., Allen, C.D., Millar, C.I., Swetnam, T.W., Michaelsen, J., Still, C.J., *et al*. (2010). Forest responses to increasing aridity and warmth in the Southwestern United States. *Proceedings of the National Academy of Sciences*, 107, 21289–21294.

Williams, A.P., Allen, C.D., Macalady, A.K., Griffin, D., Woodhouse, C.A., Meko, D.M., *et al*. (2013). Temperature as a potent driver of regional forest drought stress and tree mortality. *Nature Climate Change*, 3, 292–297.

Williams, L.J., Paquette, A., Cavender-Bares, J., Messier, C. & Reich, P.B. (2017). Spatial complementarity in tree crowns explains overyielding in species mixtures. *Nature Ecology and Evolution*, 1, e0063.

Windham, W.R., Fales, S.L. & Hoveland, C.S. (1988). Analysis for tannin concentration in *Sericea lespedeza* by near infrared reflectance spectroscopy. *Crop Science*, 28, 705–708.

Wold, S., Sjöström, M. & Eriksson, L. (2001). PLS-Regression: a Basic Tool of Chemometrics. In: *Chemometrics and Intelligent Laboratory Systems*. pp. 109–130.

Wolfe, B.T., Sperry, J.S. & Kursar, T.A. (2016). Does leaf shedding protect stems from cavitation during seasonal droughts? A test of the hydraulic fuse hypothesis. *New Phytologist*, 212, 1007–1018.

Wooster, M.J., Perry, G.L.W. & Zoumas, A. (2012). Fire, drought and El Niño relationships on Borneo (Southeast Asia) in the pre-MODIS era (1980-2000). *Biogeosciences*, 9, 317–340.

Wright, D.M., Jordan, G.J., Lee, W.G., Duncan, R.P., Forsyth, D.M. & Coomes, D.A. (2010). Do leaves of plants on phosphorus-impoverished soils contain high concentrations of phenolic defence compounds? *Functional Ecology*, 24, 52–61.

Wright, I.J., Reich, P.B., Westoby, M., Ackerly, D.D., Baruch, Z., Bongers, F., *et al*. (2004). The worldwide leaf economics spectrum. *Nature*, 428, 821–827.

Wright, P.S. (1975). The soils of Sabah. FAO.

Wu, J., Chavana-Bryant, C., Prohaska, N., Serbin, S.P., Guan, K., Albert, L.P., *et al*. (2016). Convergence in relationships between leaf traits, spectra and age across diverse canopy environments and two contrasting tropical forests. *New Phytologist*, 214, 1033–1048.

Yan, C.F., Han, S.J., Zhou, Y.M., Wang, C.G., Dai, G.H., Xiao, W.F., *et al*. (2012). Needle-age related variability in nitrogen, mobile carbohydrates, and δ13C within *Pinus koraiensis* tree crowns. *PLoS ONE*, 7, e35076.

Zellweger, F., Braunisch, V., Baltensweiler, A. & Bollmann, K. (2013). Remotely sensed forest structural complexity predicts multi species occurrence at the landscape scale. *Forest Ecology and Management*, 307, 303–312.

Zhao, K., Suarez, J.C., Garcia, M., Hu, T., Wang, C. & Londo, A. (2018). Utility of multitemporal LiDAR for forest and carbon monitoring: Tree growth, biomass dynamics, and carbon flux. *Remote Sensing of Environment*, 204, 883–897.

Zhao, N., Wu, Z., Zhang, Q., Shi, X., Ma, Q. & Qiao, Y. (2015). Optimization of parameter selection for partial least squares model development. *Scientific Reports*, 5, e11647.

Zolkos, S.G.G., Goetz, S.J.J. & Dubayah, R. (2013). A meta-analysis of terrestrial aboveground biomass estimation using LiDAR remote sensing. *Remote Sensing of Environment*, 128, 289–298.

Zuleta, D., Duque, A., Cardenas, D., Muller-Landau, H.C. & Davies, S.J. (2017). Drought-induced mortality patterns and rapid biomass recovery in a terra firme forest in the Colombian Amazon. *Ecology*, 98, 2538–2546.

Appendix A | Field spectroscopy in temperate forests

Trait correlations of 6 species growing on contrasting soil types

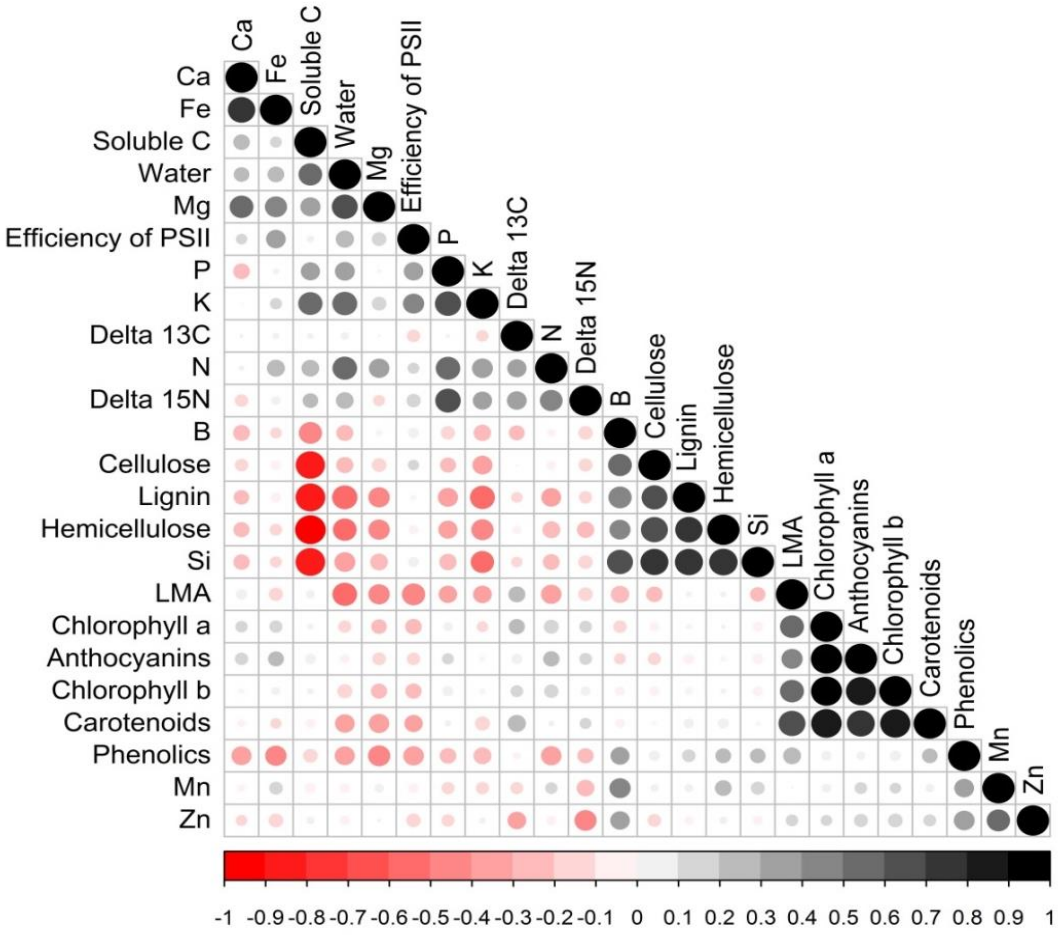

Figure A.1 | Spearman correlation rank test among leaf traits of 6 species growing on both soil types. Red and black circles mean, respectively, negative and positive correlations. Foliar traits were organised using cluster analysis.

Appendix B | El Niño effects on leaf traits and spectral properties

Trait correlations of 65 species in Borneo affected by the 2015/2016 El Niño.

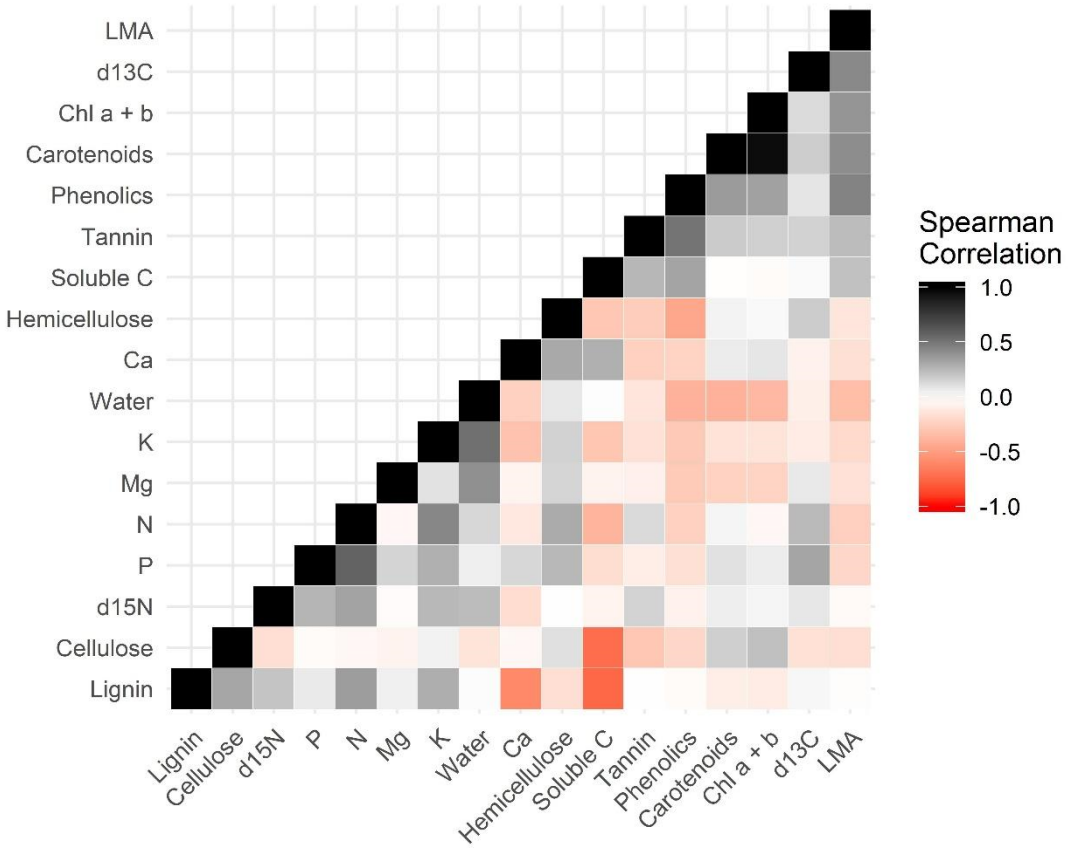

Figure B.1 | Spearman correlation matrix among all chemical traits and LMA using both year's data. The correlation matrix was reordered according to the correlation coefficient using hierarchical clustering order to identify hidden patterns in the matrix.

Appendix C | The El Niño effects on canopy structure

Microclimate variation

Field measurements of microclimatic temperature and Vapour Water-Deficit (VPD), or atmospheric dryness, across a network of 113 permanent forest plots (see Material and methods for details) showed a peak in the recorded mean annual and mean maximum daily temperatures in April 2016 (Figure S1a), and also high atmospheric dryness (Figure S1b).

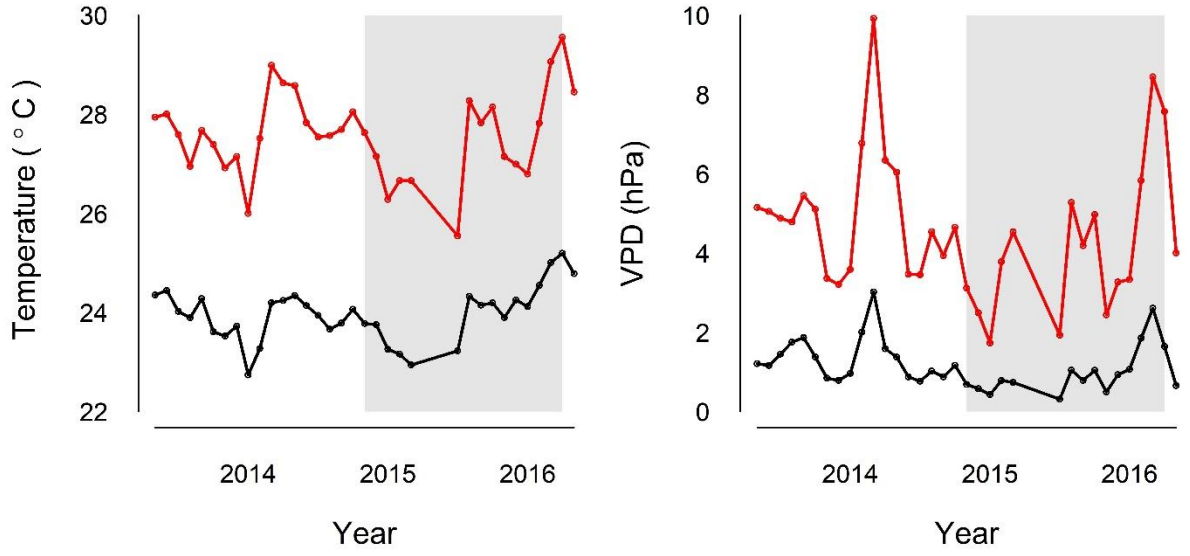

Figure C.1 | a) mean annual temperature (T_{mean}; black) and mean maximum daily temperature (T_{dmax}; red). b) annual mean Vapour-Pressure Deficit (VPD_{mean} ; black) and maximum annual VPD (VPD_{max}; red). Air temperature (T, in °C) and relative humidity (RH, in %) were measured across a network of 113 permanent forest plots (each 25 × 25 m in size). Microclimate data were collected between May 2013 and May 2016, resulting in a total of 953,789 coupled T and RH readings. We used the microclimate data to characterize atmospheric water balance by estimating VPD (in hPa). VPD, or atmospheric dryness, is the difference between the saturation water vapour pressure and the actual water vapour pressure – in other words the difference between how much moisture the air can hold before becoming saturated and the amount of moisture actually present in the air. The shaded region represents the time between both LiDAR surveys in November 2014 and April 2016.

Removing uncertainties caused by pixel size

Variance of TCH change can be overestimated owing to artefacts of repeat LiDAR data such as wind direction and within-canopy variation to reduce uncertainties of TCH change. TCH map was resampled several times until resampling would no longer affect variance (Fig. S2a). We found that 36 m resolution is the sample size that TCH distribution is no longer affected by pixel size ((Fig. S2b).

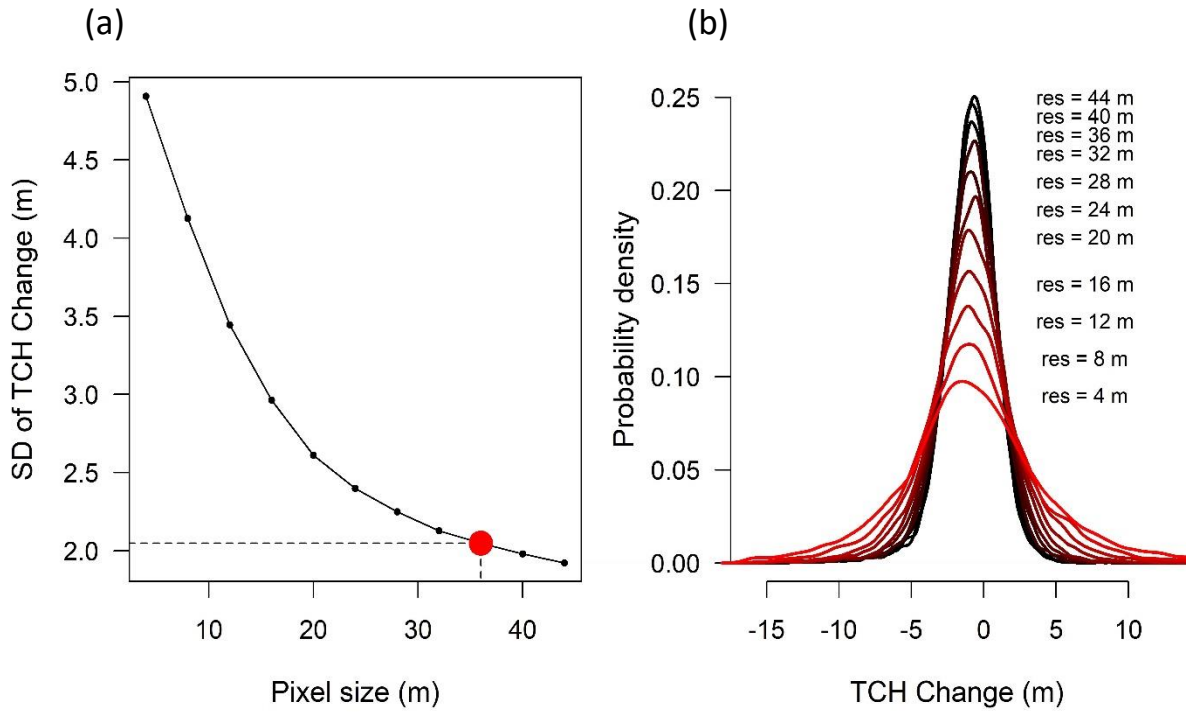

Figure C.2 | a) standard deviation versus pixel size and b) top-of-height change distribution related to pixel size.

Field top-of-canopy height calculation

A *H-DBH* and *Crown – DBH* allometric equations were locally calibrated to estimate total tree height (*H*, metres) and crown area (m^2) for individuals with missing height and crown measurements in the field (Fig. S3).

$$Crown = 0.22 \times DBH^{1.41} \quad \text{(Eqn. S1)}$$

$$Height = 2.21 \times DBH^{0.67} \quad \text{(Eqn. S2)}$$

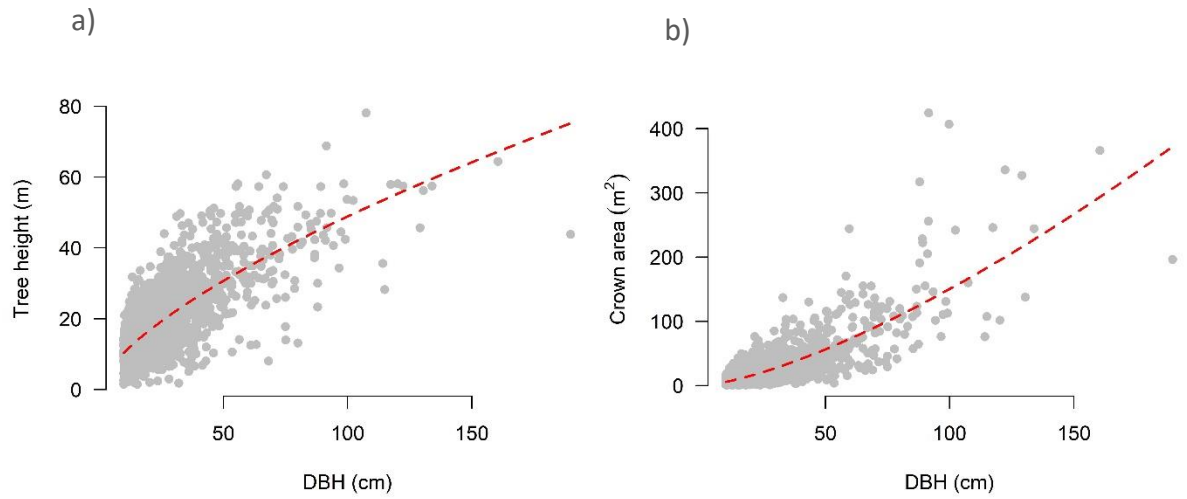

Figure C.3 | Diameter at 1.3 m (DBH; cm) explaining variation in (a) tree height (metres) and (b) crown area across a large experiment in a human modified landscape in Borneo. Each point corresponds to an individual, with fitted curves highlighting bivariate relationships captured by non-linear models.

We then apply a crown-area weighted height suited for ALS applications (Pang *et al*., 2008), where the height of each individual tree is weighted by the projected crown area. Since the upper canopy surface measured by ALS consists primarily of the tallest dominant and codominant trees, we are then able to minimise the influence of smaller stems that are incorrectly included as dominant or codominant stems. We first fitted allometric relationships between *DBH* and crown area using non-linear least-squares regression and the crown area of all trees with missing crown information was then estimated from their *DBH* values. The height of each tree was weighted by its proportional contribution to total crown area to calculate the mean top-of-canopy height as in Kent *et al*. (2015).

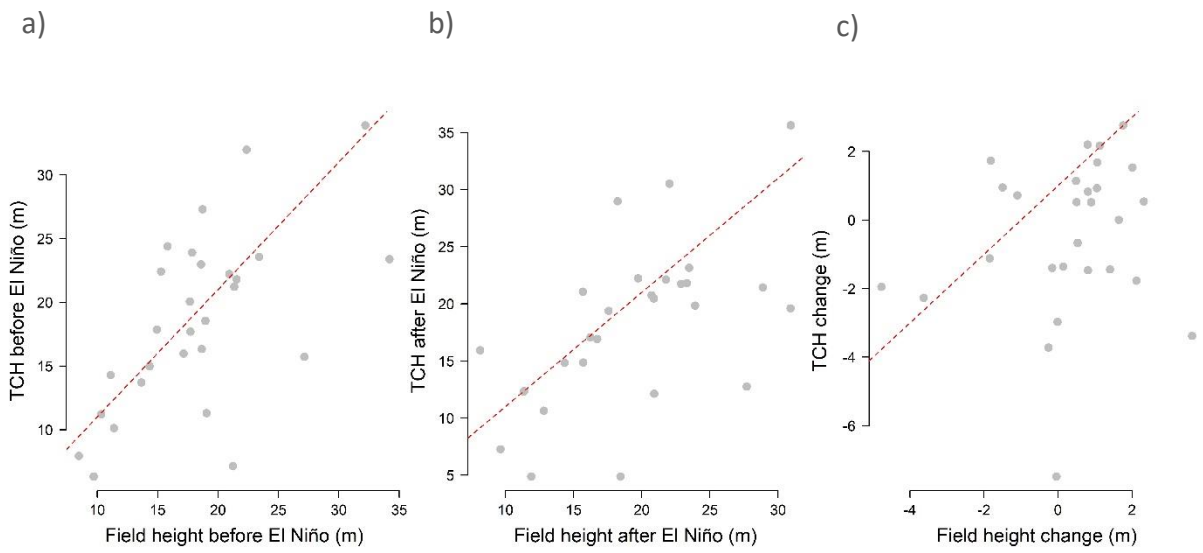

Figure C.4 | Crown-area weighted height measured in the field (a) before the El Niño in December 2014, (b) after the El Niño in February 2017, and (c) canopy height change comparing both years in comparison with the ALS-measured data. The crown-area weighted height is suited for comparison with ALS data as it minimises the influence of smaller stems that are incorrectly included as dominant or codominant stems. Each dot represents a 25 x 25 m plot.

Microclimate variables selection

Air temperature (T, in °C) and relative humidity (RH, in %) were measured across a network of 113 permanent forest plots. From the hourly temperature records we calculated the mean annual temperature (T_{mean}), the mean maximum daily temperature (T_{dmax}) and the maximum annual temperature (T_{max}) of each study plot. Having estimated VPD for each coupled hourly observation of T and RH, we then calculated annual mean VPD (VPD_{mean}), mean daily maximum VPD (VPD_{dmax}) and maximum annual VPD (VPD_{max}) for each study plot. We then coupled the mean top-of-canopy height for each plot estimated from ALS. The bivariate relationships denote the significant influences of TPI and canopy structure on microclimatic variables with the coefficient of determination (R^2) indicating the explained variation of the model (Fig. S5). Each point corresponds to a 25 x 25 m field plot (n = 37) although only 37 were under both flight paths with topographic and microclimatic data available. Even though both flights swept across all the plots, undue circumstances, like clouds, affected data availability.

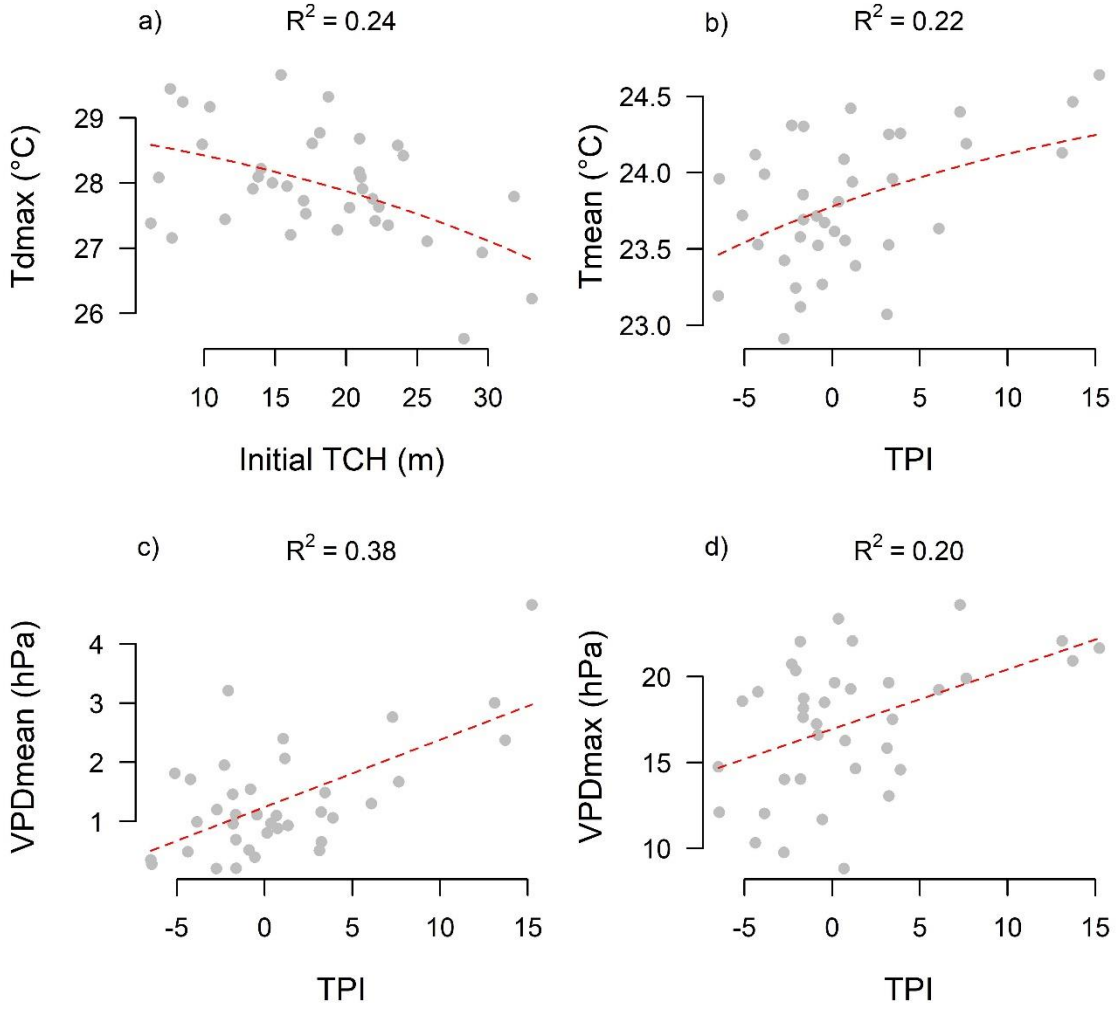

Figure C.5 | Bivariate relationships between microclimatic variables with topographic position index (TPI) and canopy structure before drought (Initial TCH); a) mean maximum daily temperature (T_{dmax}) versus Initial TCH, b) mean annual temperature (T_{mean}) versus TPI, c) annual mean Vapour-Pressure Deficit (VPD_{mean}) versus TPI and d) maximum annual VPD (VPD_{max}) versus TPI across a large experiment in a human modified landscape in Borneo. Each point corresponds to a 25 x 25 m field plot, with fitted curves highlighting bivariate relationships captured by ordinary least-square models.

Oil palm plantations offsetting forest top-of-canopy height loss

Change in top-of-canopy height was measured across 9587 hectares of oil palm plantations and 8669 hectares of logged forests in different stages of recovery before and after El Niño in Malaysian Borneo. Overall, oil palm plantations had an increase of 0.93 metres in total which

represents a change in carbon stocks of 2.2 Mg C ha^{-1} $year^{-1}$ whereas forests lost on average 0.92 m in height (Fig. S6). Aboveground carbon stocks of oil palm plantations were calculated as in Nunes *et al*. (2017b) and annual estimates were divided by 1.41. Although oil palm exhibits some definite symptoms of water stress during the dry season, there is no visible wilting because of the nature of the leaves (fibrous, thick hypodermis and well-developed cuticle) (Rees, 1961). Furthermore, the less dense canopies in oil palm plantations than tropical forests transpire less water (Hardwick *et al*., 2015), so are expected to be less affected by short-term drought. We are confident that the height change results are not an artefact of having two different LiDAR sensors and flight specifications.

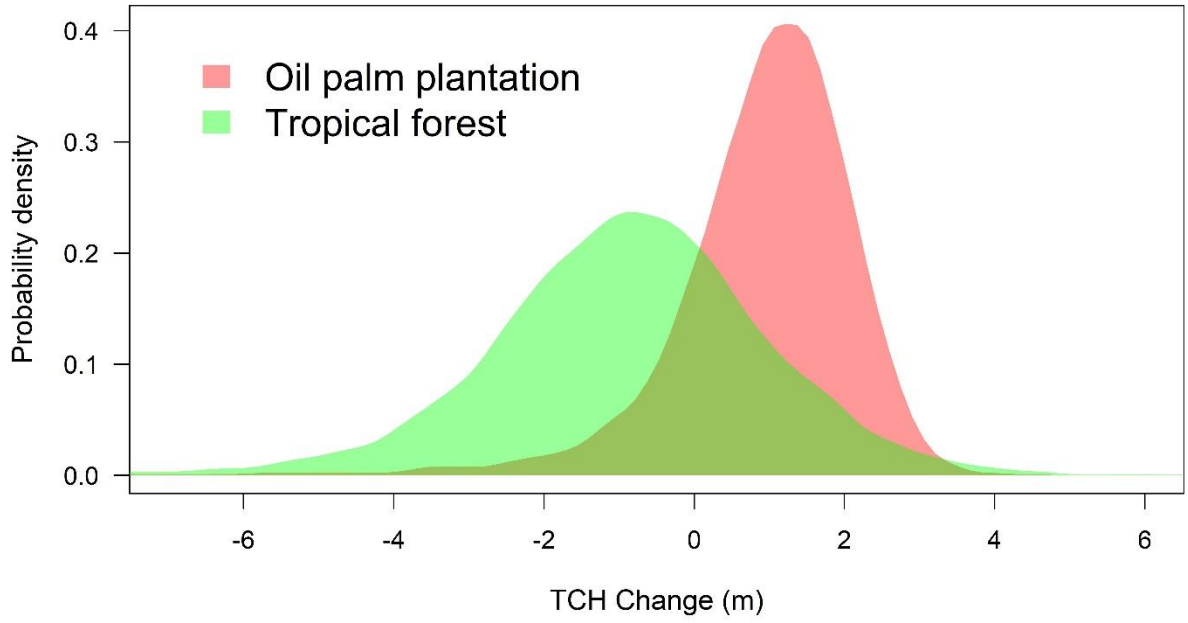

Figure C.6 | Change in top-of-canopy height in 9587 hectares of oil palm plantation and 8669 hectares of logged forests in different stages of recovery for forests and oil palm plantations before and after El Niño in Malaysian Borneo.